CELL-MATERIAL INTERACTIONS IN COMPLEX MICROENVIRONMENTS

by

Thomas William Eyster

A dissertation submitted in partial fulfillment
of the requirements for the degree of
Doctor of Philosophy
(Chemical Engineering)
in the University of Michigan
2013

Doctoral Committee:

Professor Joerg Lahann, Chair
Professor Nicholas Kotov
Professor Paul H. Krebsbach
Professor Jennifer J. Linderman

To my mother, my father, my brother, and Jilian

ACKNOWLEDGEMENTS

Having been in pursuit of a PhD for over seven years, it's difficult to condense all of the collaborators, institutions, and friends who deserve acknowledgement into a few pages. I have always told people since coming to Michigan that I am one of the luckiest graduate students for having an advisor like Dr. Joerg Lahann. He is one of the best mentors I have ever worked under, and I am a better scientist because of him. I also would like to acknowledge my committee (Dr. Jennifer Linderman, Dr. Paul Krebsbach, and Dr. Nick Kotov) for their help and guidance over the years.

I want to thank current and former members of the Lahann group, especially Xiaopei Deng, Jaewon Yoon, Himabindu Nandivada, Srijinani Bhaskar, Gowthamy Venkidasubramonian, Asish Misra, Jake Jordahl, Aftin Ross, Sahar Rahmani, Yaseen Elkasabi, Dong Woo, Tae-Hong Park, Sangyeul Hwang, Sampa Saha, Stacy Ramcharan, Ramya Kumar, Hyesun Jun, Kenneth Chang, Nathan Jones, Kathleen McEnnis, Bradley Plummer, and Hakan Durmaz. I want to independently acknowledge Dr. Xiaopei Deng for her guidance and collaborative efforts through the years along with her friendship – this PhD thesis would literally not be possible without her. I also would like to thank Dr. Jaewon Yoon for our very productive collaboration over the years – she is an excellent scientist who creatively solved many of the technical issues we encountered. The same can be said for Jacob Jordahl, Tae-Hong Park, and Aftin Ross, each of whom I collaborated with extensively and learned much from. I also must acknowledge Srijinani Bhaskar for being the only person in our group to attend both of my Super Bowl parties, even the night before her own PhD defense. I also want to thank the extraordinary undergraduates I have mentored over the years – Nicholas Sherman, Sonya Kavalam, HaeJee Yoon, and Kathy Liu. Ashley Sullivan was also a hard worker, and I'm lucky to have had such a great first mentee. All of you guys were great, and I will miss working with you. Huanan Zhang also deserves acknowledgement, because that guy rocks.

My family has been enormously supportive of me during my 7 years in graduate school. My mother, my father, and my brother have endured countless phone calls about every issue that has come up. I would have never made it through this program without them, and I want to acknowledge their love and support, as well as all the furniture they have found for me. Mid-century modern is a great style that I hope never dies out. My grandparents Bill Sr. and Margie Eyster also deserve acknowledgement for their love and support – they managed to visit me at every single college I attended (which was not an easy feat given how many there were). I also would like to acknowledge my cousin John Thomas, who I've been happy to reconnect with since moving to Michigan. Some of my best memories of my time here took place at the Liberty St. Brewery with him and his brother-in-law Gary Lanier.

I want to thank my girlfriend Jilian Bohn. When I started writing this thesis, she was there every single step of the way to listen to my complaints, bring me food, and most of all be there for me. I don't know if I could have finished this without her love. She also did a fantastic job proof-reading this dissertation. I am so lucky to have her by my side through all the rights and lefts that have been the summer of 2013. She is the best, and I love her a lot. I also would like to acknowledge her parents, Pat and Mike Bohn, for their mutual support and the cooked meals.

I want to thank Amy Baek not only as a valued collaborator and colleague biologist, but as a great friend. Thanks for being there for me when I needed to talk, and thanks for organizing the best fascinator party I've ever attended. I hope we continue to cross paths.

I want to thank Sonu Mishra for her support and friendship over the last years of my work at the university. Lunches on Central Campus and time spent killing spiders were a welcome respite from the laboratory, and I cannot repay her and Amy's support of me and my family during difficult times in 2011 and 2012.

I want to thank Stephanie Nunez for not only being a great friend over the past years at Michigan, but also the best dentist I ever had and probably ever will have. She was also a great swimming and lifting buddy, a comrade at arms during Applebees Trivia, and she knew how to put on the best Super Bowl party.

I would also like to thank my adviser at Princeton University (now at Ohio State University), Dr. David Wood. When everything wasn't working out, he gave me a chance. I will never be able to repay him. I would also like to acknowledge my friends from Princeton – Meghan Peterson, Luc Peterson, Jessica Baumgaertel, Justin Spaeth, Bob Batten, and Josh Kalman. Each is a lifelong friend and I can't think of better people to have gone through what we did together. The Finer Things Club will never die – though I apologize regarding Sartor Resartus.

Finally, I want to thank two of my best friends from high school, Jon Stotts and Mike Johnson. We've managed to stay friends for over a decade since graduation, and I wish them the best of luck as they go through graduate school themselves. I also would be remiss if I did not also mention my friend Jessica Moore (the only other chemical engineer in my class), and I wish her much luck as she pursues her new career in the Peace Corp.

TABLE OF CONTENTS

List of Figures

Abstract

Recently, effort has been placed on creating biomaterials that can directly interact biologically with cells and tissue. In this dissertation, mammalian cells are cultured on a variety of engineered microenvironments, designed to elicit a specific cellular response. In Chapter 2, chemical vapor deposition is used to create multi-modal substrates that can co-immobilize two biomolecules at precise ratios. The substrates were characterized, and the biological potency of each of the tethered biomolecules was confirmed by cell culture with the HUVEC and A431 cell lines, respectively. We also demonstrated that a CVD coating created by polymerization of pyridinophane has higher rates of cell adhesion in comparison to traditional Parylene. In Chapter 3, surface-initiated graft polymerization and atom-transfer radical polymerization were used to generate substrates coated with a thin film of poly[2-(methacryloyloxy)ethyl dimethyl-(3-sulfopropyl)ammonium hydroxide] (PMEDSAH). We characterized the proliferation, markers of pluripotency, and morphology of human mesenchymal stem cells (hMSCs) grown on these substrates and compared them to tissue culture polystyrene (TCPS). We found that hMSCs grown on PMEDSAH retain their characteristic markers, but those on grafted PMEDSAH grow at a slower rate than those on TCPS or ATRP PMEDSAH. In Chapter 4 we created bioactuators. Flexible microcylinders spatially selective for cell adhesion were fabricated via electrohydrodynamic co-jetting. Cell selectivity was subsequently demonstrated first with fibroblasts, then neonatal rat cardiomyocytes. We showed that the cardiomyocytes selectively bound to our microcylinders could bend them with a significant amount of force in comparison to other reported bioactuators. Finally, in Chapter 5 we produced microenvironments conducive to forming cell sheets, which will be used as building blocks for

higher ordered tissues. PLGA grid scaffolds were generated via electrohydrodynamic co-jetting. We created sheets of fibroblasts and hMSCs by growing them on scaffolds in rotator culture, and characterized sheet development by examining the distribution of extracellular matrix proteins over time. We also created keratinocyte sheets by co-culture with a feeder cell sheet of fibroblasts. In conclusion, we controlled cell behaviors on our engineered microenvironments to obtain desired biological outcomes.

CHAPTER 1

Introduction, Motivation, and Themes

Introduction

Using artificial materials to heal the human body arguably dates back thousands of years, with examples found throughout history. A Gallo-Roman corpse dated to the 1-2nd century CE was found fitted with an iron false tooth - one of the earliest examples of a functional oral medical prosthesis [1, 2]. Archeologists have also discovered in Iran an ancient ocular prosthesis ('glass eye') that was dated to 2800 BCE [3]. A prosthetic wooden toe dated to 1064-740 BCE was recovered in Egypt near Thebes [4]. Beyond merely attaching wood or metal to the human body, the legend of Saints Cosmas and Damian (in which the two saints replace a Caucasian man's wounded leg with that of an Ethiopian) depicts an early example of a limb transplant [5]. This miracle is celebrated in Western art and has been referenced by Vacanti (a pioneer in the field of biotechnology) as a depiction of the goals of tissue engineering, though Vacanti argues that an even earlier reference may be found in Genesis 1:1 (subject of perhaps Michelangelo's best known work, The Creation of Adam) [2, 5].

The advent of modern science, the rapid advancement of medicine in the past century, and the even more recent breakthroughs achieved in molecular biology and genetics has given scientists and medical clinicians new tools for engineering materials that interact with life. In particular, biomaterials have become a key field in medicine and biotechnology, with applications in areas ranging from biomedical devices such as stents to *in vitro* cell culture to tissue engineering[4]. A

'biomaterial' can be broadly defined as any material that is designed to interact with living tissue, but this encompasses a large family of polymers, metals, ceramics, hydrogels, and even 'natural' materials that have been re-engineered or modified, such as proteins like collagen [6, 7]. However, it has been argued that natural tissues themselves (such as a skull) are not biomaterials[8]. Picking a particular biomaterial depends on the application – metals are often used for stents, while polymers are more commonly used as catheters and ceramics for dental fillings[6]. Essentially, biomaterials serve as an artificial microenvironment for cells to grow, die, and differentiate in. By controlling a cell's microenvironment through proper design of biomaterials, its behavior can also be controlled.

Initially, biomaterials were simply the bulk material of whatever was being used; however, they have been increasingly surface modified in order to induce some biological activity[4]. In particular, the extracellular matrix (ECM) has served as both a source of inspiration and a source of functional groups for enhancing the activity of biomaterials[9]. The ECM is essentially a dynamic scaffolding secreted by cells in tissue and composed of a large variety of structural proteins, glycoproteins, proteoglycans, and bound signaling factors[10]. The ECM is not merely a static background onto which cells bind; it can directly influence cell behavior via pathways like integrin signaling, including differentiation and cell proliferation[10, 11]. It is this feature of the ECM that inspired many of the recent advances in making cell culture surfaces bioactive, rather than simply inert platforms. Choi et al. engineered a hybrid protein which fused short peptides derived from ECM molecules that promoted cell adhesion (such as argine-glycine-aspartic acid (RGD), derived from fibronectin) with another previously engineered protein based on extremely adhesive proteins secreted by mussels (so-called 'MAPs') – the adhesive protein would then stick to an inert surface such as polystyrene, while presenting the bound small peptide for cultured cells to bind[12]. This is a great example of modifying the surface of a polymer with something that directly interacts with cells – a theme that will reoccur again and again in this dissertation. Multiple reviewers refer to a new paradigm in biomaterials,

where bottom-up construction via self-assembly (much like how ECM is constructed *in vivo*) should be the strategy for creating new substrates[4, 9].

Dissertation Overview

The overarching theme of this thesis is studying how mammalian cells interact with functionalized materials. In this dissertation, a variety of material synthesis techniques are applied to create multimodal susbtrates. Much as biomaterials have many uses and applications, each project also has a different end use (Chapter 2 details multimodal substrates created via chemical vapor deposition for potential use in medical devices or cell culture, while Chapter 4 reports a project in which 'biorobots' are the goal). Yet fundamentally each involves the incubation of a line of mammalian cells with a biomaterial and a designed set of experiments meant to confirm or reject a logical sequence of hypotheses. Cell area and spreading, protein expression, and cell morphology were characterized and quantified as a way of gaining insight into the complex interactions between the cells and the biomaterial to which they are attached.

Answering the question of how mammalian cells will behave given a particular modified biomaterial that compromises an entire microenvironment serves as a unifying theme for this thesis. Chapters 2 and 3 involve the culture of cells on two-dimensional substrates designed to somehow influence or even change their behavior. Cells are presented with an environment that has multiple ligands, and their reaction to this multimodal substrate is carefully quantified in Chapter 2. In Chapter 3 human mesenchymal stem cell proliferation are compared for culture on different substrates; expression of characteristic markers is also compared. In Chapter 4, substrates are also multimodal (for example, biphasic fibers and cylinders with different cell-selective properties on each phase); however, instead of being flat 2D surfaces they are now cylindrical three-dimensional particles and fibers designed to be chemically selective for cells on only one particular side. Finally, Chapter 5 expands on this

theme. Instead of using only a collection of microcylinders or single fibers, a three-dimensional scaffold composed of stacks of many fibers is used to perform true three-dimensional cell cultures. This is important, as 2D cell culture has increasingly been recognized as unrepresentative of the physiological environment cells naturally reside in (for example, the quintessential cell 'focal adhesion point' was characterized on 2D substrates, but more recent work suggests that these FAPs are quite different on 3D substrates)[13, 14]. Fig 1.1 summarizes both the individual aims of each chapter in this thesis, and emphasizes that while the individual projects are not directly related, they all ask fundamentally what the resulting gross cell behavior will be when presented with a particular microenvironment.

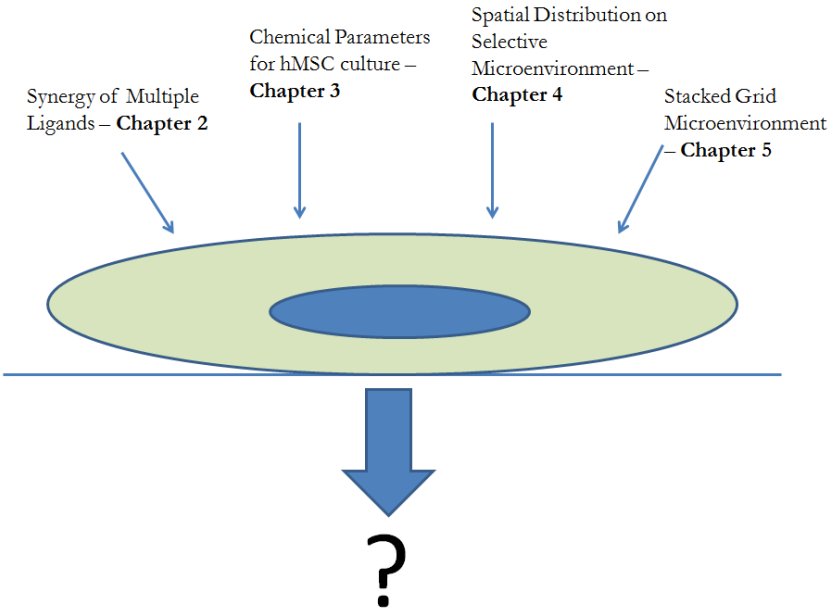

Figure 1.1: In this thesis, we created multiple selected microenvironments (the blue line) designed to influence cell behavior (illustrated in this figure as a green oval with a blue nucleus), and we seek to understand the outcome of culturing cells in these surroundings

All four projects have relevant applications in tissue engineering and medicine (especially Chapters 2 and 5). They are proof-of-concept projects that demonstrate the ability of each microenvironment platform in obtaining a certain cell behavior or morphology (for example, growth of cells as sheets, or the activation of an epidermal growth factor receptor, or the bending of a microcylinder). In

summary, biomaterials will continue to play an important role in modern medicine and clinical sciences, and by better understanding how to design them so we can observe a desired cell behavior as a result, we hope to both advance new toolboxes for producing complex functionalized substrates (from chemical vapor deposition to atom transfer radical polymerization to electrohydrodynamic co-jetting) and continue to improve on our understanding of how mammalian cells interact with artificial materials.

References

1. Crubezy, E., Murail, P., Girard, L. & Bernadou, J.P. False teeth of the Roman world. *Nature* **391**, 29 (1998).
2. Meyer, U. Fundamentals of tissue engineering and regenerative medicine. (Springer, Berlin; 2009).
3. Zargaran, A., Fazelzadeh, A. & Mohagheghzadeh, A. Surgeons and surgery from ancient persia (5,000 years of surgical history). *World journal of surgery* **37**, 2002-2004 (2013).
4. Huebsch, N. & Mooney, D.J. Inspiration and application in the evolution of biomaterials. *Nature* **462**, 426-432 (2009).
5. Vacanti, C.A. The history of tissue engineering. *J Cell Mol Med* **10**, 569-576 (2006).
6. Binyamin, G., Shafi, B.M. & Mery, C.M. Biomaterials: a primer for surgeons. *Seminars in pediatric surgery* **15**, 276-283 (2006).
7. Parenteau-Bareil, R., Gauvin, R. & Berthod, F. Collagen-Based Biomaterials for Tissue Engineering Applications. *Materials* **3**, 1863-1887 (2010).
8. Williams, D.F. On the nature of biomaterials. *Biomaterials* **30**, 5897-5909 (2009).
9. Shekaran, A. & Garcia, A.J. Nanoscale engineering of extracellular matrix-mimetic bioadhesive surfaces and implants for tissue engineering. *Biochimica et biophysica acta* **1810**, 350-360 (2011).
10. Robbins, S.L. et al., Edn. 8th 1 electronic text. (Saunders/Elsevier, Philadelphia, PA; 2009).
11. Castner, D.G. & Ratner, B.D. Biomedical surface science: Foundations to frontiers. *Surf Sci* **500**, 28-60 (2002).
12. Choi, B.H. et al. Cell behavior on extracellular matrix mimic materials based on mussel adhesive protein fused with functional peptides. *Biomaterials* **31**, 8980-8988 (2010).
13. Derda, R. et al. Paper-supported 3D cell culture for tissue-based bioassays. *Proceedings of the National Academy of Sciences of the United States of America* **106**, 18457-18462 (2009).
14. Cukierman, E., Pankov, R., Stevens, D.R. & Yamada, K.M. Taking cell-matrix adhesions to the third dimension. *Science* **294**, 1708-1712 (2001).

CHAPTER 2

Chemical Vapor Deposition Coatings for Orthogonal Dual Biomolecule Immobilization

Parts of this chapter have been adapted and/or paraphrased from the following published articles with minor modifications (reproduced by permission from John Wiley and Sons).

1. Deng, X., Eyster, T.W., Elkasabi, Y. and Lahann, J. (2012), Bio-Orthogonal Polymer Coatings for Co-Presentation of Biomolecules., Macromol. Rapid Commun., 33: 640-645.

Overview

In this chapter, we take advantage of chemical vapor deposition (CVD) to create a multimodal substrate that can bind two biomolecules in precise ratios. While there exist many methods for attaching biomolecules to surfaces, there are relatively few for precise immobilization of multiple biomolecules. In the **Introduction**, we discuss the motivating factors behind the development of techniques for modifying surfaces for biological and medical applications, along with the current state of the field for tethering molecules to a surface. We address those techniques' inherent advantages and disadvantages. In particular, the issue of precise immobilization arises as a key disadvantage for a lot of strategies available. Residual toxic solvents left behind during the immobilization step can also be a detriment. We also provide background on the chemical reactions we plan to use in tethering biomolecules, including substitution via Pfp-ester and copper catalyzed click chemistry. CVD of functionalized poly-*p*-xylylene co-polymers presents a convenient technique for creating surfaces that can bind biomolecules in predetermined ratios. We used CVD to bind two biomolecules: epidermal growth factor (EGF) and the cell adhesive factor arginine-

glycine-aspartic acid (RGD). We next demonstrate that these biomolecules remain active by culturing the model cell lines HUVEC and A431 respectively on CVD-coated surfaces featuring tethered RGD, EGF, and RGD simultaneously with EGF. We also examine the capability of a new *p*-lutidinylene-co-*p*-xylylene coating to induce HUVEC spreading.

Introduction and Background – Bulk and Surface Modification of Substrates

Ever since some of the first bacteria cultures were grown on agar in glass Petri dishes, scientists have used artificial substances to grow and support proliferating cells and tissues [1]. Traditionally these bulk materials were simple (unlike the incredibly complicated milieu of structural proteins, signaling proteins, and small molecules that make up the environment that cells typically occupy in a tissue). Glass was the original substrate used for culturing cells – this has mostly been replaced by polystyrene (which is sometimes labeled 'tissue culture polystyrene' as it is often rendered more hydrophilic by a gas plasma treatment to enhance its ability to adhere cells) due to its similar optical properties, superior reproducibility, disposability, and relative ease of production and molding into a variety of different products[2]. Recently though, there has been interest in further modifying substrates through chemical functionalization in order to influence cell behavior. By modifying substrates through attaching proteins, short peptides, nucleotides, and other small biologically active molecules ('biomolecules'), materials can be constructed that interact with living tissue and microscopic life, including bacteria and cells. Having such factors incorporated in or coated on a bulk material can radically change how it interacts with cultured cells. For example, conjugating transforming growth factor-β (TGF-β) into a polyethylene glycol (PEG) hydrogel led to a significant increase in extracellular matrix (ECM) protein production by cultured vascular smooth muscle cells in comparison to a control which lacked this growth factor [3]. Tethering a peptide that promotes cell adhesion such as arginine-glycine-aspartic acid (the cell binding motif in the ECM protein

fibronectin) to a surface or scaffold is a very common strategy[4, 5]. Other times one may wish to limit the adhesion or spreading of cells – polymers like PEG or proteins like albumin (which resists cell adhesion) can be polymerized or tethered onto a surface [6, 7]. There are applications where the mechanical properties of a certain bulk material might be very ideal (e.g., Young's modulus, or Poisson's ratio, or density), but the surface properties (for example its ability to bind cells or induce an immune response) may be very non-ideal. For instance, titanium is an ideal substrate for medical implants because it is generally biocompatible and can induce osseointegration (i.e., growth of new bone on the implant itself and its integration into the skeletal structure) – however, it has been known to fail and not integrate[8, 9]. Hauser et al. improved a titanium alloy's ability to bind SAOS-2 cells (an osteosarcoma line) by a plasma-mediated coating of collagen I, thus demonstrating a successful change to a material's ability to bind cells without changing its bulk mechanical properties[10]. By changing the surface properties of the bulk material, one can effectively separate the two. The properties of the bulk material can be decoupled from the surface through a thin polymer film coating, thus retaining the gross mechanical properties of the substrate while (sometimes greatly) altering how its surface interacts with proteins or cells [11].

Appropriate surface functionalization could also be designed to ward off or minimize undesirable biological responses (such as the immunogenic response common with implanted materials, or unwanted thrombosis)[12, 13]. Heparin (which prevents blood clotting) has been coated onto poly(vinyl) chloride (a common material found in medical devices) in order to favorably alter this material's biological interactions with blood [14]. Such materials have many applications, including as biosensors, implanted medical devices (e.g., mechanical stents, pacemakers, catheters), and components of engineered tissue [3, 15, 16].

Surfaces can be modified and functionalized directly, either through a chemical reaction resulting in a covalent bond with the bulk material, or adsorption as exemplified with self-assembled monolayers (SAMs). For example, alkanes have been covalently bonded to a hydrogen-terminated silicon substrate by submerging the substrate in molten diacyl peroxide [17]. SAMs are commonly created by adsorbing long amphiphilic molecules featuring a functional group on one end, and a 'head' group on the other that strongly (but non-covalently) interacts with the substrate[18]. Alkanethiols for example strongly interact with a gold substrate, and are commonly used to pattern mammalian cells on a surface[18, 19]. One disadvantage of SAMs is that they usually require a metal substrate such as gold (they can also be assembled on silicon), which may not always be desired for a particular application[20, 21]. Thermal grafting is another method for coating surfaces – materials are placed in a UV/ozone environment to generate peroxides on the substrate, followed by submersion in a high temperature solution of monomer[22]. The monomers then polymerize on the substrate by reacting with the peroxides[22]. To support feeder cell-free human embryonic stem cell culture, Villa-Diaz and Nandivada et al. used thermal grafting to prepare poly[2-(mathacryloyloxy)ethyl dimethyl-(3-sulfopropyl) ammonium hydroxide] (PMEDSAH) surfaces[23]. However, polymer grafting generally involves liquid solvents (which can include toxins such as acetone)[24], which along with the sometimes high temperatures required can damage the substrates that need to be coated (such as medical devices containing sensitive electronics), or leave behind toxic residues. In fact, residual toxic chemicals from materials processing can be a critical problem in biomaterials manufacturing[25, 26]. A technique for immobilizing biomolecules onto a surface that does not require a liquid solvent would thus be ideal.

Aside from generating SAMs on metallic surfaces and thermal grafting, there are many other methods for modifying substrates or depositing thin films onto surfaces. These include electroplating, layer-by-layer assembly, Langmuir-Blodgett deposition, and chemical bath deposition

[27-30]. However, one of the most versatile and well-characterized techniques available is chemical vapor deposition.

Chemical Vapor Deposition

Chemical vapor deposition (CVD) can be generally thought of as a process for depositing a chemically homogenous film from a gas via a heterogeneous reaction between the surface of the solid being coated and the gas which is being deposited [31]. The gas or vapor itself is typically generated by high temperature heating of solid reactants, which then can undergo reactions in the vapor phase before deposition [31]. CVD is commonly used to deposit metals and inorganic films such as titanium nitride, copper, and aluminum, and finds wide application in the semiconductor industry[31-34]. CVD can also be used to deposit thin films of polymers for a broad range of applications[35]. Perhaps the most well-known CVD polymerization reaction is the Gorham process[36, 37].

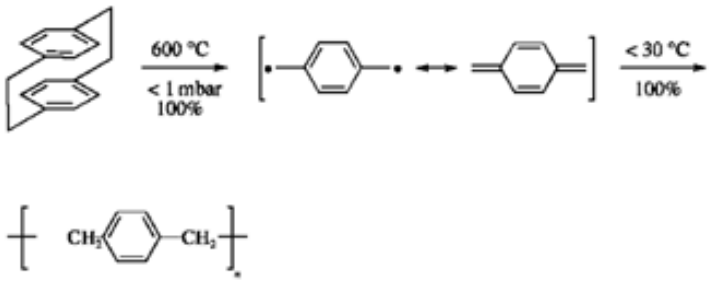

Figure 2.1: Radical polymerization of [2.2] paracyclophane to form poly-p-xylylene (parylene) (adapted from Hopf et al. with permission)[37]

Developed in 1966 by a scientist at Union Carbide, the Gorham process creates thin films of poly-*p*-xylylenes (PPX) (commonly referred to as 'parylene') from the free radical polymerization of [2.2] paracyclophanes through thermal pyrolysis at low pressures (near vacuum) (Fig. 2.1)[36, 37]. Solid monomer [2.2] paracyclophane is loaded into a quartz deposition chamber, and then placed under

vacuum (Fig 2.2)[35]. A stream of argon gas then carries the monomer into a pyrolysis chamber, which is heated to a temperature hot enough to symmetrically cleave the paracylcophane (between 550-600 C°)[35]. This leads to the formation of two diradicals (*p*-quinodimethane); once these are carried into a low temperature deposition chamber (15-30 C°), they undergo free radical polymerization to form PPX [35, 37].

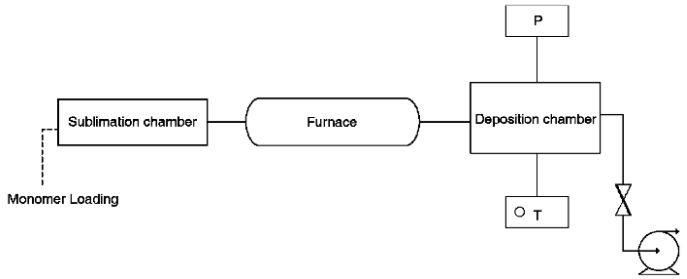

Figure 2.2: Basic chemical vapor deposition (CVD) schematic for deposition of poly(*p*-xylylene) (the Gorham process) (adapted from Lahann with permission)[35]

In addition to its use in the biomedical field, parylene and parylene-derivatives have also found application in gas chromatography and microfluidic devices [38-40]. In particular, CVD has certain advantages over other surface modification strategies that make it ideal for biomedical applications. It is a solventless process (e.g., no worries about toxic residues being left behind, or about the compatibility of what is being coated with a liquid solvent such as water or chloroform), does not require a catalyst, generates few byproducts, and the film undergoes deposition at relatively moderate temperatures (10-25 °C) so substrates that might otherwise be temperature sensitive (such as anything electronic) could be coated as well [41].

While parylene does not feature any reactive functional groups, Lahann et al. have generated a large library of modified paracylcophanes featuring a wide variety of different chemical moieties [35, 41, 42]. These groups are attached to one of the benzyl carbons on [2.2] paracyclophane via various synthetic routes; there are now many such substituted paracyclophanes available. These include

paracylcophanes featuring amines, alkynes, aldehydes, hydroxides, halogens such as bromine, ethers, esters, carboxylic acids, nitrates, and lactones [35, 41]. Paracyclophanes with these functional groups can be polymerized by CVD to form reactive thin functionalized PPX films, which can go on to react with such things as proteins, nucleic acids, or other functional groups such as linkers for further chemistries, divorcing in a single step the bulk chemistry of the substrate from its surface in a completely customized fashion. Limitations include difficulties in synthesis, the non-biodegradability of PPX, and the necessity for the functional group to not independently react during pyrolysis. For example, proteins tethered to a paracyclophane could not be coated via CVD because the intense heat would immediately denature them. However, functional groups like Pfp-esters or aldehydes could be incorporated into a substituted paracyclophane, coated onto a surface, and then through a variety of available reactions allow for the post-CVD immobilization of proteins. This has already been successfully done with several proteins, including EGF and r-hirulin[11, 43]. Picking the right functional group to immobilize a protein depends greatly on the protein being tethered (along with whether or not it needs modifications such as biotintylation or azido groups attached) and the desired outcome.

Furthermore, multiple reactive groups can be deposited in precise ratios on surfaces, as demonstrated by Elkasabi et al.[42]. This is important for immobilization of biomolecules such as peptides, nucleic acids, and proteins, as control over their ratio on the surface of a material is directly related to the ratio of the initial reactive groups present[42]. In this work, Elkasabi et al. used CVD to deposit co-polymer films with various starting ratios of precursor monomers (paracyclophanes functionalized with an amine and trifluoroacetyl group respectively) – subsequent FTIR results showed that as the molar feed ratio of amine to trifluoroacetyl groups changed, the resulting C-F band adjusted up or down accordingly, and that a 1:1 molar feed of each monomer resulted in the expected N/F ratio of 0.332 (as measured by XPS)[42]. Further studies were conducted by varying the

molar loading ratios of paracyclophanes functionalized with an amine versus a ketone (-COC_2H_5) – as the amount of ketone to amine was increased from 1:5 to 5:1, the FTIR showed the characteristic C=O peak at 1687.2 cm^{-1} increasing while the N-H stretch peak at 3361.6 cm^{-1} went away[44]. Also, 1:1 ratios of PPX-NH_2 to PPX-COC_6H_5, PPX-COC_2H_5, PPX-COC_2F_5, and $COCF_3$ mostly showed the predicted ratios of surface-bound atoms and bonds via XPS, though there were exceptions[44].

Cell Adhesion and Small Peptides

Cell spreading has been found to be critical for avoiding apoptosis[45]. By careful patterning of ECM protein islands, Chen et al. demonstrated that as the area of endothelial cells becomes smaller, their likelihood of dying becomes higher[45]. This seems to imply that the larger the area of a cell on a surface, the better chance it has of surviving, making it clear why tissue engineers and material scientists focus so much on generating substrates that can support cell adhesion. In fact, most mammalian cells in culture proliferate and survive much better when adhered to a surface (this is referred to as anchorage-dependence), with a few exceptions such as blood cells, transformed cells and certain cell lines grown under special conditions (for example, Peehl et al. grew anchorage independent non-tumor fibroblasts with high cortisol and serum concentration in the growth media) [46, 47]. Cell adhesion is a critical part of native tissues, and understanding it is important for trying to recapitulate these tissues artificially[48]. Methods such as CVD can be used to adhere cell adhesive factors onto artificial substrates.

When promoting cell adhesion on a surface, the membrane proteins that mediate this response are often targets. Integrins are the main family of proteins who anchor a cell to its environment – they are heterodimers composed of an α and β subunit of which there are many variants (e.g., α_V, α_5, β_1, etc)[49-51]. Integrins not only help coordinate cell binding, but can also act as signaling receptors and regulate apoptosis and cell survival[52, 53]. Thus, they are an important regulator of cell behavior and

can be actively targeted by proteins and peptides which they bind to elicit a desired cell response – usually cell adhesion. Artificial materials can be coated with extracellular matrix proteins such as vitronectin or fibronectin to enhance their ability to bind cells [49]. However, while using whole proteins can be fine for simple cell culture, using them to promote cell adhesion *in vivo* could lead to unwanted immunogenic effects[49]. Kantlehner et al. also points out that whole proteins are ripe targets for degradation by proteases[49]. The solution is to tether only the parts of the ECM protein that directly participate in integrin-protein interactions during cell binding, so that immunogenicity and degradation is minimized. Many of these small peptides have been successfully synthesized and used to bind cells on scaffolds or surfaces, including REDV (which is selective for endothelial cells), IKVAV (derived from laminin), and KQAGDV[3, 54, 55]. However, the most popular small adhesive peptide is RGD (mentioned previously), mostly thanks to the many different integrin heterodimers it is able to bind (nearly half of those known)[51]. The geometric patterning of RGD in a material is also important in how it influences cell spreading, signaling, and proliferation – alginate hydrogels containing RGD spaced by hydrogels lacking RGD can be generated, and it has been shown that the relative distance between these RGD 'islands' can directly regulate several key cell behaviors[56]. This indicates that the density of RGD bound to a surface could play an important role in cell culture – thus, techniques for modifying surfaces which can tune this density (such as those generated by CVD) would be a powerful tool. One disadvantage of using small peptides is their propensity to actually lower the long term production of ECM molecules by cells[3]. Mann et al. helped remedy this by co-immobilization of the growth factor TGF-β with a variety of small peptides – the growth factor subsequently stimulated new ECM production by cells cultured on these small adhesive peptides[3].

Bioconjugation and Click Chemistry

The ability to functionalize a surface with single or multiple chemical groups allows for the conjugation of biomolecules such as proteins or small peptides to a surface. Aside from those already discussed, there are several reasons this may be useful in material design – tethered proteins have been shown in multiple studies to exert different effects than their soluble counterparts (such as superior *in vivo* wound healing)[57, 58]. In particular, the tethering of growth factors such as EGF or FGF has been the goal of many projects[59]. In his large review of the subject, Ito postulates that immobilized proteins which signal through receptors can avoid down regulation by receptor-ligand degradation and recycling, as ligands (in this case the proteins) which are tethered cannot be taken up by the cell[59]. Chen et al. tethered EGF to a polystyrene surface via UV photo-irradiation (the EGF was previously modified with an *N*-(4-azidobenzoyloxy)succinimide to form an azidobenzoyl derivatized EGF, which could then be photo-immobilized to polystyrene via a secondary amine linker)[60]. They found that tethered EGF had a greater proliferative effect than soluble EGF for anchorage dependent cells, and attribute it to a lack of receptor-ligand internalization, which would subsequently down regulate the effect of EGF[60]. To support this hypothesis, they demonstrated via a radiolabeled EGF that tethered EGF was not subsequently found inside the cell after incubation, while soluble EGF was[60]. Sometimes it can be advantage to immobilize more than one protein, in order to obtain a synergistic effect. Ito et al. did exactly this by immobilizing insulin with the cell adhesive protein fibronectin[61]. They found synergistically that cell growth was stronger with both proteins tethered compared to only insulin or fibronectin alone – this makes sense given the hypothesis of long-term signaling through inhibition of receptor-ligand internalization (the more area the cells occupy as promoted by fibronectin, the more signaling that can occur via tethered insulin)[61]. Taking advantage of this potential for synergy thus could require techniques (such as CVD) which allow for the presentation of multiple tethered biomolecules on a surface.

There are many different available strategies for covalently tethering proteins to a substrate, and almost all take advantage of reactive functional groups present on proteins. These include amines and sulfhydryls among others, and are targets for a variety of chemistries that result in a protein (or peptide) being linked to another protein or substrate[62]. These strategies of covalently linking biomolecules together (which includes proteins, nucleic acids, peptides, carbohydrates, and lipids) to other materials such as polymers are generally referred to as 'bioconjugation'[63]. There are also other non-covalent methods for tethering proteins to a surface – these can be as simple as adsorption or involve more complicated strategies such as the relationship between biotin and streptavidin[40]. Pfp-ester protein linkage is a popular way to tether proteins to a surface. These highly reactive esters will react with any primary amine to form an amide bond – all amino acids have a primary amine at their N-terminus, and the amino acid lysine also contains a primary amine as its side chain [50, 64]. Lee et al. used Pfp-ester to tether amine-terminated RGD and biotin to a poly(glycolic acid) (PGA) substrate in patterns; subsequently, they were able to grow cells in patterns that followed the patterned Pfp-ester [64]. One disadvantage of using Pfp-ester is the lack of control over which primary amine it will react with – a protein with three lysine groups (and thus four primary amines) could react with a tethered Pfp-ester via any of those amines. Tethering a protein always limits its degrees of freedom – if the Pfp-ester immobilizes the protein in an orientation that is incompatible with a cell receptor (which requires a specific protein orientation to signal downstream), then it is possible that the protein will not lead to a downstream biological effect even though the protein itself has been successfully tethered to the surface. Lahann et al. had a similar problem with the protein r-hiuridin (which was tethered via reactive CVD using a different chemistry than Pfp-ester but still involved immobilizing a protein on the surface using a reactive primary amine)[43]. This was solved by temporarily protecting the amine that they did not want to react with the surface via protection with a *N*-(methyl sulfonyl ethoxy carbonyloxy) sucinimide, then deprotecting it after

immobilization with piperidine[43]. A similar strategy could be pursued with proteins containing biologically critical primary amines that are to be tethered with Pfp-ester. Attaching the protein to a spacer molecule through which the protein is linked to the surface can also increase its flexibility and allow it to act more like its soluble counterpart[59] - this could also be employed to help cope with initially poor binding orientation through Pfp-ester tethering.

Other methods of protein bioconjugation in addition to Pfp-ester include NHS-EDC chemistry (in which a carboxylic acid and amine are coupled to form an amide, with NHS ester helping to increase the reaction efficiency), sulfydryl reactions such as those which use 4-(4-*N*-maleimidophenyl)butyric acid hydrazide to link sulhydryls to carbonyls (there are other types of these reactions, many of which use a maleimide to form a thioester bond), and crosslinking a carboxylated protein with another protein containing a strong nucleophile (such as a primary amine) via photoactivated 4-(*p*-azidosalicylamido)butylamine[62].

"Click" chemistry has recently emerged as a powerful new strategy for conjugating molecules. Click chemistry is not a particular reaction or even family of reactions, but a general philosophy that Sharpless et al. and Nandivada et al. succinctly summarized as follows (paraphrased here): a click reaction is any reaction which binds two molecules together that react completely (typically with a thermodynamic driving force higher than 20 kcal/mol), has a minimal number of byproducts (and ideally only one product), has low cross-reactivity with functional groups other than its target (an important feature of bioorthgonality), results in stereospecific products if applicable, generates products which are easy to separate after the reaction is complete (Sharpless specifies it must be nonchromatographic), and can happen at simple laboratory conditions (such as at room temperature, atmospheric pressure, use non-caustic solvents such as water, etc) [65, 66]. It is a powerful tool for

functionalizing materials such as polymers in the hands of chemists, material engineers, and increasingly medical scientists[65].

While there are many reactions that can fall under the umbrella of 'click' (such as the Diels-Alder reaction – another sort of cycloaddition), the two used in this thesis are the Huisgen's 1,3-dipolar cycloaddition and strain promoted cycloaddition of cyclooctyne[67]. 1,3-dipolar cycloaddition can link two molecules together via a five-membered heterocyclic ring by a reaction between what Huisgen terms a dipole and a "dipolarophile"[68]. The dipole is generated by resonance across double or triple bonds (such as an azide with its double bonds), which can then react with a dipolarophile such as an alkyne[68]. Copper catalyzed 1,3-dipolar cycloaddition between an azide and an alkyne is commonly referred to as CuAAC, while the five-membered heterocyclic ring is defined as a 1,2,3-triazole[69]. A copper(I) catalyst is often used in order to keep the reaction conditions at room temperature and pressure (though other catalysts have been reported, such as the ruthenium catalyst $Cp^*RuCl(PPh_3)_2$) – copper (II) sulfate can be added to the reaction solvent and kept reduced via the further addition of ascorbic acid (other copper catalysts are also used depending on the solvent, such as $CuBr(PPh_3)_4$)[67, 69, 70]. In the language of cycloaddition chemistry, this sort of addition is termed "[3+2]" (as three atoms from the 1,3-dipole form a 5 member ring with two atoms on the dipolarophile)[68]. CuAAC has been used with great success in such fields as drug synthesis, activity-based protein profiling, polymer architecture, and surface modification for cell adhesion[69,11, 71, 72]. Proteins modified at their N-terminal to feature an azide or an alkyne have been joined together to form dimers through CuAAC, making it a powerful bioconjugation technique [73].

However, CuAAC suffers from a potentially critical defect when it comes to surface modification for cell culture. Copper is toxic to mammalian cells – Cao et al. demonstrated that L929 mouse fibroblasts have a greater than 99% incident of death within 24 hours after exposure to only 62 μM of copper ion[74]. This is much lower than the standard 100 μM used for CuAAC in Deng et al.[11].

While residual copper can be washed off with a phosphate buffer saline solution (PBS) or even chelated with ethylenediaminetetraacetic acid (EDTA), this still sometimes does not fully eliminate it – and there are instances where a click chemistry reaction would be desirable to occur *in situ* with living cells or tissue (in which case the strategy of washing away copper catalyst would be moot)[75]. Thus, a variety of copper-free click chemistry reactions have been developed and characterized – such reactions could then be exploited for things like live *in vivo* imaging (where copper would not be tolerated)[75].

One such copper-free click chemistry is cyclooctyne strain promoted [3+2] azide-alkyne cycloaddition, developed by Bertozzi et al.[67]. Here, the ring strain itself provides the thermodynamic driving energy (measured at 18 kcal/mol) and a catalyst is not required – Bertozzi proceeded to use this new click chemistry to do live labeling of Jurkat cells (a T-lymphocyte), and did not observe any toxic effect[67]. Other catalyst-free triazole-forming chemistries include a 1,3-dipolar cycloaddition-retro-Diels-Alder reaction with oxanorbornadiene as the dipolarophile – this was successfully used to tether cyclic RGD to a radiolabeled diethylenetriaminepentaacetic acid (DTPA)[76].

Rationale, Project Goals, and Hypotheses

As discussed in the previous section, there are many different methods and techniques available for functionalizing surfaces aside from chemical vapor deposition. However, there exist several problems in the field that need to be addressed. Having precise control over the ratios of immobilized proteins can be critical for fine tuning some biological processes (such as tissue morphogenesis, where the concentration of a signaling factor can dictate tissue development), yet the ability to do so with current methods is limited[42, 77]. For example, if one is trying to adsorb two proteins to a surface to get a defined surface ratio (say, 10 molecules of insulin for every 1 of epidermal growth factor (EGF)), it is simple to alter their ratio in solution to be 10:1. However, the hypothesis that this ratio of proteins in solution (10:1) will be the ratio of proteins on the surface is not true, as the proteins will diffuse down to the surface at different rates and can displace each other over time[78, 79]. This replacement of low molecular weight proteins initially adsorbed to a surface (due to having a high rate of diffusion down to the substrate interface) by other larger molecular weight proteins which have a higher affinity for it is termed the 'Vroman effect,' and has been observed with blood proteins adsorbed to glass[79, 80]. The same would generally be true if instead of absorption, one was attempting to react two biomolecules onto a surface using the same surface chemistry (for example, both insulin and EGF featured azido-groups and were to be clicked via CuAAC onto a surface functionalized with an alkyne)[81]. Each protein competes with the other during the reaction for alkyne sites and would react at different rates, resulting in a ratio of proteins that is different from that in the solution. The ultimate ratio of proteins tethered on the surface in this case would *not* be the ratio of proteins in the solution during the reaction[81]. Thus, if one was immobilizing multiple biofactors, a reasonable strategy would be to bind them to a reactive coating which *itself* had a defined ratio of functional groups. Furthermore, these two functional groups must react independently of one another and uniquely to only one of the population of biomolecules

being immobilized in order to preserve this desired ratio (otherwise side reactions may 'use up' some of the reactive groups intended for a separate immobilization reaction). Of course, one may still not get the exact desired ratios of proteins due to steric hindrance of the reactive groups on the surface and nonspecific adsorption, but this will be far closer than simple adsorption or reaction with only one functional group [44]. Controlling this ratio at the level of the attached reactive functional groups themselves can be difficult by methods other than chemical vapor deposition – by developing a multimodal substrate where there are two (rather than one) functional groups that undergo reactions which are independent of each other, we can create a surface that will immobilize different biomolecules with precision. There are many different methods for coating substrates (as reviewed earlier) – we want a method that is pinhole free, results in a homogenous coating regardless of the geometry of the substrate, and allows us to deposit precise ratios of functional groups. Chemical vapor deposition is the preferred thin polymer film deposition method that has all these features. Herein, we used CVD to fabricate multipotent polymer coatings with controlled ratios of alkyne and pentafluorophenyl ester groups (Fig. 2.3). As outlined in Fig. 2.3, we accomplished this by performing CVD with two initial monomers: 4-pentafluorophenyl ester[2.2]paracyclophane and 4-ethynyl[2.2]paracyclophane. With regards to the labeling in Fig. 2.3, polymer **1** is poly[(4-ethynyl-p-xylylene)-co-(p-xylylene), polymer **2** is poly[(4-pentafluorophyenyl ester-p-xylyene)-co-(p-xylylene), and polymer **3** is our copolymer poly[(4-ethynyl-p-xylylene)-co-(4-pentafluorophenyl ester p-xylylene)-co-(p-xylylene).

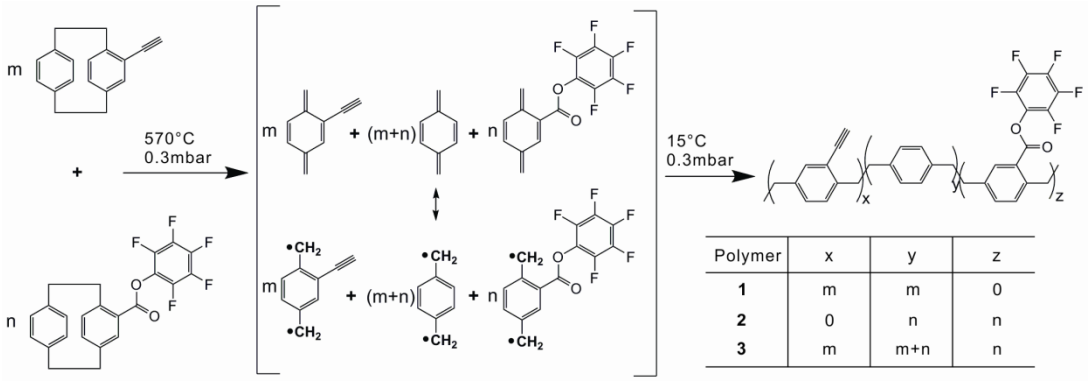

Figure 2.3: CVD copolymerization of [2.2] paracyclophanes functionalized with either alkyne or pentafluorophenyl ester groups (figure by Dr. Xiaopei Deng)

We refer to the idea of two independent reactions (which will not react with bioligands other than those targeted to them – in other words no cross reactions) as 'bioorthogonality.' This is critical for precise immobilization of multiple biomolecules. As proof of the concept of bioorthogonal co-presentation, we picked two biomolecules to conjugate to our surface, each reacting independently with one or the other functional group present (effectively decoupling their chemistries). The first is a cyclo-RGD-azide, which we tethered via CuAAC. We then picked human epidermal growth factor (EGF), and orthogonally bound it through reaction with the pentalfuorophenyl ester (Pfp-ester). We used human EGF because it is inexpensive, small (~6 kDa), has only one known receptor (EGFR), and possesses only three primary amines, limiting the degrees of freedom which it has with respect to reacting with the Pfp-ester[82, 83]. EGF has been tethered via EDC chemistry to nanofibers functionalized with primary amines in order to heal diabetic ulcers, and showed better outcomes in a mouse diabetic ulcer model over a nanofiber scaffold that was only soaked with a solution of EGF (and not immobilized with it)[58]. Thus, there is clearly medical benefit to tethered EGF. Finally, to demonstrate that these biomolecules were still active biologically after binding them to our surfaces, we cultured our substrates with either human umbilical vein endothelial cells (HUVECs) or A431 epithelial carcinoma cells (Fig 2.4).

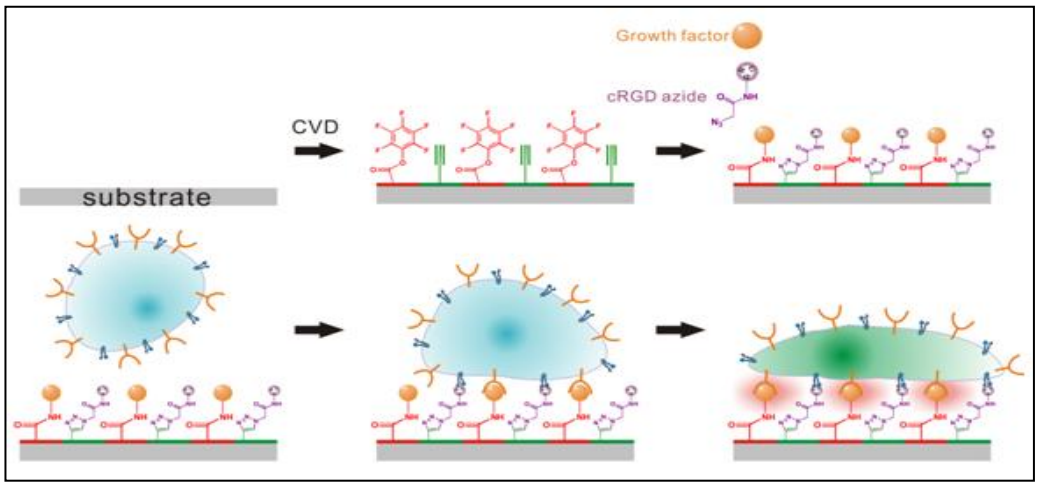

Figure 2.4: Cartoon illustrating the overall project aims: CVD of multiple functional groups in controlled ratios, reactions for biomolecule immobilization, and cultured cell's gross physiological response (figure by Dr. Xiaopei Deng)

We first hypothesize that *the copolymer will possess both functional groups, and that a 1:1 ratio of monomer will lead to a 1:1 ratio of the functional groups on the surface. No cross-reactions between the functional groups will occur during CVD.* The first hypothesis was tested by loading a 1:1 molar ratio of monomer into the CVD, then examining the resulting Fourier transform infrared spectroscopy (FTIR) and x-ray photoelectron spectroscopy (XPS). This was compared to coatings made by using the individual monomers. The FTIR spectra should demonstrate that the functional groups we claim are present with the single polymers and copolymer are in fact present, and that they have not cross reacted with each other (thus eliminating their characteristic bands). XPS will reveal the chemical composition and confirm the concentrations of Pfp-ester and acetylene present on the surface conform to a 1:1 ratio if the amount of monomer loaded into the CVD is also set at a 1:1 ratio. Secondly, we hypothesize that *EGF and cyclo-RGD-azide can be tethered to CVD-coated multipotent surfaces featuring a reactive Pfp-ester and acetylene, respectively.* This will be tested with two experiments. First, EGF will be microcontact printed (μCP) on CVD-coated surfaces in a grid pattern. If the Pfp-ester is still reactive and tethers the EGF, then after washing, the bound EGF should still be detectable using

immunofluorescence. Secondly and on a separate surface, cyclo-RGD will be μCP and reacted in a grid pattern with the acetylene. While immunofluorescence is not possible for such a small peptide, it could be indirectly detected as a height difference between where the RGD was printed on the grid line, and the surrounding area where it was not. If the RGD is there, there should be a measureable height difference that can be observed with imaging ellipsometry.

Next, we hypothesize that *the RGD remains biologically active after CuAAC with the multipotent surfaces. The presence of EGF on the surface (both by itself and with RGD) will not affect their spreading.* This will be tested by incubating the surfaces with human umbilical vein endothelial cells (HUVECs). HUVECs, which express integrins and are already known to attach and spread preferentially on cyclic RGD, should show greater cell area when cultured on coated surfaces that have been clicked with azide-RGD[84]. This was measured by incubating the cells for a limited amount of time with media *sans* serum. This was done in order to minimize unknown variables, and to prevent any proteins in the serum from reacting with any leftover unreacted Pfp-ester. Pfp-ester was passivated on all surfaces (except for the ones reacted with EGF) by a reaction with 2-(2-aminoethoxy)ethanol – this was done in order to prevent any unreacted Pfp-ester from inadvertently binding any proteins the cells generate while incubated with the coated substrates, potentially leading to confusing results. Furthermore, we hypothesize that the presence of EGF on the surfaces alongside RGD will not greatly impact cell spreading, given that HUVECs do not have appreciable levels of EGFR[85].

Finally, we hypothesize that *EGF tethered to our surfaces via reaction with Pfp-ester will remain biologically active and induce tyrosine phosphorylation on their receptor, EGFR. The presence of RGD will not impact their ability to do so.* This hypothesis cannot be tested with HUVECs, as they have a relatively low level of EGFR expression[85]. Thus, we tested the viability of our tethered EGF using the A431 epithelial carcinoma cell line, which overexpresses EGFR [86]. We will incubate serum-starved A431 cells in

media *sans* serum with our surfaces, then perform immunofluorescence for the phosphorylated EGFR (pEGFR). The presence of pEGFR indicates EGF activation of that receptor, which is powerful evidence that our tethered EGF remains biologically potent. These will be compared to AEE-passivated surfaces which do not have tethered EGF. In addition, we hypothesize that the presence of RGD will not interfere with tethered EGF signaling. Furthermore, we compared tethered EGF to soluble EGF at varying concentrations.

In addition, we performed CVD with a new monomer – pyridinophane (synthesized by Joshua Kramer at the Karlsruhe Institute of Technology). Pyridinophane is nearly identical in molecular structure to paracylcophane, except for the replacement of one of the benzyl carbons with a nitrogen atom, creating a pyridine-like aryl group. An alkyne-functionalized pyridinophane monomer was also synthesized (4-ethynylpyridinophane), and both were successfully polymerized via CVD, with pyridinophane polymerizing to poly(*p*-lutidinylene-co-*p*-xylylene) and 4-ethynylpyridinophane polymerizing to the alkyne-functionalized copolymer poly(4-ethynyl-*p* -lutidinylene-co-*p*-xylylene) (Fig 2.5).

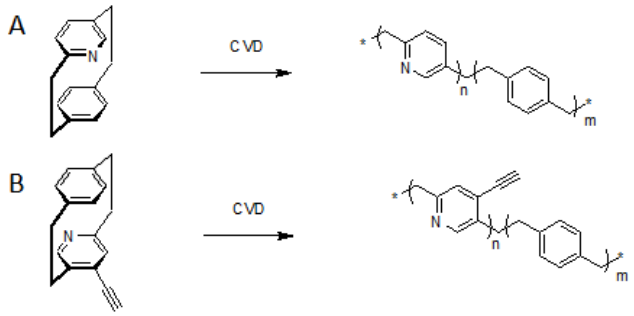

Figure 2.5: Polymerization of (a) pyridinophane and (b) 4-ethynylpyridinophane via CVD to form poly(*p*-lutidinylene-co-*p*-xylylene) and 4-ethynyl-*p*-lutidinylene-co-*p*-xylylene)(figure by Dr. Florence Bally)

The presence of the predicted polymer was verified via FTIR and XPS by Dr. Florence Bally.

Among other measured properties, it was noticed that contact angles for the *p*-lutidinylene-co-*p*-xylylene surfaces were lower than those for PPX surfaces (Fig. 2.6)

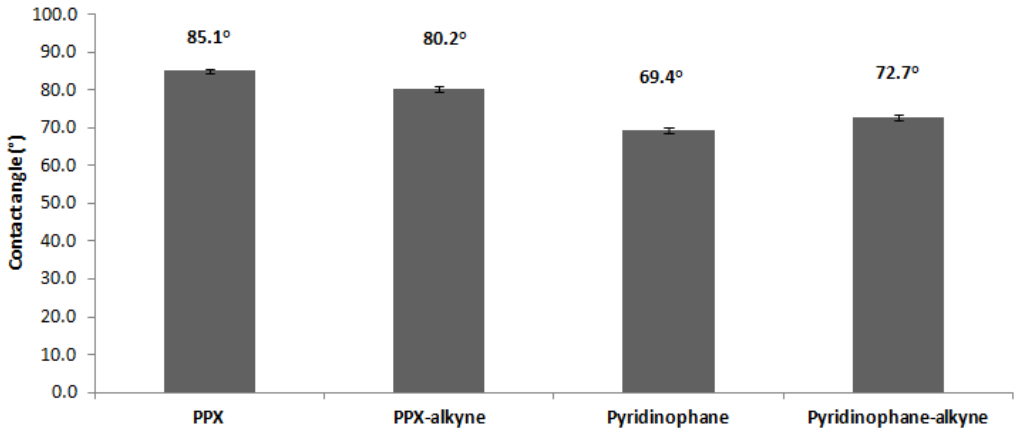

Figure 2.6: Contact angle measurements for PPX, PPX-alkyne, poly(*p*-lutidinylene-co-*p*-xylylene), and poly(4-ethynyl-*p*-lutidinylene-co-*p*-xylylene) (figure by Dr. Florence Bally)

It is not surprising that polymerizing pyridinophanes onto surfaces leads to a higher wettability than paracyclophanes, given that the nitrogen has a lone pair of electrons (which can act as a Lewis base) and the polymer exhibits some polarity. We believe this is due to the presence of a partial charge on the surface. A cell's ability to adhere to a surface based on hydrophilicity is difficult to predict, and quite a few studies initially focused on this parameter and its relationship to a cell's ability to adhere. Endothelial cells grown on poly(N-isopropylacrylamide) (PIPAAm) will detach at temperatures below the material's lower critical solution temperature, which leads to PIPAAm becoming hydrated and thus more hydrophilic[87]. Thus, it would seem that cells favor surfaces which are more hydrophobic. However, another study found that mesenchymal stem cells preferred hydrophilic surfaces which were topologically rough over smooth hydrophobic surfaces[88]. van Wachem et al. also examined endothelial cells on a variety of polymer coatings featuring different hydrophilicities[89]. They discovered that cells would adhere well to what they called 'moderately wettable surfaces' (such as tissue culture polystyrene (TCPS) and tissue culture poly(ethylene terephthalate)), while not

adhering well to surfaces that had extremely large or small contact angles[89]. But confusingly, when they alter the wettability of cellophane (by esterfication of its hydroxyl groups) to three different contact angles, as hydrophobicity increased (from 16° to 52°) cell adhesion also increased[89]. Furthermore, they hypothesize that the ability of fibronectin from the serum to adsorb onto a surface was key to cell adhesion and spreading, and that extremely hydrophilic monomers would not absorb protein well due to their tendency to expand when placed in water (but glass does not do this and can adsorb proteins, which is why despite being very hydrophilic it can also readily support cell adhesion and spreading)[89]. It is not as simple as just saying that a surface with X contact angle will be good or bad for cell adhesion.

Any charge present on a surface will also play a role in cell adhesion. Surfaces featuring a positive charge such as those grafted with N,N-dimethyl aminopropyl acrylamide (DMAPPA) when cultured with CHO cells (Chinese hamster ovary) show a large amount of cell adhesion, which is not surprising given that cell plasma membranes are negatively charged (due to the charges present on phosphatidylserine and phosphatidylinositol) [90, 91]. This is likely why cells attach so well to a surface modified with low amounts of poly-l-lysine (PLL), as it carries a strong cationic charge (high concentrations have been found to be toxic to human mesenchymal stem cells however)[92]. However, negatively charged surfaces present more of a problem – some have been shown to repel cells (like acrylic acid) while others have been shown to support cells (such as sodium *p*-styrene sulphonate)[90]. There have been attempts to decouple surface charge from surface wettability to independently study their effects on cell adhesion. When Lee et al. controlled for hydrophilicity by testing a polymer coating of polyethylene featuring four different functional groups with roughly similar contact angles (within 13°) but different charges (a positively charged -CH_2NH_2, neutral – $CONH_2$ and CH_2OH, and negatively charged –COOH), they discovered that CHO cells preferred the positively charged amine groups the most, followed by the hydroxyl group, then the amide, and

finally the carboxylic acid [93]. Furthermore, they noted that they and others have observed that ECM proteins (e.g., fibronectin) found in media serum adhere better to positively charged surfaces[93].

Non-functionalized parylene generally resists cell adhesion, but the conversion of the benzyl carbon to a nitrogen gives this surface a partially positive charge. We hypothesized that this *polymer will demonstrate enhanced cell adhesion and spreading over those cultured on n-PPX*. We tested this hypothesis by culturing primary human umbilical vein endothelial cells (HUVECs) on them in media *sans* serum, and after fixation and staining we measured the average cell areas and numbers of cells on each sample. It would also make sense to take zeta-potential measurements of our coated surfaces to determine their charges; however, at the time of writing this thesis those experiments have not been performed (data from them would go a long way towards confirming this hypothesis).

Experimental Section

Parts of the experimental section and the results section are paraphrased or unaltered directly from originally published text in

1. Deng, X., Eyster, T.W., Elkasabi, Y. and Lahann, J. (2012), Bio-Orthogonal Polymer Coatings for Co-Presentation of Biomolecules., Macromol. Rapid Commun., 33: 640-645

Other parts are paraphrased from unpublished text by collaborator Dr. Florence Bally

CVD co-polymerization

Monomer precursors' 4-pentafluorophenyl ester [2.2] paracyclophane and 4-ethynyl [2.2] paracyclophane synthesis is described elsewhere[21, 94]. Co-polymerization via chemical vapor deposition was accomplished with a 1:1 molar ratio of the monomers (as shown in Fig. 2.3). The monomers first underwent sublimation at 0.3 mbar and a temperature above 100 °C. They were then carried by a stream of argon gas (20 sccm) to a pyrolysis zone (560 °C), where they reacted to form diradicals. After this reaction, the diradicals entered the deposition chamber. Deposition was optimized with a chamber wall temperature of 120 °C and substrates temperature of 15 °C, along with rotation of the substrates to guarantee a uniform polymer film thickness.

Surface Characterization

A Nicolet 6700 spectrometer equipped with a grazing angle accessory (Smart SAGA) was used to perform IR spectroscopy (grazing angle = 85°) on the surfaces. An Axis Ultra X-ray photoelectron spectrometer (Kratos Analyticals, UK) outfitted with a monochromatized AlKα X-ray source further characterized the surfaces via XPS. A non-functionalized aliphatic carbon showing a binding energy of 285.0 eV was used to calibrate the spectra obtained. An Imaging Spectroscopic Ellipsometer

(Accurion, Nanofilm EP³-SE) measured the polymer film thicknesses. A Cauchy model was used to fit the ellipsometric parameters. The 10× objective has an imaging lateral resolution of roughly 2 μm.

Immobilization of EGF

The PDMS stamps used for microcontact printing (μCP) were generated as described elsewhere[95]. Oxidation of the stamps was first performed with a UV-ozone cleaner for 20 minutes. Next, an EGF solution (10 μg/ml in PBS) was inked to the stamps, and then placed onto the surface for 10 minutes. The now-patterned surfaces were then rinsed in PBS. EGF *sans* μCP was immobilized to surfaces at the same concentrations as those used for μCP, but the incubation time was 1 hr as opposed to 10 minutes. For immunofluorescence, the substrates were first incubated with an anti-EGF antibody (mouse IgG), diluted in PBS containing 0.1 % (w/v) bovine albumin and Tween 20 (0.02 % (v/v)) (10 μg/ml) for 1 hr. These were then washed in a PBS/BSA/Tween buffer, then incubated with a FITC-conjugated anti-mouse IgG secondary antibody for 1 hr (10 μg/ml in a PBS/BSA/Tween buffer). Finally, the now-stained samples were thoroughly washed with PBS, rinsed with distilled water, and examined with a fluorescence microscope (Olympus BX-51, Tokyo, Japan).

Immobilization of the cRGD peptide

Azide-functionazed cycloRGD (cyclo(azidoK-RGDf), Kinexus, Canada) previously aliquoted in PBS was added to an aqueous solution of sodium ascorbate (50 mg/ml) and the catalyst copper(II) sulfate (0.1 mM) at a concentration of 50 μg/ml. A PDMS stamp inked with this peptide-catalyst solution was placed on a substrate sample for 4 hr. Finally, this substrate was washed with PBS and deionized water. The concentration of cRGD was the same for non-μCP modification of surfaces, but the reaction was allowed to take place over night.

Adhesion and Spreading of Endothelial Cells

Copolymer **3** was deposited via CVD onto silicon and modified as outlined above to present tethered EGF, cRGD, EGF+cRGD, or passivated with 2-(2-aminoethoxy)ethanol (AEE). Once modified, these surfaces were washed thoroughly and placed in a 24-well plate. Human umbilical vein endothelial cells (HUVEC, Lonza) were cultured on the modified surfaces at a concentration of 5×10^4 cells/ml for 4 hours in serum-free EBM (Lonza). Passages 3-6 were used for all experiments. The cells were then fixed with 4% paraformaldehyde in DPBS and stained for actin with Alexa Fluor® 568-phallodin (Life Technologies). The surfaces were mounted with ProLong Gold + DAPI (Life Technologies) and imaged using an Olympus BX-51 fluorescence microscope. The average area of the cells was measured via ImageJ, and performed by dividing total cell area by total number of cells (equated to total number of individually counted DAPI stains). The results show three independent trials averaged; error bars are standard error (standard deviation divided by the square root of the total number of images taken over three trials), and p-values are calculated using all images from all trials.

Phosphorylated EGFR Immunofluorescence

The epidermal carcinoma line A431 (ATCC, Manassas, VA) was cultured in polystyrene flasks (Corning, Lowell, MA) at 37 ºC and in a humidified 5% CO_2 atmosphere until 100% cell confluence was observed. Passage 3 was used for all experiments. 18 hours prior to incubation with the modified surfaces, the A431 culture was serum-starved. A431 cells were trypsinized, spun down at 100xg, and resuspended with serum-free DMEM (ATCC) to a cell concentration of 5×10^4 cells/ml. A volume of 0.5 ml of A431 suspension was added to each well containing a surface. After 90 minutes of incubation at 37 ºC/5% CO_2, the cells were briefly washed with PBS, and then fixed with 4% paraformaldehyde. After three 5 minute PBS washes, the surfaces were incubated with blocking

buffer (5% normal goat serum (Life Technologies, Carlsbad, CA), 0.3% Triton-X 100 (Sigma-Aldrich) in PBS) for 1 hour followed by overnight incubation with primary antibody Phospho-EGF Receptor (Tyr1068) (D7A5) XP™ Rabbit mAb (Cell Signaling Technology, Danvers, MA). Incubation with secondary antibody anti-rabbit IgG (H+L), F(ab')2 Fragment (Alexa Fluor® 488 Conjugate) for 2 hours followed; finally the surfaces were mounted on glass slides with ProLong Gold + DAPI (Life Technologies) and imaged using an Olympus BX-51 fluorescence microscope. The quantity of immunofluorescence as a ratio of total grey pixilation to cell area minus threshold was measured via ImageJ. The results show three independent trials averaged; error bars are standard error (standard deviation divided by the square root of the total number of images taken over three trials), and p-values are calculated using all images from all trials (treating each image as statistically independent).

EGF EC_{50} measurement

A431 cells were cultured as previously described, and starved for 18 hours prior to incubation. Cells were trypsonized and cultured on AEE-modified surfaces, then incubated with a range of soluble EGF concentrations from 0.1 to 1000 ng/ml for 1 hour. pEGFR was then measured via the immunofluorescence protocol described above, including the same primary and secondary antibodies. EC_{50} data was fitted and analyzed using GraphPad Prism version 5.01 for Windows (GraphPad Software, San Diego California USA) using the modified variable slope model.

Chemical Vapor Deposition of Pyridinophane Surfaces

The monomers were first sublimated at near vacuum (<0.007 torr) and high temperature (100 °C), and were transported into a furnace by an argon gas stream (20 sccm) where they underwent

pyrolysis. The products of pyrolysis then entered a cooled deposition chamber (15 °C) where they polymerized onto substrates which were rotating to ensure uniform thickness.

*Endothelial Cell Adhesion on Poly(*p*-lutidinylene-co-*p*-xylylene) Surfaces*

Primary HUVECs at passage 2 were initially harvested by Amy Baek and obtained as a kind gift from the Pinsky group (University of Michigan). Silicon substrates were coated using CVD, then placed into a 24-well plate. We used n-PPX, alkyne-functionalized PPX, poly(*p*-lutidinylene-co-*p*-xylylene), and poly(4-ethynyl-*p*-lutidinylene-co-*p*-xylylene). Samples were run in triplicate. After trypsonization, 30,000 cells in Medium 199 (no serum) (Life Technologies) were added to each well, and the cells were allowed to incubate for 4 hours. After incubation, the surfaces were fixed with 4% formaldehyde, then stained with phalloidin and mounted with DAPI-containing ProLong Gold for imaging with an Olympus BX-51 fluorescence microscope.

Image and Statistical Analysis

The software package ImageJ (NIH) was used to analyze all images. Normalized cell spreading was quantified by measuring the total cell area and dividing by the total number of cells (counted by DAPI spot). Magnitude of fluorescence quantification was performed by converting the images to a 32-bit gray scale and then measuring the mean gray value. All error bars with the exception of the EC_{50} graph (which show standard deviation) represent standard error (one standard deviation from the mean divided by the square root of the total number of images averaged). Statistical significance was determined using Student's two-tailed t-test assuming unequal variance, with $p<0.05$ considered significant unless otherwise specified.

Results

A copolymer coating of poly[(4-ethynyl-p-xylylene)-co-(4-pentafluorophenyl ester p-xylylene)-co-(p-xylylene) (polymer **3**) was deposited by co-deposition of monomers 4-pentafluorophenyl ester[2.2] paracyclophane and 4-ethynyl[2.2] paracyclophane. We also coated surfaces with polymer **1** (poly[(4-ethynyl-p-xylylene)-co-(p-xylylene)] by deposition of the monomer 4-ethynyl[2.2] paracyclophane, and polymer **2** (poly[(4-pentafluorophyenyl ester-p-xylyene)-co-(p-xylylene)] by deposition of 4-pentafluorophenyl ester[2.2] paracyclophane; these served as controls. Fourier transform infrared spectroscopy of polymer **3** can be compared to that of polymer **1** and **2** – as Fig. 2.7 shows the expected functional groups (alkyne and pentafluoroester) are present in polymer **3** (with bands at 3287 and 2101 cm^{-1} for the alkyne, and 1762, 1523, and 1250-990 cm^{-1} for the pentafluoroester).

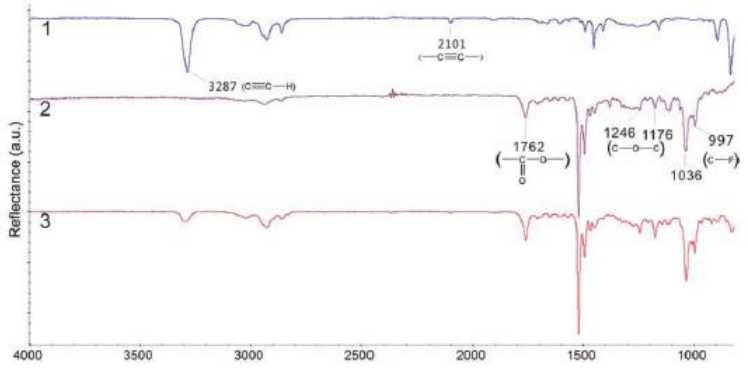

Figure 2.7: FTIR spectra for the three polymers (**1**, **2**, and **3**) (experiment performed by Dr. Xiaopei Deng)

X-ray photoelectron spectroscopy (XPS) was also used to further characterize the coated surfaces, and confirm the functional groups were deposited and did not undergo cross-reactions in the CVD chamber before deposition. As shown in Fig. 2.8, the measured values are close to those expected based on the chemical formulas of the monomers and stoichiometric conversion into the polymer. The concentration of F-C bonds in polymer **3** are roughly half of polymer **2** – this confirms the hypothesis that feeding monomers at a molar ratio of 1:1 will result in a 1:1 ratio of functional

groups on the surface. In addition, this demonstrates the power of CVD in exerting precise control over the surface coating composition.

Chemical States/ Elements	Peak Position (eV)	1	2	3
C-C/H	285.0	94.7 (100.0)	46.1 (50.0)	67.1 (74.7)
C-C=O	285.7	- (-)	3.3 (3.3)	2.4 (1.7)
C-O	286.6	- (-)	2.8 (3.3)	1.7 (1.7)
C-F	288.1	- (-)	18.9 (16.7)	9.9 (8.4)
O-C=O	289.2	- (-)	3.0 (3.3)	1.9 (1.7)
$\pi \rightarrow \pi^*$	291.5	4.0 (-)	1.4 (-)	2.6 (-)
O	533	1.3 (-)	4.8 (6.7)	3.7 (3.4)
F	688	- (-)	19.7 (16.7)	10.7 (8.4)

Figure 2.8: Chemical composition in atom% shown as experimental values (with the calculated values based on stoichiometry in the brackets) measured by XPS; experimental values of O and F atom ratios [%] were obtained from survey results and other experimental values are from high resolution C 1s spectra peak fitting calculated based on an equimolar distribution of monomers. (experiment performed by Dr. Xiaopei Deng)

Next, we need to verify that our functionalized polymers can be conjugated to our peptide and growth factor. First we microcontact printed cRGD via Huisgen's [1,3] dipolar cycloaddition, with the unstamped area serving as an internal control. We then examined the printed substrate with imaging ellipsometry – the resulting thickness of the stamped area was roughly 0.5 nm above the background unpatterned area (Fig. 2.9). This confirms that the alkyne remained reactive and that we had successfully conjugated cRGD to our functionalized surface.

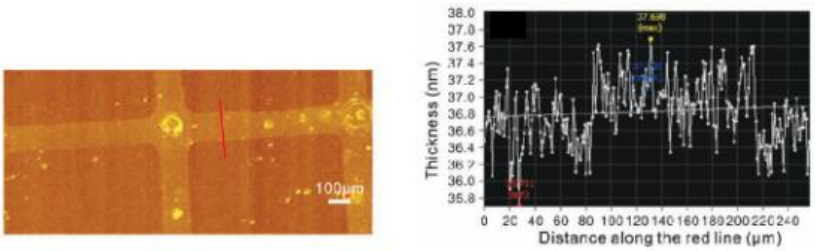

Figure 2.9: Imaging ellipsometry thickness map of patterned cRGD with thickness profile (measured along the red line) (experiment performed by Dr. Xiaopei Deng)

We next evaluated the Pfp-ester's ability to conjugate EGF. EGF was reacted with Pfp-ester via microcontact printing (a primary amine on EGF reacts with the ester to form an amide bind), then immunostained with anti-EGF antibody and a FITC-conjugated secondary antibody. We then imaged the substrate with fluorescence microscopy to see if the immobilization of EGF worked as hypothesized.

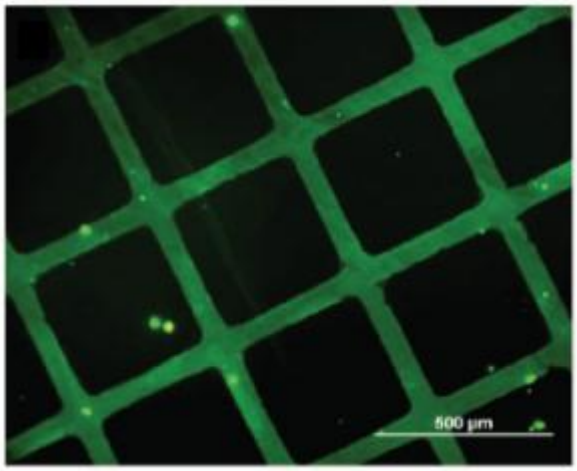

Figure 2.10: Fluorescence microscopy of microcontact printed EGF on surfaces functionalized with Pfp-ester (experiment performed by Dr. Xiaopei Deng)

As shown in Fig 2.10, the area where EGF was printed (the grid lines) was the only area to show fluorescence (besides occasional spots caused by non-specific binding of the secondary antibody). As immunofluorescence is relatively specific for the antibody being stained for, this is strong evidence that our EGF is tethered to our surface. Thus, we can claim that our substrates have been successfully functionalized with two independent reactive groups that can tether biofunctional molecules independently of each other.

We then evaluated the immobilization of cRGD via click reaction and assessed peptide activity in the presence of immobilized growth factor. The RGD tripeptide is a well-studied cell adhesion motif present in many proteins, but perhaps most prominently in extracellular matrix (ECM) molecules, such as fibronectin and vitronectin (among others)[96]. RGD (and other small peptide adhesion

molecules) have been widely explored for use in tissue engineering and presents several advantages over full-length proteins such as fibronectin (as discussed previously)[97]. A cRGD peptide was employed in this study. The major advantages of these cyclic peptides are automatable synthesis, resistance against proteolysis, weak immunogenicity, high specificity to integrin $\alpha_v\beta_3$, and enhanced biological activity (up to 240 times of linear analogues)[98].

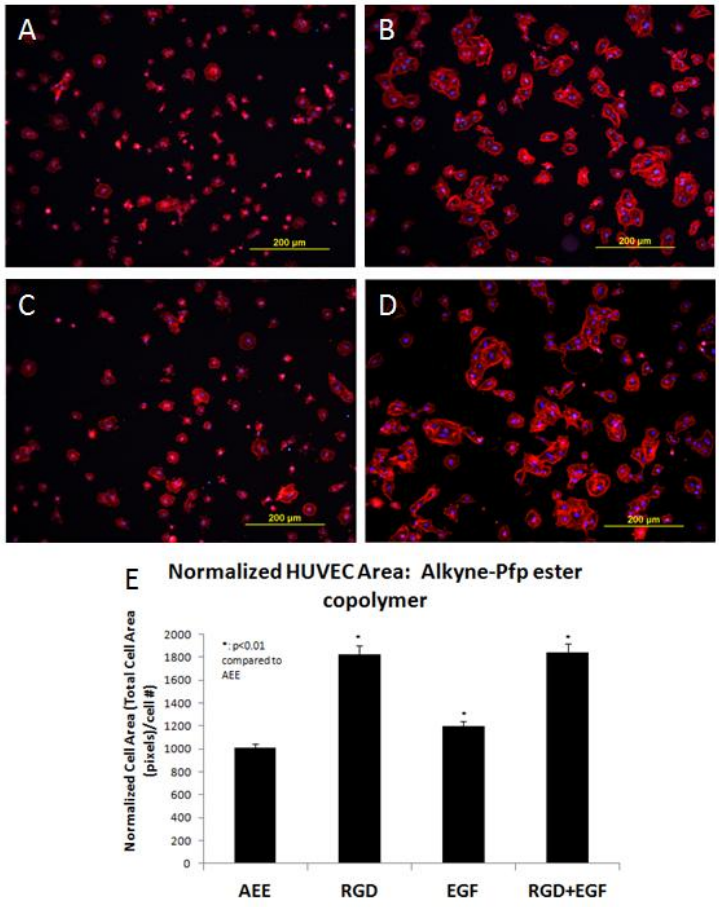

Figure 2.11: Fluorescence micrographs of HUVEC line seeded onto modified surfaces of polymer **3** after 4 h incubation. The surfaces were tethered with: (a) AEE, (b) cRGD-only, (c) EGF-only, (d) cRGD + EGF. (e) Quantification of spreading by ImageJ (three trials combined).

Human umbilical vein endothelial cells (HUVEC) spreading on polymer **3** surfaces with different treatments was shown in Fig. 2.11. The surfaces were passivated with 2-(2-aminoethoxy) ethanol (AEE), immobilized only with cRGD, only with EGF or with both biomolecules, respectively[99].

HUVEC spreading is significantly enhanced by the presence of cRGD (Fig. 2.11). The cell area on the surface with both cRGD and EGF was approximately the same as the one with only cRGD. The surface immobilized only with EGF only had a slight increase in cell area. The observance that EGF did not have any obvious effect on HUVECs is consistent with other studies showing the absence of EGFR expression in normal HUVECs[85].

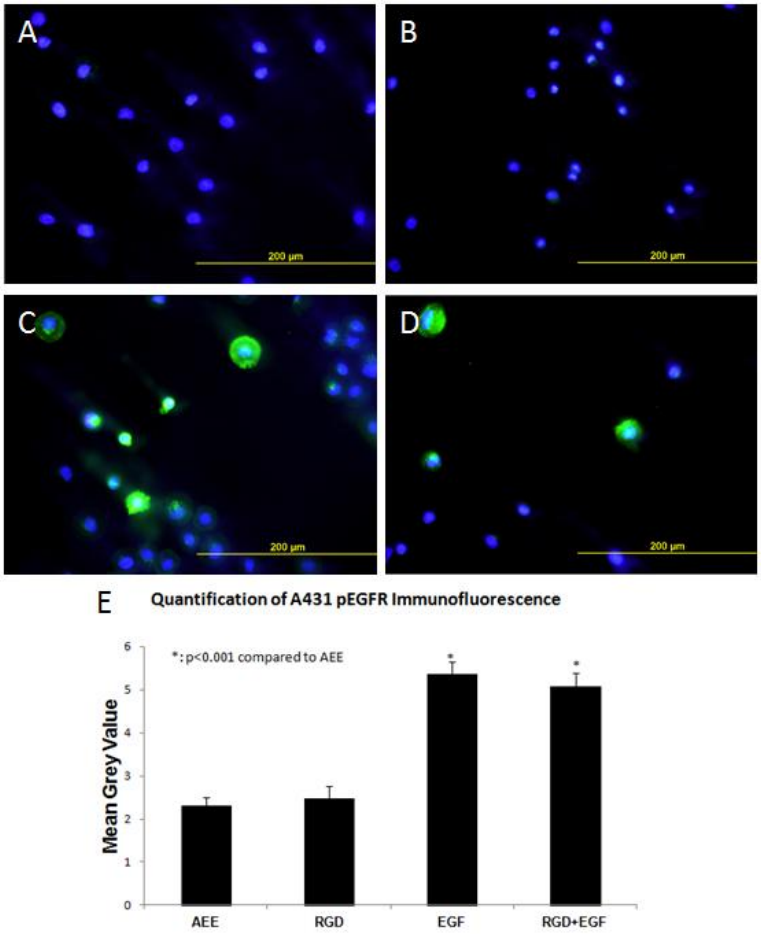

Figure 2.12: Immunofluorescence of phosphorylated EGFR in A431 cells cultured on CVD-coated surfaces with tethered (a) AEE, (b) cRGD, (c) EGF, and (D) cRGD+EGF. (e) Quantification of pEGFR immunofluorescence (three trials combined).

Tethering growth factors has gained more interest from the scientific community within the last three decades[100]. Studies showed that the immobilized growth factors, compared to the soluble ones,

had higher mitogenic effect, longer-term signal transduction and were resistant to endocytosis, degradation and diffusion [82]. In order to verify that the immobilized EGF still has biological activity, we investigated our modified surfaces' ability to induce phosphorylation of EGFR (pEGFR), the receptor of EGF. The A431 line is a human epidermal carcinoma and a well-characterized positive control for EGFR activity[101]. A431 cells overexpress EGFR roughly 10–50-fold over many other cell lines, and thus are an ideal cell type for examining the bioactivity of tethered EGF [86]. Surfaces with tethered EGF successfully induce phosphorylation of EGFR in serum-starved A431 cells, as observed using immunofluorescence (Fig. 2.12). This shows that the immobilized EGF on polymer **3** maintained its biological activity. Surfaces exhibiting both the adhesion factor cRGD and EGF show statistically similar ($p < 0.001$, with data from all three trials combined) pEGFR phosphorylation compared to those exhibiting EGF alone, demonstrating that multiple biofactors do not affect this particular growth factor's ability to interact with its receptor. We next examined A431 EGFR phosphorylation in response to soluble EGF and compared it to tethered EGF (Fig. 2.13). Various literature indicate that A431 respond to EGF with EC_{50} values of 12.1 ng mL^{-1} and 20 ng mL^{-1}, respectively [102, 103]. From four independent trials, an average EC_{50} value was 14.8 ng mL^{-1} ± 3.02 ng mL^{-1} (standard error), well matching the reported literature values previously cited. In all four trials, EGFR phosphorylation of tethered EGF as measured by quantification of immunofluorescence was either statistically equivalent to or higher ($p < 0.05$) than the highest concentration of soluble EGF tested (1000 ng mL^{-1}), demonstrating the potency of tethered EGF.

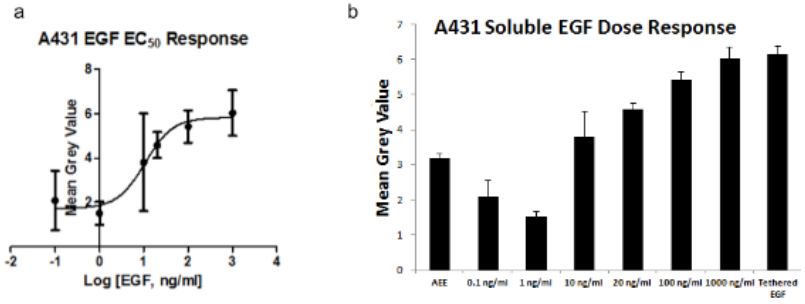

Figure 2.13: (a) EC_{50} plot for EGF (individual trial); (b) Quantification of pEGFR immunfluorescence of phosphorylated EGFR in A431 cells in bar graph form (individual trial). The cells were cultured on CVD-coated surfaces passivated with AEE and in media with soluble EGF from 0-1000 ng/ml, in comparison with surface with tethered EGF in soluble EGF-free media.

Primary HUVECs (harvested at the University of Michigan from umbilical cords by a collaborator) were next cultured on pyridinophane-derived surfaces, with n-PPX and n-PPX-alkyne surfaces as controls (Fig. 2.14).

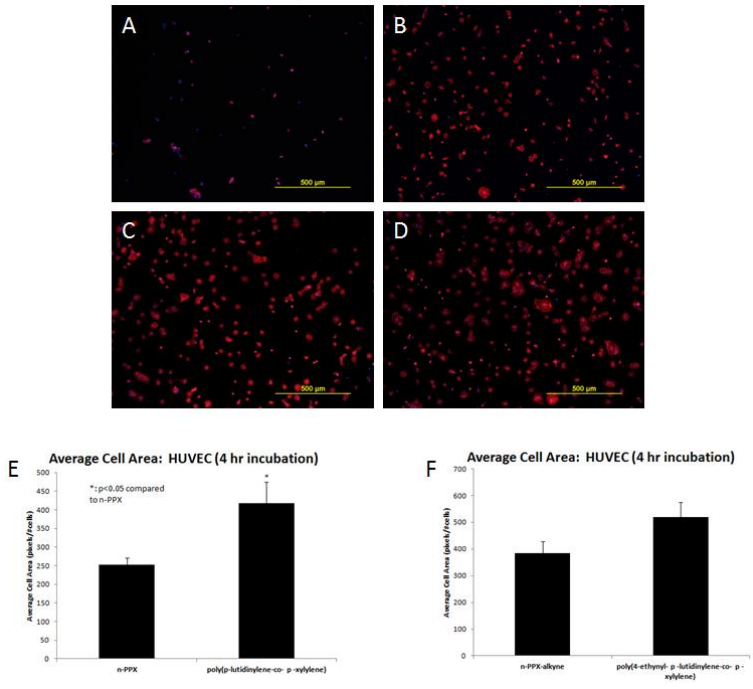

Figure 2.14: Fluorescence microscopy of HUVECs cultured for four hours sans serum and stained with phalloidin/DAPI on (a) n-PPX, (b) n-PPX-alkyne, (c) poly(*p*-lutidinylene-co-*p* -xylylene) and (d) poly(4-ethynyl- *p* -lutidinylene-co-*p*-xylylene). Average cell areas on (e) non-functionalized substrates and (f) alkyne-functionalized substrates

HUVECs spread out significantly better on n-PPX functionalized with alkyne, (poly(*p*-lutidinylene-co *p*-xylylene), and poly(4-ethynyl-*p*-lutidinylene-co-*p*-xylylene). Thus, the pyridinophane-based substrates showed a marked enhancement over n-PPX with respect to cell spreading - there was also no difference in cell spreading between (*p*-lutidinylene-co-*p*-xylylene) and poly(4-ethynyl-*p*-lutidinylene-co-*p*-xylylene). However, HUVECs grown on poly(4-ethynyl-*p*-lutidinylene-co-*p*-xylylene) did not spread significantly less than those on n-PPX-alkyne. We next looked at the average number of cells per surface by taking three images of each substrate, counting the number of cells individually, and then adding those three numbers to get a 'total' count based on three representative images. These were then averaged with other substrates with the same surfaces across three trials (for n = 9), and compared via Student's t-test (Fig. 2.15):

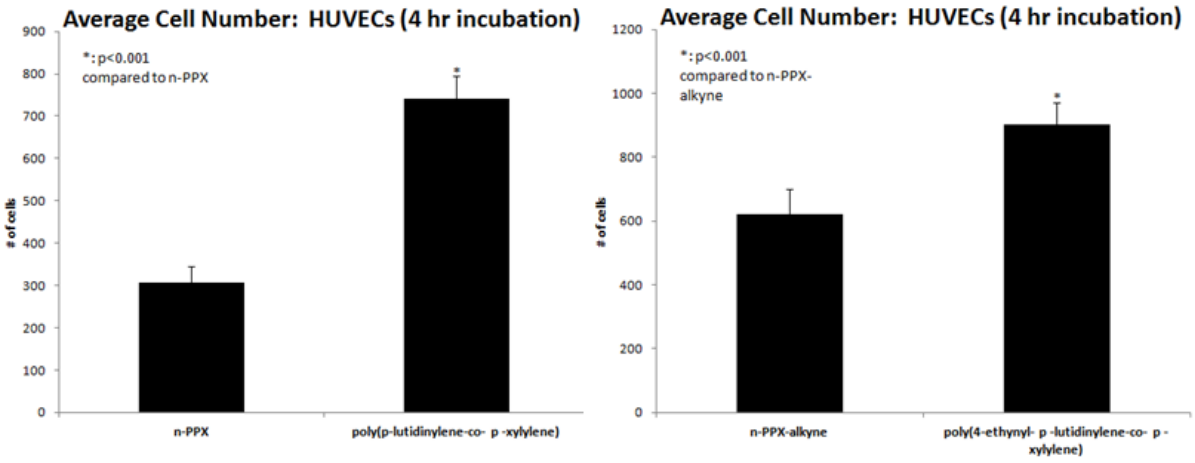

Figure 2.15: Quantification of the number of cells for three images taken per substrate and averaged (three trials combined) for both non-functionalized and alkyne-functionalized substrates

Once again, the hypothesis bears out as pyridinophane-based substrates show a far higher number of HUVECs attached over paracyclophane-based substrates. In this case, the functionalization of the polymer with ethylene has no effect on the enhancement to cell attachment with respect to the polymer backbone.

Conclusions and Future Work

In this chapter, we have successfully bound two different ligands (an azido-cyclic RGD and EGF) onto a surface with a controlled ratio of reactive groups. Furthermore, we demonstrated that these ligands remained potent biologically by culturing surfaces that featured them with two model cell lines (HUVEC and A431). We also demonstrated that the individual tethered biomolecules did not interfere with one another – RGD induced HUVECs to spread just as much whether or not EGF was present, and A431 EGF receptors showed the same amount of phosphorylation regardless of the presence or absence of RGD. This is an important result, as it demonstrates the true bioorthogonality of these reactions and the resulting immobilized biomolecules influence cell behavior independently. However, no real synergistic interaction between the two ligands was observed with either cell line, though by casual observation it appears that A431 cells actually show some inhibited spreading on surfaces coated with RGD and EGF in comparison to cells grown on EGF only. However, this was not formally measured and quantified, and did not affect the measurement of EGFR phosphorylation via ImageJ analysis, which is normalized to cell area. Shahal et al. observed that high concentrations of EGF co-immobilized with RGD on surfaces leads to A431 detachment[104]. This could potentially explain this observation – though we never measured the density of EGF or RGD on our surfaces, we know that the amount of bound EGF is likely high as the resulting EGFR phosphorylation is similar to that observed with soluble EGF at 1000 ng/ml.

Clearly, there are drawbacks to the strategies used above. While Pfp-ester is an excellent functional group for constructing polypeptides and binding proteins to a surface, it is indiscriminate in how it binds proteins featuring multiple primary amines. This means it may bind proteins in an unfavorable confirmation. Even if a protein only has a terminal primary amine and no others, it is possible that this amine plays a role in how the protein functions with its receptor or another protein, making Pfp-ester a poor functional group for tethering it. However, the functional group could

instead be biotin– then a protein could be biotintylated at a point where if it interacts with streptavidin it will be in an ideal confirmation. Of course, this means biotintylating every protein one wants to put on a surface, which would require some synthetic chemistry beforehand (whereas immobilizing via Pfp-ester requires no such modifications). Another strategy could be to copolymerize an aldehyde-functionalized paracyclophane over a Pfp-ester, then tether heparin to the surface via a carbohydrazide linker. Many proteins associate non-covalently with heparin, and would thus likely bind to the surface with a favorable conformation[81]. In fact, this strategy has also been studied by a colleague, and will hopefully pave a way forward for binding some growth factors (such as VEGF) that currently do not show much activity on our surfaces when tethered via Pfp-ester (data not shown) [81]. Furthermore, PPX films are not biodegradable, which could present problems for certain biomedical applications.

We have also demonstrated how altering even one atom (in this case, exchanging a carbon atom on a benzyl ring in paracylcophane for a nitrogen atom to create pyridinophane) can radically change how cells behave on our surface. We hypothesize that this effect is due to the presence of a partial charge on the surface, but this needs to be confirmed with zeta-potential measurements. Nevertheless, we can create a surface that attracts and adheres cells even in media which has no serum proteins present to pre-adsorb onto the surface. We also have already functionalized this new CVD precursor with an alkyne group (poly(4-ethynyl-*p*-lutidinylene-co-*p*-xylylene)) – thus, we hypothesize that after patterned atomic transfer radical polymerization of poly(ethylene glycol), HUVECs will only grow in areas where PEG is not present. This would demonstrate that the coating remains reactive after CVD and can be used to create surfaces that are selective for cell adhesion. If this is true, then we can generate coatings with all the listed advantages of CVD (including reactive functional groups which can then be modified orthogonally with further factors)

which cells tightly bind to and spread on without any sort of biological modification (such as attaching a cyclic adhesion peptide, or fibronectin, etc).

References

1. Puchkov, E.O. Computer image analysis of microbial colonies. *Microbiology*+ **79**, 141-146 (2010).
2. Freshney, R.I. Culture of animal cells : a manual of basic technique, Edn. 5th. (Wiley-Liss, Hoboken, N.J.; 2005).
3. Mann, B.K., Schmedlen, R.H. & West, J.L. Tethered-TGF-beta increases extracellular matrix production of vascular smooth muscle cells. *Biomaterials* **22**, 439-444 (2001).
4. Tirrell, M., Kokkoli, E. & Biesalski, M. The role of surface science in bioengineered materials. *Surf Sci* **500**, 61-83 (2002).
5. Wang, D.A. et al. In situ immobilization of proteins and RGD peptide on polyurethane surfaces via poly(ethylene oxide) coupling polymers for human endothelial cell growth. *Biomacromolecules* **3**, 1286-1295 (2002).
6. Nicodemus, G.D. & Bryant, S.J. Cell encapsulation in biodegradable hydrogels for tissue engineering applications. *Tissue engineering. Part B, Reviews* **14**, 149-165 (2008).
7. Yamazoe, H., Okuyama, T., Suzuki, H. & Fukuda, J. Fabrication of patterned cell co-cultures on albumin-based substrate: applications for microfluidic devices. *Acta biomaterialia* **6**, 526-533 (2010).
8. Sutherland, D.S., Forshaw, P.D., Allen, G.C., Brown, I.T. & Williams, K.R. Surface analysis of titanium implants. *Biomaterials* **14**, 893-899 (1993).
9. Esposito, M., Lausmaa, J., Hirsch, J.M. & Thomsen, P. Surface analysis of failed oral titanium implants. *Journal of biomedical materials research* **48**, 559-568 (1999).
10. Hauser, J. et al. Plasma mediated collagen-I-coating of metal implant materials to improve biocompatibility. *J Biomed Mater Res A* **94**, 19-26 (2010).
11. Deng, X., Eyster, T.W., Elkasabi, Y. & Lahann, J. Bio-orthogonal polymer coatings for co-presentation of biomolecules. *Macromolecular rapid communications* **33**, 640-645 (2012).
12. Kallrot, M., Edlund, U. & Albertsson, A.C. Surface functionalization of degradable polymers by covalent grafting. *Biomaterials* **27**, 1788-1796 (2006).
13. Schlosser, M. et al. Immunogenicity of polymeric implants: Long-term antibody response against polyester (Dacron) following the implantation of vascular prostheses into LEW.1A rats. *Journal of biomedical materials research* **61**, 450-457 (2002).
14. Xie, Y.C. & Yang, Q.F. Surface modification of poly(vinyl chloride) for antithrombogenicity study. *J Appl Polym Sci* **85**, 1013-1018 (2002).
15. Babapulle, M.N. & Eisenberg, M.J. Coated stents for the prevention of restenosis: Part I. *Circulation* **106**, 2734-2740 (2002).
16. Medintz, I.L. et al. General strategy for biosensor design and construction employing multifunctional surface-tethered components. *Analytical chemistry* **76**, 5620-5629 (2004).
17. Linford, M.R. & Chidsey, C.E.D. Alkyl Monolayers Covalently Bonded to Silicon Surfaces. *Journal of the American Chemical Society* **115**, 12631-12632 (1993).
18. Love, J.C., Estroff, L.A., Kriebel, J.K., Nuzzo, R.G. & Whitesides, G.M. Self-assembled monolayers of thiolates on metals as a form of nanotechnology. *Chem Rev* **105**, 1103-1169 (2005).

19. Lopez, G.P. et al. Convenient Methods for Patterning the Adhesion of Mammalian-Cells to Surfaces Using Self-Assembled Monolayers of Alkanethiolates on Gold. *Journal of the American Chemical Society* **115**, 5877-5878 (1993).
20. Onclin, S., Ravoo, B.J. & Reinhoudt, D.N. Engineering silicon oxide surfaces using self-assembled monolayers. *Angew Chem Int Edit* **44**, 6282-6304 (2005).
21. Lahann, J. et al. Reactive polymer coatings: A platform for patterning proteins and mammalian cells onto a broad range of materials. *Langmuir : the ACS journal of surfaces and colloids* **18**, 3632-3638 (2002).
22. Liu, S.X., Kim, J.T. & Kim, S. Effect of polymer surface modification on polymer-protein interaction via hydrophilic polymer grafting. *J Food Sci* **73**, E143-E150 (2008).
23. Villa-Diaz, L.G. et al. Synthetic polymer coatings for long-term growth of human embryonic stem cells. *Nature biotechnology* **28**, 581-583 (2010).
24. Asano, M. et al. Novel UV-induced photografting process for preparing poly(tetrafluoroethylene)-based proton-conducting membranes. *J Polym Sci Pol Chem* **45**, 2624-2637 (2007).
25. Sachlos, E. & Czernuszka, J.T. Making tissue engineering scaffolds work. Review: the application of solid freeform fabrication technology to the production of tissue engineering scaffolds. *European cells & materials* **5**, 29-39; discussion 39-40 (2003).
26. Ginty, P.J., Barry, J.J.A., White, L.J., Howdle, S.M. & Shakesheff, K.M. Controlling protein release from scaffolds using polymer blends and composites. *Eur J Pharm Biopharm* **68**, 82-89 (2008).
27. Deleeuw, D.M., Kraakman, P.A., Bongaerts, P.E.G., Mutsaers, C.M.J. & Klaassen, D.B.M. Electroplating of Conductive Polymers for the Metallization of Insulators. *Synthetic Met* **66**, 263-273 (1994).
28. Tang, Z.Y., Wang, Y., Podsiadlo, P. & Kotov, N.A. Biomedical applications of layer-by-layer assembly: From biomimetics to tissue engineering. *Advanced Materials* **18**, 3203-3224 (2006).
29. Baker, S.M., Leach, K.A., Devereaux, C.E. & Gragson, D.E. Controlled patterning of diblock copolymers by monolayer Langmuir-Blodgett deposition. *Macromolecules* **33**, 5432-5436 (2000).
30. Lu, Y.J., Meng, X., Yi, G.W. & Jia, J.H. In situ growth of CuS thin films on functionalized self-assembled monolayers using chemical bath deposition. *J Colloid Interf Sci* **356**, 726-733 (2011).
31. Choy, K.L. Chemical vapour deposition of coatings. *Prog Mater Sci* **48**, 57-170 (2003).
32. Faltermeier, C.G. et al. The effects of processing parameters in the low-temperature chemical vapor deposition of titanium nitride from tetraiodotitanium. *J Electrochem Soc* **145**, 676-683 (1998).
33. Cohen, S.L., Liehr, M. & Kasi, S. Mechanisms of Copper Chemical Vapor-Deposition. *Appl Phys Lett* **60**, 50-52 (1992).
34. Yun, J.H., Kim, B.Y. & Rhee, S.W. Metal-organic chemical vapor deposition of aluminum from dimethylethylamine alane. *Thin Solid Films* **312**, 259-264 (1998).
35. Lahann, J. Vapor-based polymer coatings for potential biomedical applications. *Polym Int* **55**, 1361-1370 (2006).
36. Gorham, W.F. A New General Synthetic Method for Preparation of Linear Poly-P-Xylylenes. *J Polym Sci A1* **4**, 3027-& (1966).
37. Hopf, H. [2.2]Paracyclophanes in Polymer Chemistry and Materials Science. *Angew Chem Int Edit* **47**, 9808-9812 (2008).
38. Noh, H.S., Hesketh, P.J. & Frye-Mason, G.C. Parylene gas chromatographic column for rapid thermal cycling. *J Microelectromech S* **11**, 718-725 (2002).

39. Sasaki, H., Onoe, H., Osaki, T., Kawano, R. & Takeuchi, S. Parylene-coating in PDMS microfluidic channels prevents the absorption of fluorescent dyes. *Sensor Actuat B-Chem* **150**, 478-482 (2010).
40. Lahann, J. et al. Reactive polymer coatings: A first step toward surface engineering of microfluidic devices. *Analytical chemistry* **75**, 2117-2122 (2003).
41. Lahann, J. & Langer, R. Novel poly(p-xylylenes): Thin films with tailored chemical and optical properties. *Macromolecules* **35**, 4380-4386 (2002).
42. Elkasabi, Y., Chen, H.Y. & Lahann, J. Multipotent polymer coatings based on chemical vapor deposition copolymerization. *Advanced Materials* **18**, 1521-+ (2006).
43. Lahann, J., Klee, D., Pluester, W. & Hoecker, H. Bioactive immobilization of r-hirudin on CVD-coated metallic implant devices. *Biomaterials* **22**, 817-826 (2001).
44. Elkasabi, Y., Yoshida, M., Nandivada, H., Chen, H.Y. & Lahann, J. Towards multipotent coatings: Chemical vapor deposition and biofunctionalization of carbonyl-substituted copolymers. *Macromolecular rapid communications* **29**, 855-870 (2008).
45. Chen, C.S., Mrksich, M., Huang, S., Whitesides, G.M. & Ingber, D.E. Geometric control of cell life and death. *Science* **276**, 1425-1428 (1997).
46. Peehl, D.M. & Stanbridge, E.J. Anchorage-independent growth of normal human fibroblasts. *Proceedings of the National Academy of Sciences of the United States of America* **78**, 3053-3057 (1981).
47. Chan, B.P. & Leong, K.W. Scaffolding in tissue engineering: general approaches and tissue-specific considerations. *European spine journal : official publication of the European Spine Society, the European Spinal Deformity Society, and the European Section of the Cervical Spine Research Society* **17 Suppl 4**, 467-479 (2008).
48. Thery, M., Pepin, A., Dressaire, E., Chen, Y. & Bornens, M. Cell distribution of stress fibres in response to the geometry of the adhesive environment. *Cell Motil Cytoskel* **63**, 341-355 (2006).
49. Kantlehner, M. et al. Surface coating with cyclic RGD peptides stimulates osteoblast adhesion and proliferation as well as bone formation. *Chembiochem : a European journal of chemical biology* **1**, 107-114 (2000).
50. Alberts, B. Molecular biology of the cell, Edn. 4th. (Garland Science, New York; 2002).
51. Ruoslahti, E. RGD and other recognition sequences for integrins. *Annual review of cell and developmental biology* **12**, 697-715 (1996).
52. Stupack, D.G. & Cheresh, D.A. Get a ligand, get a life: integrins, signaling and cell survival. *J Cell Sci* **115**, 3729-3738 (2002).
53. Vachon, P.H. Integrin signaling, cell survival, and anoikis: distinctions, differences, and differentiation. *Journal of signal transduction* **2011**, 738137 (2011).
54. Hubbell, J.A., Massia, S.P., Desai, N.P. & Drumheller, P.D. Endothelial cell-selective materials for tissue engineering in the vascular graft via a new receptor. *Biotechnology (N Y)* **9**, 568-572 (1991).
55. Mandal, S., Bhaskar, S. & Lahann, J. Micropatterned Fiber Scaffolds for Spatially Controlled Cell Adhesion. *Macromolecular rapid communications* **30**, 1638-1644 (2009).
56. Comisar, W.A., Kazmers, N.H., Mooney, D.J. & Linderman, J.J. Engineering RGD nanopatterned hydrogels to control preosteoblast behavior: A combined computational and experimental approach. *Biomaterials* **28**, 4409-4417 (2007).
57. Ogiwara, K., Nagaoka, M., Cho, C.S. & Akaike, T. Effect of photo-immobilization of epidermal growth factor on the cellular behaviors. *Biochemical and biophysical research communications* **345**, 255-259 (2006).

58. Choi, J.S., Leong, K.W. & Yoo, H.S. In vivo wound healing of diabetic ulcers using electrospun nanofibers immobilized with human epidermal growth factor (EGF). *Biomaterials* **29**, 587-596 (2008).
59. Ito, Y. Covalently immobilized biosignal molecule materials for tissue engineering. *Soft Matter* **4**, 46-56 (2008).
60. Chen, G., Ito, Y. & Imanishi, Y. Photo-immobilization of epidermal growth factor enhances its mitogenic effect by artificial juxtacrine signaling. *Biochimica et biophysica acta* **1358**, 200-208 (1997).
61. Ito, Y., Inoue, M., Liu, S.Q. & Imanishi, Y. Cell-Growth on Immobilized Cell-Growth Factor .6. Enhancement of Fibroblast Cell-Growth by Immobilized Insulin and or Fibronectin. *Journal of biomedical materials research* **27**, 901-907 (1993).
62. Hermanson, G.T. & ScienceDirect (Online service) Bioconjugate techniques, Edn. 2nd. (Elsevier Academic Press, Amsterdam ; Boston; 2008).
63. Kalia, J. & Raines, R.T. Advances in Bioconjugation. *Current organic chemistry* **14**, 138-147 (2010).
64. Lee, K.B., Kim, D.J., Lee, Z.W., Woo, S.I. & Choi, I.S. Pattern generation of biological ligands on a biodegradable poly(glycolic acid) film. *Langmuir : the ACS journal of surfaces and colloids* **20**, 2531-2535 (2004).
65. Nandivada, H., Jiang, X.W. & Lahann, J. Click chemistry: Versatility and control in the hands of materials scientists. *Advanced Materials* **19**, 2197-2208 (2007).
66. Kolb, H.C., Finn, M.G. & Sharpless, K.B. Click chemistry: Diverse chemical function from a few good reactions. *Angew Chem Int Edit* **40**, 2004-+ (2001).
67. Agard, N.J., Prescher, J.A. & Bertozzi, C.R. A strain-promoted [3+2] azide-alkyne cycloaddition for covalent modification of blomolecules in living systems. *Journal of the American Chemical Society* **126**, 15046-15047 (2004).
68. Huisgen, R. Kinetik Und Mechanismus 1.3-Dipolarer Cycloadditionen. *Angew Chem Int Edit* **75**, 742-& (1963).
69. Tron, G.C. et al. Click chemistry reactions in medicinal chemistry: Applications of the 1,3-dipolar cycloaddition between azides and alkynes. *Med Res Rev* **28**, 278-308 (2008).
70. Majireck, M.M. & Weinreb, S.M. A study of the scope and regioselectivity of the ruthenium-catalyzed [3+2]-cycloaddition of azides with internal alkynes. *J Org Chem* **71**, 8680-8683 (2006).
71. Speers, A.E., Adam, G.C. & Cravatt, B.F. Activity-based protein profiling in vivo using a copper(I)-catalyzed azide-alkyne [3+2] cycloaddition. *Journal of the American Chemical Society* **125**, 4686-4687 (2003).
72. Fournier, D., Hoogenboom, R. & Schubert, U.S. Clicking polymers: a straightforward approach to novel macromolecular architectures. *Chem Soc Rev* **36**, 1369-1380 (2007).
73. Xiao, J. & Tolbert, T.J. Synthesis of N-terminally linked protein dimers and trimers by a combined native chemical ligation-CuAAC click chemistry strategy. *Organic letters* **11**, 4144-4147 (2009).
74. Cao, B. et al. Concentration-dependent cytotoxicity of copper ions on mouse fibroblasts in vitro: effects of copper ion release from TCu380A vs TCu220C intra-uterine devices. *Biomedical microdevices* **14**, 709-720 (2012).
75. Baskin, J.M. et al. Copper-free click chemistry for dynamic in vivo imaging. *Proceedings of the National Academy of Sciences of the United States of America* **104**, 16793-16797 (2007).
76. van Berkel, S.S. et al. Application of metal-free triazole formation in the synthesis of cyclic RGD-DTPA conjugates. *Chembiochem : a European journal of chemical biology* **9**, 1805-1815 (2008).

77. Jaeger, J. & Reinitz, J. On the dynamic nature of positional information. *Bioessays* **28**, 1102-1111 (2006).
78. Castner, D.G. & Ratner, B.D. Biomedical surface science: Foundations to frontiers. *Surf Sci* **500**, 28-60 (2002).
79. Hirsh, S.L. et al. The Vroman effect: Competitive protein exchange with dynamic multilayer protein aggregates. *Colloid Surface B* **103**, 395-404 (2013).
80. Vroman, L., Adams, A.L., Fischer, G.C. & Munoz, P.C. Interaction of high molecular weight kininogen, factor XII, and fibrinogen in plasma at interfaces. *Blood* **55**, 156-159 (1980).
81. Deng, X. & Lahann, J. A generic strategy for co-presentation of heparin-binding growth factors based on CVD polymerization. *Macromolecular rapid communications* **33**, 1459-1465 (2012).
82. Kuhl, P.R. & GriffithCima, L.G. Tethered epidermal growth factor as a paradigm for growth factor-induced stimulation from the solid phase. *Nature medicine* **2**, 1022-1027 (1996).
83. Njieha, F.K. & Shalaby, S.W. Stabilization of Epidermal Growth-Factor. *J Bioact Compat Pol* **7**, 288-299 (1992).
84. Patel, P.R. et al. Synthesis and cell adhesive properties of linear and cyclic RGD functionalized polynorbornene thin films. *Biomacromolecules* **13**, 2546-2553 (2012).
85. Al-Nedawi, K., Meehan, B., Kerbel, R.S., Allison, A.C. & Rak, J. Endothelial expression of autocrine VEGF upon the uptake of tumor-derived microvesicles containing oncogenic EGFR. *Proceedings of the National Academy of Sciences of the United States of America* **106**, 3794-3799 (2009).
86. Ullrich, A. et al. Human epidermal growth factor receptor cDNA sequence and aberrant expression of the amplified gene in A431 epidermoid carcinoma cells. *Nature* **309**, 418-425 (1984).
87. Okano, T., Yamada, N., Okuhara, M., Sakai, H. & Sakurai, Y. Mechanism of cell detachment from temperature-modulated, hydrophilic-hydrophobic polymer surfaces. *Biomaterials* **16**, 297-303 (1995).
88. Kim, M.S. et al. Adhesion behavior of human bone marrow stromal cells on differentially wettable polymer surfaces. *Tissue engineering* **13**, 2095-2103 (2007).
89. van Wachem, P.B. et al. Interaction of cultured human endothelial cells with polymeric surfaces of different wettabilities. *Biomaterials* **6**, 403-408 (1985).
90. Lee, J.H., Lee, J.W., Khang, G. & Lee, H.B. Interaction of cells on chargeable functional group gradient surfaces. *Biomaterials* **18**, 351-358 (1997).
91. Cooper, G.M. The cell : a molecular approach, Edn. 2nd. (ASM Press ;Sinauer Associates, Washington, D.C.Sunderland, Mass.; 2000).
92. Lu, H., Guo, L., Kawazoe, N., Tateishi, T. & Chen, G. Effects of poly(L-lysine), poly(acrylic acid) and poly(ethylene glycol) on the adhesion, proliferation and chondrogenic differentiation of human mesenchymal stem cells. *Journal of biomaterials science. Polymer edition* **20**, 577-589 (2009).
93. Lee, J.H., Jung, H.W., Kang, I.K. & Lee, H.B. Cell Behavior on Polymer Surfaces with Different Functional-Groups. *Biomaterials* **15**, 705-711 (1994).
94. Nandivada, H., Chen, H.Y., Bondarenko, L. & Lahann, J. Reactive polymer coatings that "click"". *Angew Chem Int Edit* **45**, 3360-3363 (2006).
95. Chen, H.Y. & Lahann, J. Vapor-assisted micropatterning in replica structures: A solventless approach towards topologically and chemically designable surfaces. *Advanced Materials* **19**, 3801-+ (2007).

96. Ruoslahti, E. & Pierschbacher, M.D. New Perspectives in Cell-Adhesion - Rgd and Integrins. *Science* **238**, 491-497 (1987).
97. Shakesheff, K.M., Cannizzaro, S.M. & Langer, R. Creating biomimetic micro-environments with synthetic polymer-peptide hybrid molecules. *J Biomat Sci-Polym E* **9**, 507-518 (1998).
98. Haubner, R. et al. Structural and functional aspects of RGD-containing cyclic pentapeptides as highly potent and selective integrin alpha(v)beta(3) antagonists. *Journal of the American Chemical Society* **118**, 7461-7472 (1996).
99. Lahann, J., Choi, I.S., Lee, J., Jenson, K.F. & Langer, R. A new method toward microengineered surfaces based on reactive coating. *Angew Chem Int Edit* **40**, 3166-+ (2001).
100. Liberelle, B. et al. Impact of epidermal growth factor tethering strategy on cellular response. *Bioconjugate chemistry* **21**, 2257-2266 (2010).
101. Rubin Grandis, J. et al. Levels of TGF-alpha and EGFR protein in head and neck squamous cell carcinoma and patient survival. *Journal of the National Cancer Institute* **90**, 824-832 (1998).
102. Westover, E.J., Covey, D.F., Brockman, H.L., Brown, R.E. & Pike, L.J. Cholesterol depletion results in site-specific increases in epidermal growth factor receptor phosphorylation due to membrane level effects - Studies with cholesterol enantiomers. *J Biol Chem* **278**, 51125-51133 (2003).
103. Waddleton, D., Ramachandran, C. & Wang, Q. Development of a time-resolved fluorescent assay for measuring tyrosine-phosphorylated proteins in cells. *Analytical biochemistry* **309**, 150-157 (2002).
104. Shahal, T., Geiger, B., Dunlop, I.E. & Spatz, J.P. Regulation of integrin adhesions by varying the density of substrate-bound epidermal growth factor. *Biointerphases* **7**, 23 (2012).

CHAPTER 3

Human Mesenchymal Stem Cell Culture on PMEDSAH Modified Substrates

Overview

In this chapter, we characterize the behavior of mesenchymal stem cells on the zwitterionic hydrogel poly[2-(methacryloyloxy)ethyl dimethyl-(3-sulfopropyl)ammonium hydroxide] (PMEDSAH), previously shown to maintain embryonic stem cells and prevent spontaneous differentiation. We deposited this hydrogel onto polystyrene using both thermal grafting and atom transfer radical polymerization (ATRP) respectively, and examined mesenchymal stem cell morphology, proliferation, and characteristic markers after culture on these surfaces. Embryonic stem cells are normally cultured on feeder layers or substrates with adsorbed or tethered biomolecules – when these are differentiated into a mesenchymal-like stem cell, they are transferred and cultured on a different substrate. With PMEDSAH, we wish to create a universal substrate for stem cell culture and differentiation, obviating the need for feeder cells or expensive substrates featuring attached peptides. In the **Introduction and Background**, we discuss the biology and clinical relevance of both embryonic and mesenchymal stem cells, along with current substrates used to culture and maintain them. We focus specifically on the disadvantages of feeder cells and current alternatives available. We also briefly review ATRP and the characteristics of PMEDSAH hydrogels generated by it. We next demonstrate how mesenchymal stem cells, like embryonic stem cells, can be grown and maintained on PMEDSAH. Thermally grafted PMEDSAH leads to lower proliferation rates of mesenchymal stem cells in comparison to that of ATRP deposited PMEDSAH. However, both maintained the characteristic markers that define mesenchymal stem cells.

Introduction and Background – Stem Cells and their Maintenance on Artificial Substrates

Human stem cells, with their ability to generate nearly any type of cell found in the body, have ushered a revolution in biology and medicine, offering a possibly infinite renewable source of differentiated cells. While an obvious use for these cells could be in repairing diseased or injured tissues in patients, stem cells could also serve as a reservoir for *in vitro* cell models that were previously difficult to obtain in large quantities (such as human cardiomyocytes, or non-cancerous neural cells)[1, 2]. Some have even called embryonic stem cells' pluripotency a sort of biological alchemy[3]. Stem cells essentially can do three things: die, self-renew (i.e. proliferate as stem cells), and differentiate down tissue lineages towards functional tissues[3].

Initially isolated human embryonic stem cells (hESCs) were cultured on a mouse embryonic fibroblast feeder layer, or MEF[4-7]. These feeder cells prevent hESCs from spontaneously differentiating while in culture (important for maintaining and expanding stocks of pluripotent cells)[4, 7]. The feeder layer cells are thought to provide essential nutrients, growth factors, cytokines, and extracellular matrix proteins in order to support the hESCs, along with inducing a signaling cascade which prevents them from differentiating[8]. Activin A, basic fibroblastic growth factor (bFGF), and transformation growth factor beta (TGFβ) are among the many known proteins which play a critical role in maintaining hESC pluripotency – but while there have been many studies of the proteins produced by feeder cells, the precise mechanisms behind feeder cell maintenance remain unclear[8, 9]. Concerns rapidly arose regarding the safety behind this xenogenic cell culture, particularly with the risk of pathogenic transmission or biological factors that could provoke an immunogenic response (Villa-Diaz et al. cites animal-derived sialic acid as a major concern)[10]. Furthermore, fundamental studies of hESC biology are hampered by ill-defined substrates that can vary from batch-to-batch – their impact on the results obtained can be difficult at best to gauge[10].

Engineers and scientists began to develop methods and strategies for culturing hESCs without using a MEF feeder layer, or even any feeder layer. In an attempt to not use any feeder cells directly with hESC culture, Xu et al. coated dishes with Matrigel and conditioned their growth media with MEFs (in other words, the growth media was first incubated with MEFs so their soluble factors could enter into it, collected, supplemented with a further 4 ng/ml of bFGF, and fed to the hESCs)[11]. While this method worked (hESCs showed all the characteristics of remaining pluripotent for multiple passages, along with typical karyotype), it remains xenogenic and thus the raised concerns are not alleviated[11]. Matrigel itself is derived from tumors grown in mice, and is composed of a variety of ECM proteins and some growth factors[12].

As a result, more completely artificial environments were engineered. One of the most successful was poly[2-(methacryloyloxy)ethyl dimethyl-(3-sulfopropyl)ammonium hydroxide], or PMEDSAH. This zwitterionic polymer was one of six derivatives of poly(methyl methacrylate) tested by Villa-Diaz and Nandivada et al. –most (such as poly[[2-(methacryloyloxy)ethyl]trimethyl ammonium chloride]) (PMETAC) and poly[3-sulfopropyl methacrylate] (PSPMA)) led to spontaneous differentiation after hESCs were cultured on them (Fig. 3.1)[13]. All six polymers were coated onto TCPS by thermal grafting, in which TCPS was exposed to UV irradiation to generate ozones on the polystyrene, which could then react with a solution of the monomer plus heat to form covalently-linked polymer chains[13]. The polymers were picked systematically – PSPMA had the sulfate group of PMEDSAH, while PMETAC had the quaternary amine[13]. Nevertheless, only the two functional groups together on the same polymer led to hESC maintenance. Of the two zwitterions tested - PMEDSAH and poly[carboxybetaine methacrylate]- only PMEDSAH allowed hESCs to adhere[13]. Hydrophilicity and elastic modulus were correlated to successful hESC culture, as PMEDSAH had respectively the highest and the lowest of all the polymers tested[13].

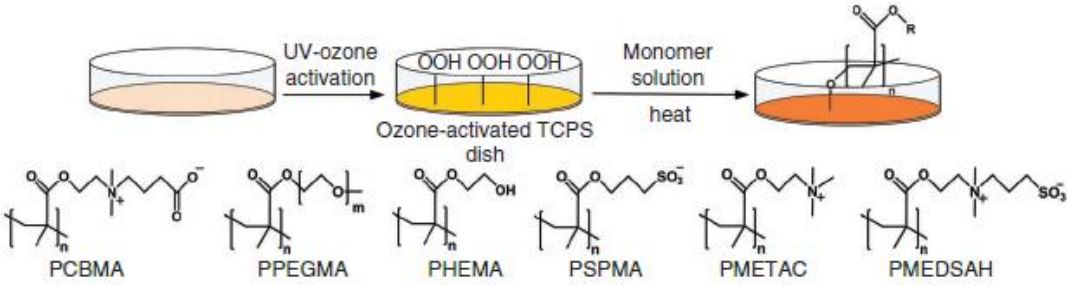

Figure 3.1: The process of thermal grafting after UV-ozone treatement, and the six different polymers grafted to TCPS for testing hESC maintenance (Nandivada and Villa-Diaz et al. with permission)[13]

hESCs were confirmed to remain pluripotent and phenotypically normal through the standard testing methodology (staining for pluripotent markers, karyotyping, differentiation down the three germ lines, etc) for up to 25 passsagings[13]. It has been hypothesized that hESC behavior on PMEDSAH is due to PMEDSAH mimicking the properties of the natural carbohydrate heparin through its charged functional groups[10]. Heparin strongly binds bFGF and has even been found to be necessary for bFGF to signal to cells through its receptor[14]. bFGF in turn is known to be essential for hESCs to maintain their undifferentiated state; even hESCs cultured with MEFs still need their media supplemented with bFGF in order to thrive and maintain pluripotency, highlighting the importance of this growth factor[15].

Other groups have attempted to directly bind heparin for xenogenic-free culture of hESCs[16]. Kolhar et al. cultured hESCs on a cyclic disulphide-bridged CRGDC functionalized substrate – compared to linear RGD, this peptide was able to also maintain hESCs, and they observed higher hESC adhesion[17]. However, this solution is not ideal in comparison to a grafted polymer, as small peptides are expensive (and are normally synthesized in small amounts) and these surfaces require

complicated chemistries (as in Kolhar et al.) or rely on non-covalent binding (such as seen by Klim et al.) [10, 16-18].

Other fully synthetic substrates have emerged which bind FGF and maintain hESC pluripotency. Chang et al. recently developed a variety of co-polymer hydrogels composed of various amounts of crosslinked monomers sodium 4-vinylbenenesulfonate and acrylamide – these were then polymerized to form polyacrylamide–co-poly(sodium-4-styrenesulfonate), or PAm_x-PSS_y (where x and y were varied depending on the desired mechanical properties and hydrophilicity)[19]. They had previously observed that the muscle progenitor cell line C2C12 grown in media with supplemented poly (sodium-4-styrenesulfonate) (PSS) had enhanced differentiation rates comparable to supplemented heparin, then proceeded to demonstrate through PAGE that bFGF binds to PSS [20]. Thus, they speculated that this polymer may support hESCs[19]. hESCs were able to maintain pluripotency for over 20 passages on the hydrogel Pam_6-PSS_2 with both MEF conditioned media and chemically defined media[19]. Yet again, it seems that an ability to bind bFGF and mimic heparin leads to a surface which can support hESCs, though this was not directly proven in this work. Interestingly, the group also noted that co-polymer hydrogels of polyacrylamide and PMEDSAH could not maintain hESCs[19]. As Villa-Diaz et al. note in their review of stem cell culture conditions, Irwin et al. are the only other group besides Villa-Diaz et al. (and now Chang et al.) who have developed a completely synthetic polymer that can maintain hESCs[10, 21]. In their work, hESCs are maintained on an amino-propylmethacrylamide (APMAAm) hydrogel, who's ability to adsorb BSA was critical for this result[21].

Mesenchymal Stem Cells

Mesenchymal stem cells (MSCs) are also able to differentiate down different lineages, though they are not as potent as embryonic stem cells (hence why they are often called 'multipotent' as opposed

to 'pluripotent'). These cells normally are thought to originate and reside in bone marrow and are often isolated from superior iliac crest marrow, though cells with similar properties have been isolated from many different other organs such as lungs, muscles, teeth, and even neural tissue in the brain [22-24]. The name 'mesenchymal' (where 'mesenchymal' itself refers to connective tissue originating from the mesodermal germ layer during embryogenesis) speaks to their general ability to differentiate down three major mesodermal lineages: osteogenic (bone), chondrogenic (cartilage), and adipogenic (fat) [25-27]. MSCs are often identified by the presence or absence of a list of markers. The International Society for Cellular Therapy recommended in 2006 that MSCs be identified based on the following: ability to adhere to a tissue culture substrate; positive expression of CD105, CD73, and CD90; negative expression of CD45, CD34 (a prime marker for another type of cell, the hematopoetic stem cell), CD14 or CD11b, CD79α or CD19, and HLA-DR; and the ability *in vitro* to differentiate down the three primary lineages (chondrogenesis, osteogenesis, and adiposgenesis)[28, 29]. They have also successfully been differentiated into other lineages, including cardiomyocytes, neural-like cells, and even hepatocytes [30-32]. When cultured *in vitro*, human mesenchymal stem cells (hMSCs) have a fibroblastic morphology – smaller hMSCs tend to be more multipotent than larger ones[33]. They are of interest to biologists who study skeletal development, tissue engineers interested in creating bone-like scaffolding, and even for use in personalized biosensors for diagnostics and medicine (a patient's own hMSCs can be isolated and examined with a variety of assays looking at toxicity or gene expression – with an eye towards then recommending treatments based on the results)[25, 27]. They also lack the ethical controversy (and resulting limitations and regulations) that surround hESC research and use in treatments[29].

hMSCs are normally differentiated down three main mesenchymal lineages – bone, cartilage, and fat. This is often done by adding a cocktail of growth factors, hormones, and small molecules along with altered culture conditions (such as pellet culture or elimination of serum)[29]. Osteoblasts, for

example, are created by the addition of dexamethasone (a steroid) and β-glycerophosphate to normal growth media (at final concentrations of 0.1 μM and 2 mM respectively), while hMSCs can be differentiated into adipocytes by the same amount of dexamethasone as used for osteoblastic differentiation, but also require 3-isobutyl-1-methylxanthine and indomethacin[34]. Cartilage is more difficult – it usually is done in pellet culture at extremely high densities of cells (250,000 cells/well in a 96-well plate is recommended by one protocol), and requires TGF-β, dexamethasone, ascorbic acid, sodium pyruvate, and ITS (insulin, transferring, and selenium) supplementation to serum-free media[35]. Differentiation of hMSCs can also be heavily influenced by their mechanical environment [36]. Engler et al. demonstrated that hMSCs grown on soft materials tended to go down a neurogenic differentiation pathway, those on stiffer materials became myogenic, and those on very stiff materials tended towards osteogenic differentiation – all incubated with the same media[36]. It is a common strategy in tissue engineering to culture hMSCs on a scaffold or construct and then differentiate them *in situ* to form whatever final lineage is desired[37-40]. hMSCs are normally grown and proliferated on standard tissue culture plastic dishes, and do not require a feeder layer or feeder-layer conditioned media like hESCs typically do[34, 35]. Like hESCs, there have been worries about using media with xenogenic products in it (like animal serum), so efforts have been made to grow hMSCs under defined conditions[33]. Furthermore, hMSCs lose their potency after too many passages (and thus are not infinitely self-renewing like hESCs), and eventually will only be able to go down the osteogenic lineage[41]. Thus, it is important to know that if they are to be cultured on a new material (like PMEDSAH) they will continue to have similar growth rates to what they have on standard TCPS, as a slower proliferation rate might impact their clinical use given that too many cell divisions results in a loss of potency.

Native adult hMSCs can be difficult to harvest though and it is a painful and invasive process, so recently there has been an effort to differentiate hMSC-like cells directly from hESCs and other stem

cell lines[18, 42]. hESCs, thanks to their self-renewing properties, could potentially generate an enormous number of hMSCs[43]. Barberi et al. generated hMSC-like cells from hESCs; they appropriately expressed markers associated with hMSCs, and could be differentiated into mesenchymal lineages like adipocytes, osteocytes, and chondrocytes [44]. However, a feeder layer was used to maintain the hESCs before differentiation, and in order to differentiate into hMSC-like cells, the group cultured hESCs on a layer of mouse OP9 stromal cells [44]. The resulting hMSC-like cells were separated out via fluorescence-activated cell sorting (FACS) and then replated onto TCPS – a complicated procedure requiring three different substrates (two of which are xenogenic co-cultures)[44]. PMEDSAH could potentially replace these two substrates, if mesenchymal stem cells can be shown to grow and maintain multipotency when cultured on it. Villa-Diaz et al. was able to generate hMSCs from a pluripotent stem cell without using any feeder cell layers; however, instead of hESCs they used induced pluripotent stem cells (hiPSCs)[18]. iPSCs were initially generated by Takahashi et al. from an adult mouse fibroblast line by transfection of four hESC pluripotency markers (OCT4, c-MYC, SOX2, and KLF4) – they were found to express hESC pluripotency markers and could differentiate much like hESCs when transplanted into mice[45, 46]. This was a very exciting development, as it potentially means that cells with the same advantages as hESCs but with none of the ethical concerns or immunogenic issues could be generated on demand for patients[46]. While the creation of iPSC cells took place on MEF feeder layers, Villa-Diaz et al. subsequently transferred them to PMEDSAH substrates to grow in feeder-free conditions[18]. hMSCs were then obtained by creating embryoid bodies, growing these in suspension culture with low-attachment substrates, and then culturing these again on a gelatin coated substrate and subculturing them until the cells looked like fibroblasts (the gross morphology of hMSCs)[18]. These cells could then differentiate down the three major mesenchymal stem cell lineages, had all the appropriate markers, and osteogenic cells generated from them resulted in new bone growth with a bone defect mouse

model[18]. Nevertheless, there is still little known about how hMSCs would behave if cultured on PMEDSAH-coated dishes. Letsche et al. tried to culture hMSCs on a variety of polymer brushes coated onto silicon substrates in patterns, and found that hMSCs prefer to grow in between the patterned PMEDSAH rather than on it[47]. Furthermore, thermal grafting of PMEDSAH results in largely uncontrolled polymerization with respect to chain length and dispersity – both important variables in dictating surface properties such as hydrophobicity. We wish to investigate a different reaction that gives us more control over polymerization – atom transfer radical polymerization.

ATRP

Atom transfer radical polymerization (ATRP) is a recently developed reaction that uses a transition metal catalyst and halogenated initiation group to create carbon-carbon bonds, with low reaction temperatures and a large library of available monomers[48, 49]. It is categorized as a type of 'living' polymerization because there is no chain termination (though as Patten et al. points out technically there is a termination step that occurs at a very initial low rate) – this is because ATRP controls the number of radicals present during the reaction[50-52]. ATRP is able to generate a monodisperse population of polymers by having the chemical reaction equilibrium favor the non-radical form of the growing polymer chain, with the number of propagating free radical polymers in much smaller numbers than the dormant polymer[51, 53, 54]. ATRP can be combined with chemical vapor deposition by functionalizing [2.2] paracyclophane with the initiator ester bromide via Rieche formulation followed by reduction to form a hydroxylated paracyclophane[49]. 2-bromoisobutyryl bromide can react to form the new desired initiator, which can undergo CVD via the Gorham process[49]. This allows for an easy way to modify the surfaces of bulk materials with ATRP-produced polymer chains – other methods of doing so exist, but are limited by the bulk material surface chemistry given the usual difficulty of immobilizing the necessary initiator[49]. Decoupling the surface chemistry from the

bulk material via CVD solves this issue. After deposition of the resulting PPX-esterbromide on a substrate, ATRP can be performed with the initiator, growing long polymer branches from the surface (Fig. 3.2)[49].

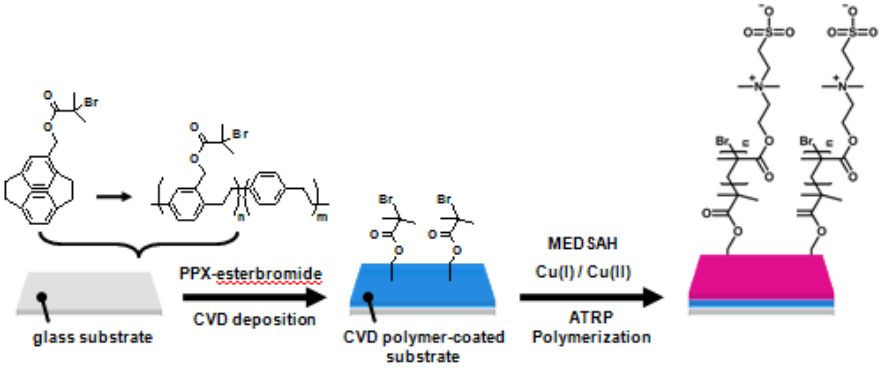

Figure 3.2 – ATRP of PMEDSAH after CVD deposition of the initiator PPX-esterbromide (figure by Dr. Jaewon Yoon)[55]

Jiang et al. used CVD and ATRP to pattern PEGMA against a PMMA background (poly(methyl methacrylate) generated on a silicon substrate via vapor-assisted micropatterning in replica structures, or 'VAMPIR')[49]. Subsequently, cultured NIH3T3 fibroblasts would only grow on the portion of the surface that did not contain the ATRP-generated PEGMA[49]. Jaewon et al. used ATRP generated PEGMA chains to prevent unwanted cell attachment during experiments[55].

PMEDSAH can also be deposited via ATRP, as illustrated in Fig. 3.3 and performed by Cheng et al [56]. ATRP allows for controllable polymer brush thickness, and Cheng wanted to study how zwitterionic brushes change with regards to certain mechanical properties such as wettability as thickness is increased [56]. Azzaroni et al. postulate that PMEDSAH chains progress through three conformational states based on the individual ionic interactions between the sulfonate and quaternary ammonium (Fig. 3.3)[57].

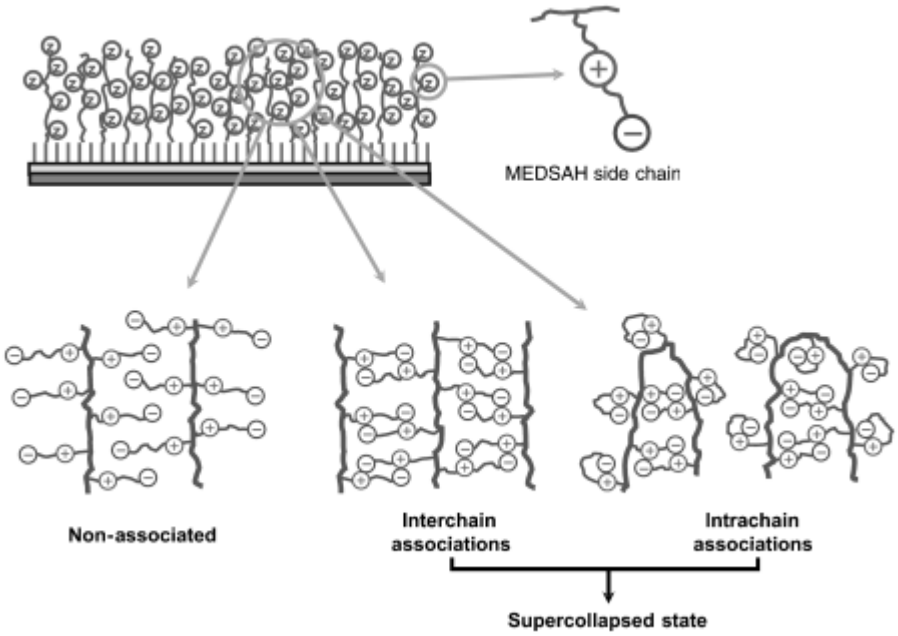

Figure 3.3 – PMEDSAH conformations based on zwitterionic interactions (reprinted with permission by Azzaroni et al.)[56]

At a shorter polymer brush height (less than 50 nm), it is hypothesized that the zwitterions do not interact and are in a non-associated conformation – but as thickness or density increases, the chains begin to interact with each other more, and eventually at a certain height will collapse onto each other with all of the ions interacting either within the individual chain itself or with ions in other chains (Fig. 3.4)[57]. Co-currently with this, Cheng et al. discovered that as the chain length is increased, the polymer brush transitions from being hydrophilic to being hydrophobic, with a critical brush height h_{crit} that depends on the chain density and rate of polymerization[56]. The change in how the zwitterionic chains associate with each other and water as height or density changes is proposed as a mechanism for explaining this transition – when ions are not associating with each other, they are free to be hydrated by water and thus show a low contact angle measurement[57]. However, once taller or denser chains start to show ion-pairing, water becomes excluded and the brush switches to a hydrophobic regime[57]. As previously discussed, surface wettability can be an important criterion for

a cell's ability to adhere or spread onto a surface – ATRP of PMEDSAH allows for precise control of this parameter as a function of the chain height and density.

Rationale, Project Goals, and Hypotheses

Clearly hMSCs represent an important and valuable type of adult multipotent stem cells that can further differentiate down lineages with critical applications in medicine and tissue engineering. While thermally grafted PMEDSAH has been very successful for maintaining hESCs and iPSCs, little work has been done to study hMSCs themselves on PMEDSAH. Early work in differentiating hESCs into mesenchymal stem cells required them to be first cultured on a MEF feeder layer, then OP9 stromal cells, then regular TCPS[44]. More recent research has attempted to remove the necessity for MEFs by using PMEDSAH as a feeder-free substrate, but this PMEDSAH was prepared using a UV-ozone thermal grafting polymerization without any control over polymer chain length[18]. Furthermore, while the iPSCs were maintained on PMEDSAH, the resulting hMSCs were not[18]. Much is known about how hESCs and iPSCs grow and maintain themselves on PMEDSAH - relatively little is known about how hMSCs would act. hMSCs can be maintained on traditional TCPS without fear of spontaneous differentiation (unlike hESCs and iPSCs). Nevertheless, if PMEDSAH is to be used as a universal substrate for hESC/iPSC differentiation towards hMSCs, it is important to know how hMSCs will behave on it (with respect to attachment, proliferation, morphology, and maintenance of multipotency). We want to grow hMSCs on PMEDSAH dishes coated via ATRP, as thermal grafting operates by an uncontrolled mechanism of polymerization. Thermally grafted PMEDSAH results in chains which are less dense and more prone to defects than those generated by ATRP. By contrast, ATRP allows us to directly control the thickness of the polymer brush, gives us a monodisperse coating (i.e. the individual chain lengths of PMEDSAH are the same height), and lets us control the wettability. Given that these parameters may play a role in embryonic stem cell maintenance[10], it is reasonable to hypothesize that they could also influence mesenchymal stem cell culture as well, yet this has not been well characterized. Thus, this chapter

characterizes and compares hMSCs grown on ATRP PMEDSAH to those grown on grafted PMEDSAH.

We cultured hMSCs on PMEDSAH surfaces coated with PMEDSAH of various chain lengths, along with grafted PMEDSAH and TCPS as controls. We measured various biological properties of the hMSCs after they were cultured in order to characterize how they grow and whether or not they remain pluripotent on the ATRP PMEDSAH. Work by Villa-Diaz et al. showed that MSCs differentiated from iPSCs grown on grafted PMEDSAH expressed all relevant markers and could be differentiated down the three major mesenchymal lineages, but the hMSCs themselves were not grown on PMEDSAH[18]. We first hypothesized that hMSCs *cultured on PMEDSAH deposited by ATRP at a similar length to grafted PMEDSAH will remain multipotent*. We tested this by growing hMSCs for seven days on ATRP PMEDSAH, grafted PMEDSAH, and TCPS then used flow cytometry to measure the presence or absence of undifferentiated hMSCs. We also did RT-PCR on hMSCs cultured on grafted PMEDSAH and TCPS, looking at the expression rates of a battery of genes related to hMSC maintenance and differentiation. While it is possible that the new orientation of the PMEDSAH chains could through mechanotransduction radically change hMSC gene expression, it was felt to be unlikely given that the overall stiffness of the material was largely the same (that of TCPS). Secondly, we hypothesized that *varying the lengths of the PMEDSAH chains by varying the ATRP reaction time will result in morphological and growth rate differences due to differing mechanical properties.* The second hypothesis was tested by culturing hMSCs on ATRP PMEDSAH of differing brush thickness for seven days, then fixing and staining them with phalloidin and DAPI/Hoescht probe. This hypothesis was shown to be incorrect – hMSCs grew to the same levels of confluency after 7 days of culture no matter the length of the PMEDSAH chains. However, there were noticeable morphological and viability differences between hMSCs grown on ATRP PMEDSAH and those grown on grafted PMEDSAH. This lead to our third hypothesis: *that due to differences in the orientation*

of the PMEDSAH chains with respect to the substrate, hMSCs cultured on ATRP PMEDSAH will grow at a different rate and have different morphological characteristics than those grown on grafted PMEDSAH of a similar height. This was partially tested by measuring the growth rate of hMSCs cultured on grafted PMEDSAH and ATRP PMEDSAH with an XTT assay over seven days, along with microscope studies, though we did not investigate the orientation of the PMEDSAH chains.

Experimental Section

Parts of this experimental section were paraphrased from original unpublished text by collaborator Dr. Aftin Ross.

Ultraviolet Ozone Thermal Grafting Polymerization

A 10 L reaction vessel was degassed through an argon-vacuum purging performed three times sequentially. During the reaction vessel purging, a solvent of 4:1 water/ethanol was prepared and degassed for 40 minutes after being placed under vacuum. After degassing, PMEDSAH (Sigma Aldrich, St. Louis, MO) was dissolved into the solvent at a concentration of 0.06 g/ml and the mixture was placed into the reaction vessel. This was then heated to 76-82 °C. During heating, tissue culture polystyrene cell culture well plates were placed in a UV ozone environment for 25 minutes to generate free radicals. The plates were then inserted into the reaction vessel for 2.5 hr for thermal grafting polymerization. After the reaction, the plates were washed with a 1% saline solution overnight at a temperature of 50 °C.

Atom Transfer Radical Polymerization

Brushes of PMEDSAH (Monomer-Polymer and Dajac Labs, Trevose, PA) were created using atom transfer radical polymerization (ATRP). A 4:1 methanol/water solvent was prepared and degassed with three freeze-pump-thaw cycles in a 50 ml Schlenk flask. Another 10 ml Schlenk flask was also degassed after three argon-vacuum cycles. At room temperature, 10% of the solvent was transferred by syringe to this 10 ml Schlenk flask, and a catalyst composed of CuCl (3.6 mg/ml), $CuCl_2$ (0.96 mg/ml) and 2'2 bipyridyl (14 mg/ml) was added to the mixture. PMEDSAH was dissolved into the remaining solvent in the 50 ml Schlenk flask at a concentration of 0.5 g/ml, and each mixture underwent ten minutes of stirring to ensure all reactants and catalysts were dissolved. The catalyst/solvent mixture was then added to the 50 mL PMEDSAH mixture, and after stirring the

mixture was placed under an argon environment in a purged glove box and aliquoted to the substrates needing to be coated (tissue culture polystyrene cell culture well plates, or flat silicon substrates in 20 ml scintillation vials that had previously been degassed – 1 ml to each sample). Substrates had previously undergone chemical vapor deposition to coat them with the initiator PPX-esterbromide. The ATRP reaction time was varied depending on the desired PMEDSAH chain length, and afterwards the substrates were washed in a 1% saline/water solution and allowed to dry. Copper catalyst was removed by washing with a 5 mM solution of EDTA along with further deionized water rinses.

RT-PCR

hMSCs at passage 6 were grown for 7 days on TCPS and thermally grafted TCPS. They were harvested with trypsin/EDTA 0.25% (Gibco), then RNA was harvested with a RNEasy Minikit and QIAshredder (Qiagen). These RNA samples were taken to the RT-PCR core facility at the NCRC, where they were converted into cDNA libraries. Gene expression for the following genes was measured using a Human Mesenchymal Stem Cell PCR Array (Qiagen) (some genes repeated for completeness of their category): FGF2, INS, LIF, POU5F1, SOX2, TERT, WNT3A, ZFP42 (stemness markers); ALCAM, ANPEP, BMP2, CASP3, ENG, ERBB2, FUT4, FZD9, ITGA6, ITGAV, KDR, MCAM, NGFR, NT5E, PDGFRB, PROM1, THY1, VCAM1 (MSC-specific markers); ANXA5, BDNF, BGLAP, BMP7, COL1A1, CSF2, CSF3, CTNNB1, EGF, FUT1, GFT3A, HGF, ICAM1, IFNG, IGF1, IL10M, IL1B, IL6, ITGB1, KITLG, MITF, MMP2, NES, NUDT6, PIGS, PTPRC, SLC17A5, TGFB3, TNF, VEGFA, VIM VWF (other genes associated with hMSCs); BMP2, BMP6, FGF10 HDAC1, HNF1A, KDR, PTK2, RUNX2, SMURF1, SMURF2, TBX5 (genes involved in osteogenesis); PPARG, RHOA, RUNX2 (genes involved in adipogenesis); ABCB1, BMP2, BMP4, BMP6, GDF5, GDF7, HAT1, ITGAX, KAT2B, SOX9,

TGFB1 (genes involved in chondrogenesis); JAG1, NOTCH1 (genes involved in myogenesis); and BMP2, GDF15, SMAD4, TGFB1 (genes involved in tenogenesis). $\Delta\Delta C_t$ values were calculated, and the natural scale fold change was outputted as $2^{-\Delta\Delta Ct}$. p-values were calculated and then adjusted for multiple comparisons via the false discovery rate.

Flow Cytometry

hMSCs (a kind gift from Dr. Paul Krebsbach, University of Michigan) at passage 6 were thawed from cryogenic storage and plated on TCPS, grafted PMEDSAH, and ATRP PMEDSAH surfaces at a concentration of 6000 cells/cm^2 (all 6 well plates). After 166 hours of proliferation in complete media (α-MEM + 10% FBS + 1% P/S), the cells were trypsonized and labeled with 1 μg/ml of antibody conjugated with a fluorescent marker. The following antibodies were used: PE (phycoerythrin) isotype-matched control, FITC (fluorescein isothiocyanate) istotype-matched control, CD34 (FITC), CD45 (FITC), CD73 (PE), CD90 (PE), and CD105 (PE). The samples were then run through a FACSCalibur 1 and analyzed.

hMSC Spreading Microscopy

hMSCs at passage 6 were seeded at a seeding density of 6000 cells/cm^2 onto silicon substrates in a 24-well plate coated with grafted PMEDSAH and ATRP PMEDSAH grown to various thicknesses. Cells were fed at 24 hr, 72 hr, and 120 hr complete media (α-MEM + 10% FBS + 1% P/S). At 168 hr (7 days), cells were fixed in 4% paraformaldehyde in DPBS and stained for actin with Alexa Fluor® 568-phallodin (Life Technologies). The surfaces were mounted with ProLong Gold + DAPI (Life Technologies) and imaged using an Olympus BX-51 fluorescence microscope. The average area of the cells was measured via ImageJ, and performed by dividing total cell area by total number of cells (equated to total number of individually counted DAPI stains). For statistical purposes, all

images were treated as independent with regards to calculating p-values. Other trials used a 6-well plate – cell seeding density was kept the same, along with feeding times and phalloidin staining technique (except Hoescht probe was used to stain nuclei instead of DAPI).

hMSC Growth Assay

hMSCs at passages 6-7 were thawed from cryogenic storage and plated on TCPS, grafted PMEDSAH, and ATRP PMEDSAH surfaces, at a plating density of 6000 cells/cm^2. Cells were fed at 24 hr, 72 hr, 120 hr, and 168 hr complete media (α-MEM + 10% FBS + 1% P/S), and an XTT assay (ATCC) was conducted to measure metabolic activity at 72 hr, 120 hr, and 168 hr. Briefly, an XTT solution composed of two parts complete media and one part XTT mixture (XTT mixture is composed of XTT reagent (2,3-bis-(2-methoxy-4-nitro-5-sulfophenyl)-2H-tetrazolium-5-carboxanilide) and activating agent (N-methyl dibenzopyrazine methyl sulfate) at a ratio of 50:1) was incubated with the cells for 65 minutes along with an equal number of blanks, and then pipetted into a 96 well plate. Using a plate reader, specific absorbance was measured at 475 nm and non-specific absorbance at 660 nm. The following formula was then used to calculate final specific absorbance: $SA = A_{475}$ (test) – A_{475} (blank) – A_{660} (test).

Results

Various surface properties of the grafted PMEDSAH and ATRP PMEDSAH plates were measured, including hydrophobicity via contact angle measurement and the brush thickness. Generally as expected with ATRP, the longer the plates spent in the ATRP reactor, the longer the branch chains became and the more hydrophobic the surfaces became (and all are much longer than the relatively short thermally grafted PMEDSAH chains) [56]. Table 3.1 highlights the measured physical properties (measured by Dr. Aftin Ross)

Time in ATRP Reactor	**Contact Angle**	**Brush Thickness**
1 hr	17°	27.1 nm
12 hr	37.7°	93.4 nm
24 hr	65.6°	108.3 nm
Grafted PMEDSAH	17°	10-20 nm

Next, differences were examined between hMSCs grown on thermally grafted PMEDSAH and ATRP PMEDSAH. The gross morphology and confluency of hMSCs on ATRP PMEDSAH surfaces of differing thickness was imaged, with growth on grafted PMEDSAH as a control. hMSCs were grown on PMEDSAH surface-modified silicon substrates for 166 hr, fixed and stained

with phalloidin and DAPI, then imaged using a fluorescence microscope (Fig.3.4)

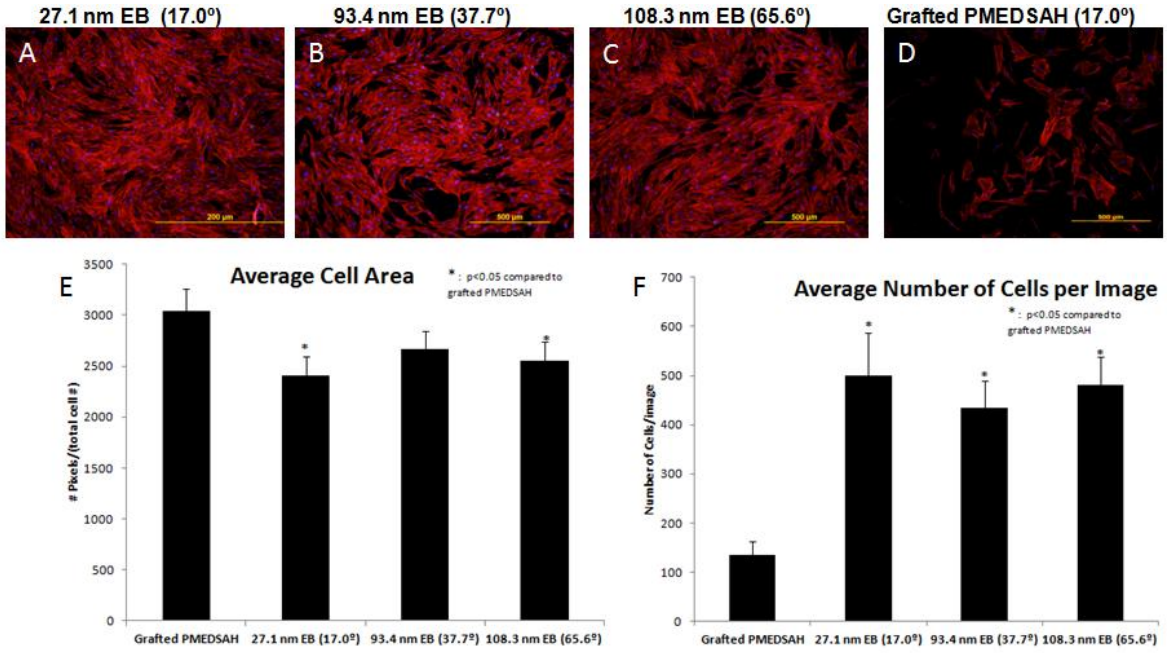

Figure 3.4: Fluorescent microscopy of hMSCs grown for 7 days on (a) 27.1 nm ATRP PMEDSAH, (b) 93.4 nm ATRP PMEDSAH, (c) 108.3 nm ATRP PMEDSAH, and (d) grafted PMEDSAH. The average cell area (e) and average number of cells per image (f) were measured as well

Interestingly, while grafted PMEDSAH surfaces (with a thickness between 10-20 nm) and ATRP surfaces coated to a thickness of 27.1 nm showed similar hydrophilicity (with a contact angle of ~17°), the behavior of the hMSCs on each was very different. hMSCs grew to confluency on all ATRP surfaces irrespective of hydrophilicity or thickness (contrary to our initial hypothesis), while the number of hMSCs on grafted PMEDSAH was significantly lower (in line with our last hypothesis). Cells grown on PMEDSAH had a marginally but statistically significantly higher average area than those grown on 27.1 nm and 108.3 nm ATRP PMEDSAH; this could be due to the overall lower level of confluency on grafted PMEDSAH, and thus greater area over which individual cells could freely spread in comparison to hMSCs grown on ATRP PMEDSAH. As the

cells had reached confluency on the ATRP surfaces by seven days, it was difficult to gauge any distinctive morphological differences.

hMSCs were also cultured on 6-well plates coated with either grafted or ATRP PMEDSAH, and grown for 7 days. The results were similar to that observed with the silicon substrates (Fig. 3.5), with cells showing near confluency on all surfaces except the grafted PMEDSAH. hMSCs grown on TCPS in a separate trial also grew to confluency after 7 days.

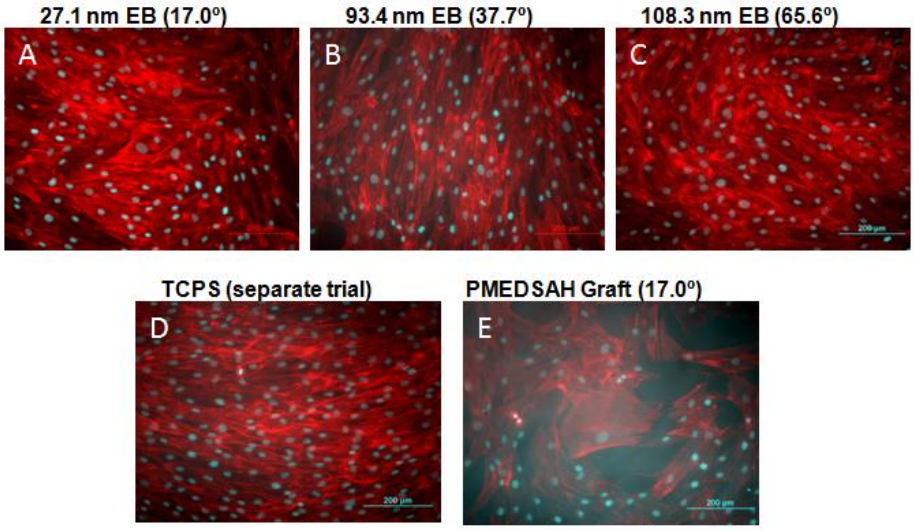

Figure 3.5: Fluorescent microscopy of hMSCs grown for 7 days on (a) 27.1 nm ATRP PMEDSAH, (b) 93.4 nm ATRP PMEDSAH, (c) 108.3 nm ATRP PMEDSAH, (d) TCPS (from a separate trial with the same conditions), and (e) Grafted PMEDSAH.

While the hMSCs grown on UV graft PMEDSAH looked very different from those grown on ATRP PMEDSAH, both the 27.1 nm ATRP PMEDSAH and the grafted PMEDSAH had the same contact angle. Thus, we decided for future experiments to only use the 27.1 nm ATRP PMEDSAH in order to keep the contact angle consistent (and thus eliminate wettability as a variable), and try to understand why hMSCs grew more vigorously on it in comparison to grafted PMEDSAH.

Flow cytometry was next performed to determine whether hMSCs spontaneously differentiate after

culture on grafted PMEDSAH and ATRP pMEDAH (27.1 nm thick). hMSCs were cultured for nearly 7 days, then removed from the surface and labeled with various markers associated with identifying hMSCs. hMSCs were also grown on TCPS as a positive control. CD34 and CD45 are negative on multipotent hMSCs, while CD73, CD90, and CD105 are positive markers.

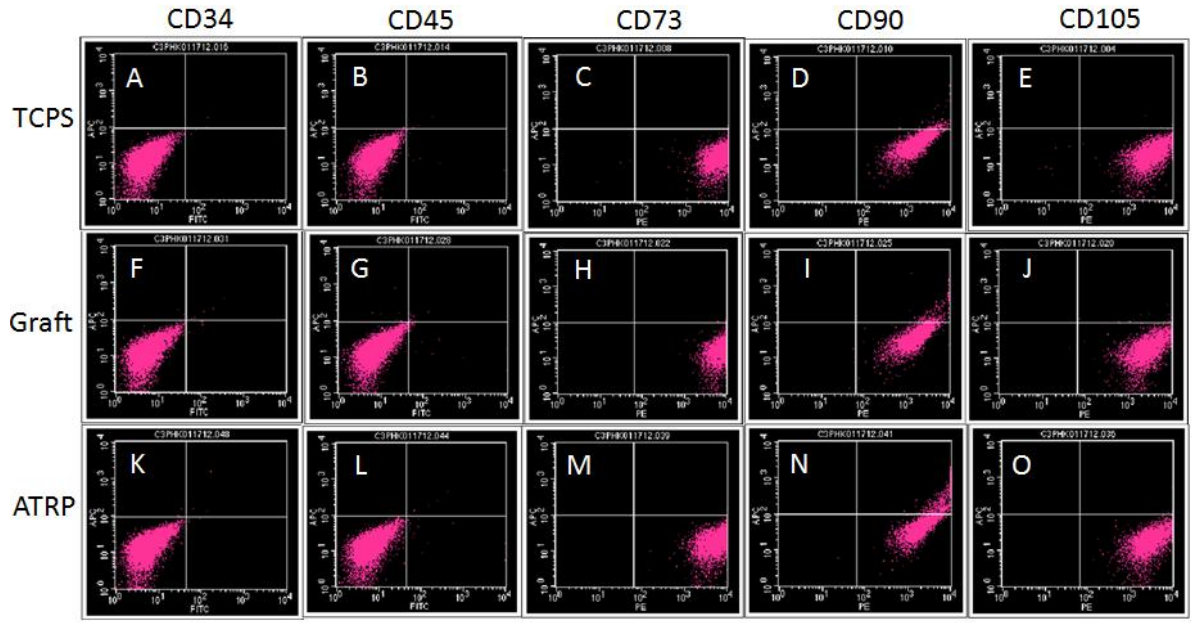

Figure 3.6: Flow cytometry dot plots (APC vs. PE or FITC) of (a-e) TCPS-grown hMSCs labeled with (a) CD34, (b) CD45, (c) CD73, (d) CD90, and (e) CD105; (f-j) Grafted PMEDSAH-grown hMSCs labeled with (f) CD34, (g)CD45, (h) CD73, (i) CD90, and (j) CD105; (k-o) ATRP PMEDSAH-grown hMSCs labeled with (k) CD34, (l)CD45, (m) CD73, (n) CD90, and (o) CD105

As shown in Fig. 3.6, hMSCs grown on all three surfaces are negative for CD34 and CD45, and positive for CD73, CD90, and CD105. This indicates that hMSCs do not spontaneously differentiate after extended culture on PMEDSAH surfaces, which is necessary if PMEDSAH is to be used as a universal substrate for stem cell culture.

Changes in gene expression on the grafted PMEDSAH (but not ATRP PMEDSAH) were also probed by RT-PCR, with TCPS as a control. A microarray able to probe 83 different genes related

to hMSC differentiation and multipotent maintenance was used. Fig. 3.7 plots $\Delta\Delta C_t$ values for a selection of these genes, related to such differentiation lineages as osteogenesis (BMP 2, RUNX2), adipogenesis (RUNX2), chondrogenesis (BMP 2, RUNX2, SOX9), myogenesis (JAG-1, NOTCH1), and other genes associated with hMSCs (EGF, FGF 2, VEGF, NGFR, IGF-1).

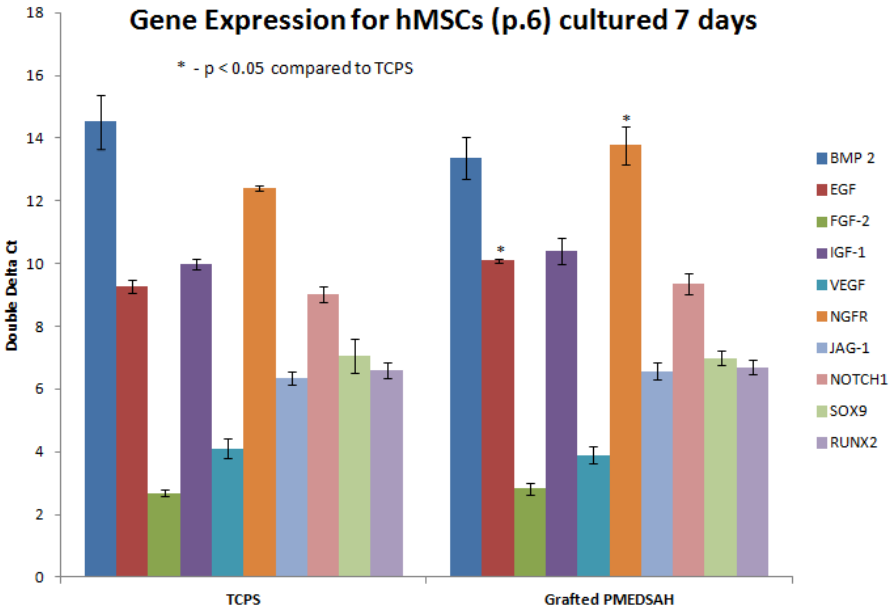

Figure 3.7: RT-PCR results for selected genes from hMSCs grown on TCPS and grafted PMEDSAH

Of the 83 genes examined, only two changed significantly in expression on grafted PMEDSAH vs. TCPS. Both EGF and NGFR were slightly downregulated after 7 days of growth on grafted PMEDSAH in comparison to those grown on TCPS ($p = 0.0367$ and $p = 0.0138$). Genes used as markers for hMSCs showed no significant changes after culture on either surfaces, and the appropriate amount of expression expected (e.g., CD29 is not expressed as it is a negative marker for undifferentiated hMSCs, while CD45 shows significant expression given that it's a positive marker for undifferentiated hMSCs) (Fig. 3.8). This corresponds well with the flow cytometry data, both of which present strong evidence that hMSCs do not undergo spontaneous differentiation when cultured on PMEDSAH.

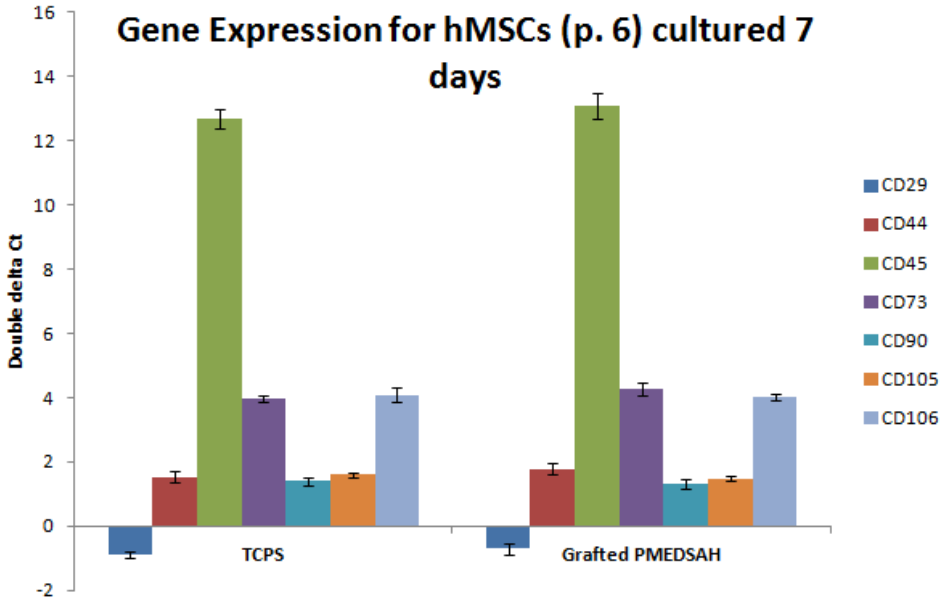

Figure 3.8: RT-PCR results of hMSC gene markers for hMSCs grown on TCPS and grafted PMEDSAH

As it seems that the growth rate on grafted PMEDSAH was much lower than that on ATRP and TCPS, growth was dynamically assessed through a measurement of metabolic activity over the course of a week. hMSCs were cultured for 7 days on TCPS, thermally grafted PMEDSAH, and ATRP grafted PMEDSAH. While growth occurred as expected with the TCPS and PMEDSAH plates, hMSCs would avoid growing in certain areas of the ATRP PMEDSAH plates while growing to full confluency in other parts. This was so apparent at times that one could even see a clear boundary which divided where the hMSCs would grow and where they would not (Fig. 3.9-b).

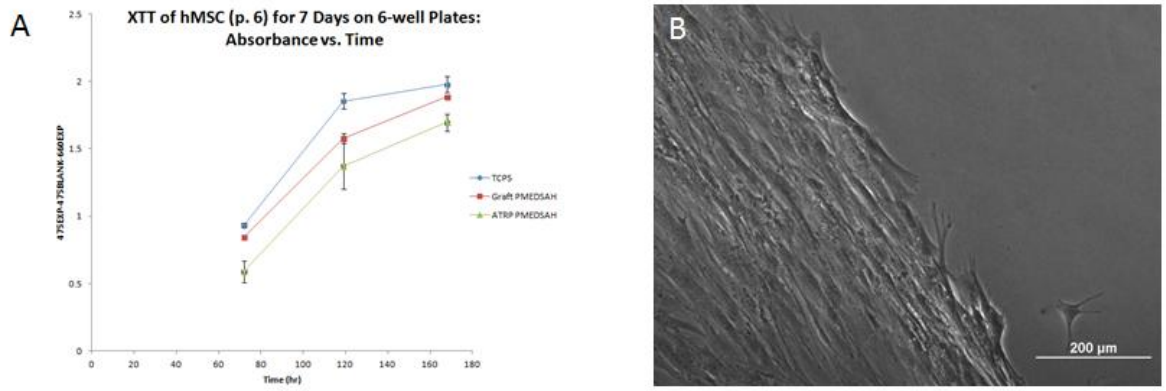

Figure 3.9: (a) XTT assay results for hMSCs grown on TCPS (blue), grafted PMEDSAH (red), and ATRP PMEDSAH (green). (b) Brightfield microscopy of the hMSCs growing on ATRP PMEDSAH after seven days in culture

The XTT results for the TCPS and grafted plates (which displayed no inhomogeneity with regards where cells would grow) were consistent with the previous microscopy results shown in Figure 3.5 – cells grew slower on the grafted PMEDSAH than the TCPS (though in the trial shown above they caught up to TCPS by day 7). The data for growth by days 3 and 5 is completely consistent through four trials, though by day 7 two of the trials showed the graft PMEDSAH cells catching up to the TCPS cells, while two others did not (Fig. 3.9, 3.10).

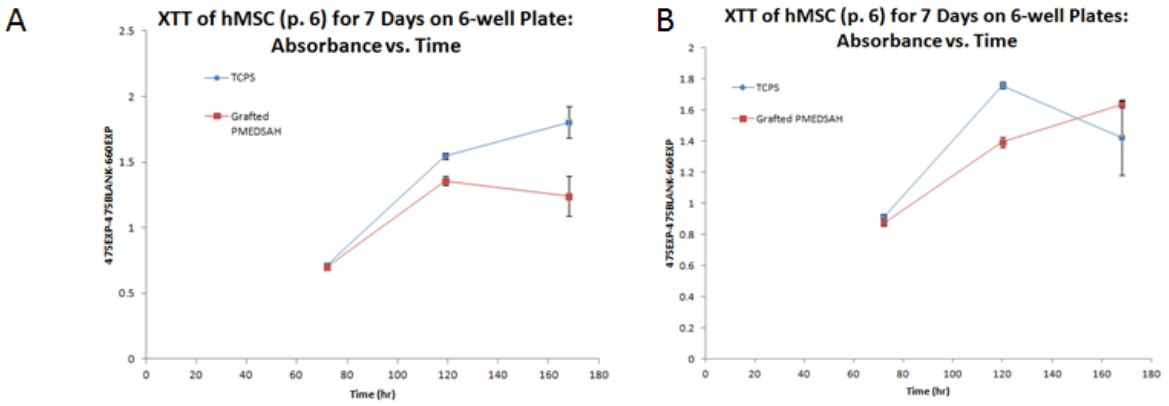

Figure 3.10: XTT assay results for hMSCs grown on TCPS (blue) and grafted PMEDSAH (red) for two different trials (a and b)

We hypothesized that the inhomogeneity occurring on the ATRP PMEDSAH was due to residual ethylenediaminetetraacetic acid (EDTA). This is normally used to wash the surfaces after ATRP to bind away all residual copper catalyst – failure to do this leads to surfaces where few cells will adhere and proliferate (data not shown). While after EDTA washing ATRP PMEDSAH surfaces could subsequently support hMSCs, we would consistently observe areas where the cells would refuse to grow despite other areas bordering them where the cells would grow to confluency. We hypothesized that as the acidic EDTA was not very soluble in water (0.4 g/L), it would remain on the surfaces despite washing. As EDTA chelates calcium, this would cause problems for cells trying to attach to each other via cadherins (which proteases will digest if calcium is not present)[26]. Therefore, we switched to a different chelation agent – EDTA disodium salt dihydride, which was far more water soluble (100 g/L).

To test our hypothesis, we washed our ATRP plates with a 5 mM solution of EDTA disodium salt dihydride and repeated the experiment (Fig. 3.11, n = 10). We no longer observed any areas on the ATRP PMEDSAH surfaces where the hMSCs would not go, strong evidence that our hypothesis was correct. As is consistent with microscopy (Fig. 3.11), hMSCs grew faster on ATRP and there were more cells present (as indirectly measured by XTT) than those on the grafted PMEDSAH surfaces. While at 72 hr the cells grown on ATRP PMEDSAH and grafted PMEDSAH show statistically similar XTT assay results, by 120 hr the cells on the ATRP surfaces have outgrown those on the grafted and continued to do so by 168 hr. As in previous trials, hMSCs grown on the grafted PMEDSAH grew far slower than those on TCPS, reinforcing this observation. TCPS also showed higher XTT assay results than the cells growing on the PMEDSAH ATRP surfaces.

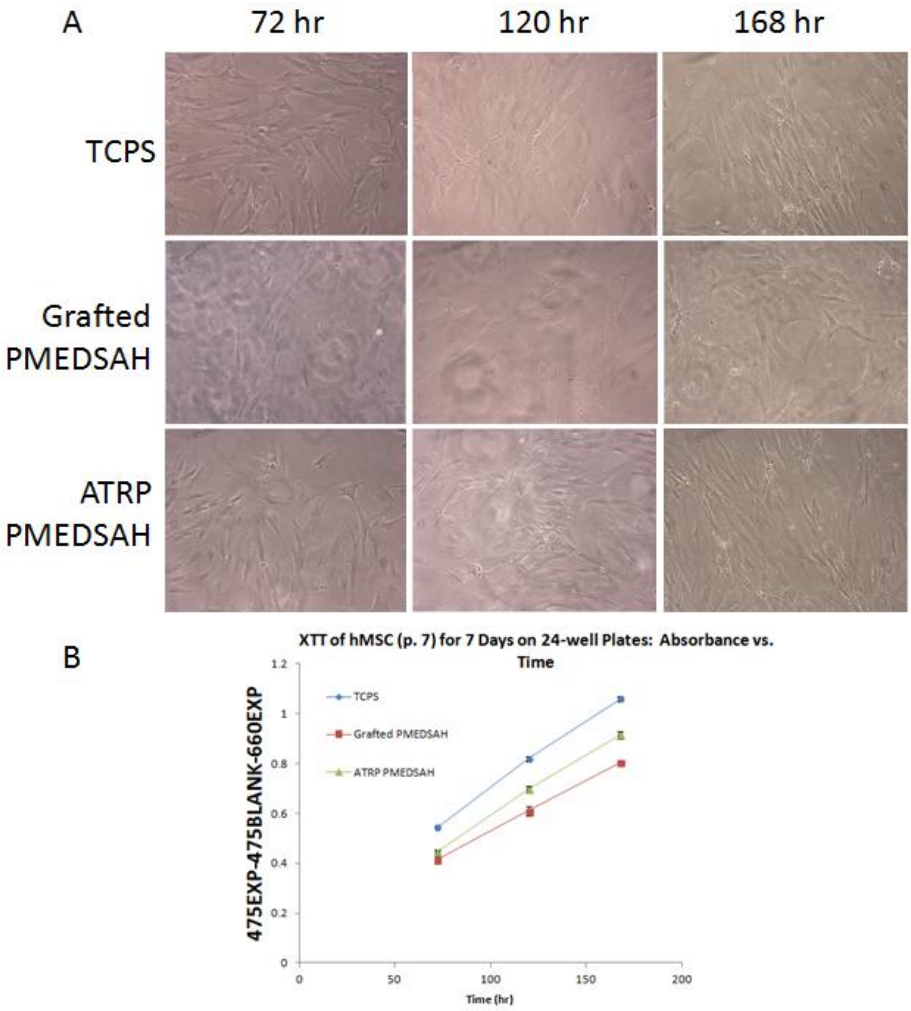

Figure 3.11: (a) Brightfield microscopy of hMSCs growing on various surfaces at indicated time points, (b) XTT results over seven days

Conclusions and Future Work

hMSCs are a valuable cell line with many desirable properties, including their relatively fast growth rate, simple culture conditions, and potential for autologous transplant . In this chapter, we confirmed that hMSCs maintain markers for multipotency when grown on grafted PMEDSAH and ATRP PMEDSAH via flow cytometry. This is further backed up for grafted PMEDSAH based on RT-PCR results. However, hMSCs do not grow as well on PMEDSAH surfaces (either the grafted or the ATRP) as they do on TCPS. This was disappointing, though it is interesting that there is a clear difference in growth rate between the thermally grafted PMEDSAH and ATRP PMEDSAH with similar contact angles. Thus, we supported our first hypothesis (hMSCs retain their characteristic markers on grafted and ATRP generated PMEDSAH surfaces), rejected our second (as the contact angle and thickness of the surfaces did not seem to affect the growth of the hMSCs when it was varied on the ATRP-generated PMEDSAH surfaces), and supported our third (hMSCs do grow at slower rates on thermally grafted pMEDSAH over ATRP pMEDSAH). Why they fail to grow as well on the grafted PMEDSAH in comparison to the other surfaces is unclear. The RT-PCR results indicate that hMSCs grown on grafted PMEDSAH very slightly downregulate expression of EGF, and EGF has been shown to increase hMSC proliferation and motility[58]. However, while the result is significant statistically, it is so small (not even two-fold) that this hypothesis is not very likely to be true. It is also unlikely to do with the hydrophilicity of the surfaces, as both grafted PMEDSAH and the thickness of ATRP pMEDAH tested (27.1 nm) have essentially the same contact angle (17°). As the conformation of the polymer chains is likely different on a short polydisperse thermally grafted coatings vs. the thicker and more monodisperse ATRP coatings, it is likely that this is the source of the difference observed. Perhaps the thermally grafted co-polymer does not support cell proliferation as well due to a difference in how it binds

proteins (such as growth factors or extracellular matrix) generated by the cells during culture in comparison to the ATRP PMEDSAH.

For future work, we need to confirm that the hMSCs still differentiate down their three major lineages (osteo, chondro, and adipo) by differentiating them *in vitro* after culture on PMEDSAH surfaces. The results with the EDTA suggest a new method for preventing cell growth on PMEDSAH surfaces. As our hypothesis seems to be correct, it may be possible to microcontact print the insoluble acidic form of EDTA onto bare PMEDSAH in order to create patterned regions where cells will not bind. Unlike reaction schemes such as ATRP deposition of PEGMA or click chemistry of azido-PEG onto a surface, this would be an incredibly simple procedure (just physisorption of EDTA) – yet it may result in resistance to cell adhesion over long times much like these already well-known surface modifications. Controlled experiments testing this are underway as of the writing of this thesis.

References

1. Ess, K.C. Patient heal thyself: modeling and treating neurological disorders using patient-derived stem cells. *Exp Biol Med (Maywood)* **238**, 308-314 (2013).
2. Pouton, C.W. & Haynes, J.M. Embryonic stem cells as a source of models for drug discovery. *Nat Rev Drug Discov* **6**, 605-616 (2007).
3. Orkin, S.H. Stem cell alchemy. *Nature medicine* **6**, 1212-1213 (2000).
4. Reubinoff, B.E., Pera, M.F., Fong, C.Y., Trounson, A. & Bongso, A. Embryonic stem cell lines from human blastocysts: somatic differentiation in vitro. *Nature biotechnology* **18**, 399-404 (2000).
5. Thomson, J.A. et al. Embryonic stem cell lines derived from human blastocysts. *Science* **282**, 1145-1147 (1998).
6. Lee, J.B. et al. Establishment and maintenance of human embryonic stem cell lines on human feeder cells derived from uterine endometrium under serum-free condition. *Biol Reprod* **72**, 42-49 (2005).
7. Richards, M., Fong, C.Y., Chan, W.K., Wong, P.C. & Bongso, A. Human feeders support prolonged undifferentiated growth of human inner cell masses and embryonic stem cells. *Nature biotechnology* **20**, 933-936 (2002).
8. Eiselleova, L. et al. Comparative study of mouse and human feeder cells for human embryonic stem cells. *The International journal of developmental biology* **52**, 353-363 (2008).
9. Hongisto, H. et al. Laminin-511 expression is associated with the functionality of feeder cells in human embryonic stem cell culture. *Stem Cell Res* **8**, 97-108 (2012).
10. Villa-Diaz, L.G., Ross, A.M., Lahann, J. & Krebsbach, P.H. Concise review: The evolution of human pluripotent stem cell culture: from feeder cells to synthetic coatings. *Stem Cells* **31**, 1-7 (2013).
11. Xu, C. et al. Feeder-free growth of undifferentiated human embryonic stem cells. *Nature biotechnology* **19**, 971-974 (2001).
12. Hughes, C.S., Postovit, L.M. & Lajoie, G.A. Matrigel: a complex protein mixture required for optimal growth of cell culture. *Proteomics* **10**, 1886-1890 (2010).
13. Villa-Diaz, L.G. et al. Synthetic polymer coatings for long-term growth of human embryonic stem cells. *Nature biotechnology* **28**, 581-583 (2010).
14. Ornitz, D.M. et al. Heparin Is Required for Cell-Free Binding of Basic Fibroblast Growth-Factor to a Soluble Receptor and for Mitogenesis in Whole Cells. *Mol Cell Biol* **12**, 240-247 (1992).
15. Eiselleova, L. et al. A Complex Role for FGF-2 in Self-Renewal, Survival, and Adhesion of Human Embryonic Stem Cells. *Stem Cells* **27**, 1847-1857 (2009).
16. Klim, J.R., Li, L., Wrighton, P.J., Piekarczyk, M.S. & Kiessling, L.L. A defined glycosaminoglycan-binding substratum for human pluripotent stem cells. *Nature methods* **7**, 989-994 (2010).
17. Kolhar, P., Kotamraju, V.R., Hikita, S.T., Clegg, D.O. & Ruoslahti, E. Synthetic surfaces for human embryonic stem cell culture. *Journal of biotechnology* **146**, 143-146 (2010).
18. Villa-Diaz, L.G. et al. Derivation of mesenchymal stem cells from human induced pluripotent stem cells cultured on synthetic substrates. *Stem Cells* **30**, 1174-1181 (2012).

19. Chang, C.W. et al. Engineering cell-material interfaces for long-term expansion of human pluripotent stem cells. *Biomaterials* **34**, 912-921 (2013).
20. Sangaj, N. et al. Heparin Mimicking Polymer Promotes Myogenic Differentiation of Muscle Progenitor Cells. *Biomacromolecules* **11**, 3294-3300 (2010).
21. Irwin, E.F., Gupta, R., Dashti, D.C. & Healy, K.E. Engineered polymer-media interfaces for the long-term self-renewal of human embryonic stem cells. *Biomaterials* **32**, 6912-6919 (2011).
22. Chamberlain, G., Fox, J., Ashton, B. & Middleton, J. Concise review: Mesenchymal stem cells: Their phenotype, differentiation capacity, immunological features, and potential for homing. *Stem Cells* **25**, 2739-2749 (2007).
23. Meirelles, L.D.S., Chagastelles, P.C. & Nardi, N.B. Mesenchymal stem cells reside in virtually all post-natal organs and tissues. *J Cell Sci* **119**, 2204-2213 (2006).
24. Barry, F.P. & Murphy, J.M. Mesenchymal stem cells: clinical applications and biological characterization. *Int J Biochem Cell B* **36**, 568-584 (2004).
25. Caplan, A.I. & Bruder, S.P. Mesenchymal stem cells: building blocks for molecular medicine in the 21st century. *Trends in molecular medicine* **7**, 259-264 (2001).
26. Alberts, B. Molecular biology of the cell, Edn. 4th. (Garland Science, New York; 2002).
27. Caplan, A.I. Mesenchymal stem cells. *J Orthopaed Res* **9**, 641-650 (1991).
28. Dominici, M. et al. Minimal criteria for defining multipotent mesenchymal stromal cells. The International Society for Cellular Therapy position statement. *Cytotherapy* **8**, 315-317 (2006).
29. Tuan, R.S., Boland, G. & Tuli, R. Adult mesenchymal stem cells and cell-based tissue engineering. *Arthritis research & therapy* **5**, 32-45 (2003).
30. Toma, C., Pittenger, M.F., Cahill, K.S., Byrne, B.J. & Kessler, P.D. Human mesenchymal stem cells differentiate to a cardiomyocyte phenotype in the adult murine heart. *Circulation* **105**, 93-98 (2002).
31. Zheng, B. et al. Neural differentiation of mesenchymal stem cells influences chemotactic responses to HGF. *Journal of cellular physiology* **228**, 149-162 (2013).
32. Stock, P. et al. The generation of hepatocytes from mesenchymal stem cells and engraftment into murine liver. *Nature protocols* **5**, 617-627 (2010).
33. Jung, S., Panchalingam, K.M., Rosenberg, L. & Behie, L.A. Ex vivo expansion of human mesenchymal stem cells in defined serum-free media. *Stem cells international* **2012**, 123030 (2012).
34. Bruedigam, C. et al. in Current Protocols in Stem Cell Biology (John Wiley & Sons, Inc., 2007).
35. Vemuri, M.C., Chase, L.G. & Rao, M.S. Mesenchymal stem cell assays and applications. (Springer, New York; 2011).
36. Engler, A.J., Sen, S., Sweeney, H.L. & Discher, D.E. Matrix elasticity directs stem cell lineage specification. *Cell* **126**, 677-689 (2006).
37. Meinel, L. et al. Engineering cartilage-like tissue using human mesenchymal stem cells and silk protein scaffolds. *Biotechnol Bioeng* **88**, 379-391 (2004).
38. Neuss, S. et al. Long-term survival and bipotent terminal differentiation of human mesenchymal stem cells (hMSC) in combination with a commercially available three-dimensional collagen scaffold. *Cell transplantation* **17**, 977-986 (2008).
39. George, J., Kuboki, Y. & Miyata, T. Differentiation of mesenchymal stem cells into osteoblasts on honeycomb collagen scaffolds. *Biotechnol Bioeng* **95**, 404-411 (2006).
40. Wang, Y., Kim, U.J., Blasioli, D.J., Kim, H.J. & Kaplan, D.L. In vitro cartilage tissue engineering with 3D porous aqueous-derived silk scaffolds and mesenchymal stem cells. *Biomaterials* **26**, 7082-7094 (2005).

41. Sensebe, L. Clinical grade production of mesenchymal stem cells. *Bio-medical materials and engineering* **18**, S3-10 (2008).
42. Olivier, E.N. & Bouhassira, E.E. Differentiation of Human Embryonic Stem Cells into Mesenchymal Stem Cells by the "Raclure" Method. *Embryonic Stem Cell Therapy for Osteo-Degenerative Diseases* **690**, 183-193 (2011).
43. Olivier, E.N., Rybicki, A.C. & Bouhassira, E.E. Differentiation of human embryonic stem cells into bipotent mesenchymal stem cells. *Stem Cells* **24**, 1914-1922 (2006).
44. Barberi, T., Willis, L.M., Socci, N.D. & Studer, L. Derivation of multipotent mesenchymal precursors from human embryonic stem cells. *PLoS medicine* **2**, e161 (2005).
45. Takahashi, K. & Yamanaka, S. Induction of pluripotent stem cells from mouse embryonic and adult fibroblast cultures by defined factors. *Cell* **126**, 663-676 (2006).
46. Robinton, D.A. & Daley, G.Q. The promise of induced pluripotent stem cells in research and therapy. *Nature* **481**, 295-305 (2012).
47. Letsche, S. et al. Usage of polymer brushes as substrates of bone cells. *Front. Mater. Sci. China* **3**, 132-144 (2009).
48. Wang, J.S. & Matyjaszewski, K. Controlled Living Radical Polymerization - Atom-Transfer Radical Polymerization in the Presence of Transition-Metal Complexes. *Journal of the American Chemical Society* **117**, 5614-5615 (1995).
49. Jiang, X.W., Chen, H.Y., Galvan, G., Yoshida, M. & Lahann, J. Vapor-based initiator coatings for atom transfer radical polymerization. *Advanced functional materials* **18**, 27-35 (2008).
50. Jenkins, A.D., Kratochvil, P., Stepto, R.F.T. & Suter, U.W. Glossary of basic terms in polymer science. *Pure Appl Chem* **68**, 2287-2311 (1996).
51. Patten, T.E. & Matyjaszewski, K. Atom transfer radical polymerization and the synthesis of polymeric materials. *Advanced Materials* **10**, 901-+ (1998).
52. He, W.W., Jiang, H.J., Zhang, L.F., Cheng, Z.P. & Zhu, X.L. Atom transfer radical polymerization of hydrophilic monomers and its applications. *Polym Chem-Uk* **4**, 2919-2938 (2013).
53. Matyjaszewski, K. Atom Transfer Radical Polymerization: From Mechanisms to Applications. *Isr J Chem* **52**, 206-220 (2012).
54. Morinaga, T., Ohkura, M., Ohno, K., Tsujii, Y. & Fukuda, T. Monodisperse silica particles grafted with concentrated oxetane-carrying polymer brushes: Their synthesis by surface-initiated atom transfer radical polymerization and use for fabrication of hollow spheres. *Macromolecules* **40**, 1159-1164 (2007).
55. Yoon, J. 2013).
56. Cheng, N., Brown, A.A., Azzaroni, O. & Huck, W.T.S. Thickness-dependent properties of polyzwitterionic brushes. *Macromolecules* **41**, 6317-6321 (2008).
57. Azzaroni, O., Brown, A.A. & Huck, W.T.S. UCST Wetting Transitions of Polyzwitterionic Brushes Driven by Self-Association. *Angewandte Chemie International Edition* **45**, 1770-1774 (2006).
58. Tamama, K., Kawasaki, H. & Wells, A. Epidermal growth factor (EGF) treatment on multipotential stromal cells (MSCs). Possible enhancement of therapeutic potential of MSC. *Journal of biomedicine & biotechnology* **2010**, 795385 (2010).

CHAPTER 4

Cardiomyocyte Bioactuators with Electrohydrodynamically Co-jetted Anisotropic Microcylinders

Overview

In this chapter, we created a biohybrid material consisting of anisotropic flexible microcylinders and mammalian cells. These microcylinders were generated using electrohydrodynamic co-jetting. We subsequently demonstrated that this resulted in bioactuators if the cell line used were spontaneously contracting rat neonatal cardiomyocytes. In the **Introduction and Background**, we discuss current bioactuators that have been crafted using muscle cells and flexible polymers. We highlight the successes as well as the shortcomings of these approaches, particularly with regards to their comparatively large size. We also briefly review the technique of electrohydrodynamic co-jetting, emphasizing the ease with which it can create anisotropic materials. We built a new free floating cylindrical bioactuator that is smaller than those currently in the literature, and characterize the force generated by cardiomyocytes attached to it using confocal microscopy.

Introduction and Background - Bioactuators

An actuator is simply defined as a mechanical device which converts energy into motion. Micro-electromechanical systems (MEMS) and devices comprise a major industry, and actuators are an important component for these devices and their ability to interact with the outside world[1]. Bell et

al. categorizes MEM actuators into four broad families based on how they function: electrostatic, piezoelectric, thermal, and magnetic[1]. Picking a particular actuator for a MEMS device is a project in determining the desired frequency, force, and displacement along with looking at factors like fatigability, efficiency, and material failure[1, 2]. For example, piezoelectric actuators can exert a maximal force between 10^{-5}-10^{-3} N, while ones based on magnetic fields range around 10^{-7}-10^{-4} N[1]. Shapeshifting materials such as polypyrrole are a popular choice for actuators, as they have high stress/strain performance and require a low voltage in order to work[3, 4]. Another factor to consider is the source of energy needed for the actuator to move and generate force[2]. For example, polypyrrole acts as an actuator by changing its volume due to the entrance or exit of ions – this is often accomplished with a battery providing the voltage necessary[5]. Recent work by Küttel et al. accomplished this same effect without a battery by adding the redox reagents hexacyanoferrate and L-ascorbic acid to a solution bathing the actuator[5]. Thus, there is interest in eliminating the necessity of batteries for actuators, especially MEMS devices which might require a sophisticated microbattery to operate[6].

A potentially new class of actuator has recently been developed. Rather than depending on inorganic substrates, they attempt to mimic an actuator already found in nature: muscle[7]. So-called 'bioactuators' have several potential advantages over traditional actuators. One of these is that unlike some microactuators, bioactuators do not require an external microbattery[6]. In fact, glucose alone has been measured to result in 1000 J of work per gram – this fact is often noted in arguments for the energy-density advantages of bioactuator[2, 8, 9]. In comparing their bioactuator to a polypyrrole actuator, Feinberg et al. note the energy advantage of using glucose over a battery, along with marked advantages in strain, frequency, and force generation (though not in stress, where polypyrrole actuators have a marked advantage over bioactuators by more than an order of magnitude)[6]. They are also able to potentially self-repair themselves if damaged[10].

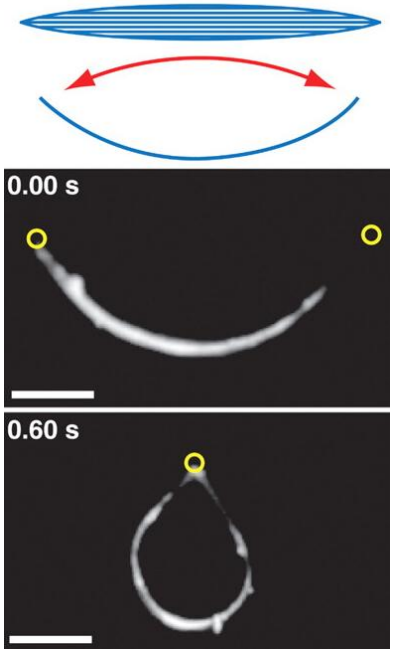

Figure 4.1: Cardiomyocytes cultured on thin films of anisotropic PDMS will bend it in culture (reprinted and modified with permission from Feinberg et al.)[6]

One class of bioactuators was engineered by Feinberg et al. PDMS was spin coated on top of poly(N-isopropylacrylamide) (PIPAAm) and then functionalized with μCP fibronectin[6]. Cardiomyocytes were then grown on top of this flat film, which could be cut with a scalpel into any shape desired[6]. Cardiomyocytes are often an ideal choice for proof-of-concept bioactuators, as neonatal cardiomyocytes will spontaneously beat in culture without any need for an external electric potential (depending on how they are cultured, adult cardiomyocytes can also exhibit spontaneous contractions)[11, 12]. The bioactuator was next placed into a colder temperature; as PIPAAm is temperature sensitive and has a tunable wettability (discussed at length in Chapter 5), the cooler temperature releases the PDMS-cardiomyocyte actuator from the PIPAAm substrate (which transitions from a hydrophobic to a hydrophilic state when the temperature is lowered)[6]. Key to this work was the anisoptropy of the initially flat thin film of PDMS – both fibronectin and cardiomyocytes were μCP/cultured on one side, thus enabling it to bend in a desired direction

without other cardiomyocytes opposing it[6]. The individual alignment of the cardiomyocytes was also a part of the anisotropy of the thin films – on films where fibronectin was printed in alternating lines of high and low concentration, the cardiomyocytes formed aligned sarcomeres and fibers and deformed the PDMS along in a uniaxial manner[6]. Cardiomyocytes grown on an isotropic surface exhibited no preferred alignment, and thus showed no net stress (which is not ideal for an actuator)[6]. Feinberg therefore demonstrates how important material anisotropy is for preparing bioactuators. This work was recently extended to create a 'heart on a chip' platform where cardiomyocytes were grown on a similar anisotropic PDMS platform as before, but that was previously cut with a laser tool to create individual cantilevers that the cardiomyocytes could bend (rather than crudely cut out with a scalpel as before)[13]. This essentially creates a high throughput assay for testing how drugs affect cardiomyocyte contractility (measured by examining diastolic, systolic, and twitch stress) – as proof of concept the experimenters looked at the dose response of the beta-adrenergic agonist isoproterenol [13]. This project demonstrates that platforms for bioactuators have more applications than simply as replacements for inorganic materials such as polypyrrole, but could also be useful for the study of cardiomyocyte biology itself in addition to their potential development as a diagnostic tool (for example, one could culture diseased or genetically altered cardiomyocytes on this heart-on-a-chip platform rather than simply healthy ones)[13].

All three types of muscle cells (cardiac, smooth, and skeletal) have been used in the production of bioactuators. Cardiomyocytes may not always be ideal depending on the application, as they spontaneously contract and would be more difficult to control in settings where actuation needs to be performed only at certain intervals[14]. Sun et al. (collaborating with Feinberg) printed lines of fibronectin on spin coated PDMS bound to PIPAAm, and then cultured the mouse muscle progenitor cell line C2C12[15]. They were then differentiated (via switching the serum in the media from 10% FBS to 2% horse serum) into myotubes[15]. As before, the anisotropy was important for

generating unaxial force, and the authors optimized the spacing between the printed fibronectin lines so cells in individual muscle fibers do not 'bridge' over to interface with cells in other muscle fibers[15]. Smooth muscle cells are also candidates for bioactuators – Tanaka et al. used vascular smooth muscle cells to bind and bend micropillar PDMS[14].

Other 'biorobots' have been developed using the principles of bioactuators. Herr et al. developed one of the earliest of these devices (colloquially referred to as swimmers) using frog muscle that had been surgically removed and incorporated into a macroscopic mechanical device[9]. Energy was provided by a solution of glucose, along with batteries for the embedded microcontrollers[9]. This biorobot could then be remotely controlled and perform swimming exercises with the ability to turn[9]. The muscle thin films produced by Feinberg et al. could be thought of as biorobots[6]. Naworth et al. in collaboration with Parker and Feinberg created a millimeter-sized biorobot they termed a 'medusoid,' as it resembled and was inspired by the swimming method of the jellyfish[16]. This was constructed out of PDMS and rat cardiomyocytes, and resembled actual jellyfish when they swam in the bath[16]. Hoshino et al. cultured a cardiomyocyte/collagen gel in a PDMS network cast into patterns such as grids and lattices, and some of these could crawl across a surface[17].

Electrohydrodynamic co-jetting (EHD jetting or electrospinning) provides an excellent platform for creating anistropic materials, and is a powerful fabrication technique that could be used to produce bioactuators. A solution of charged polymer (dissolved in either organic or aqueous solvent) is 'jetted' from a syringe via a pump and applied voltage; once the force from the electrical potential overwhelms the surface tension of the polymer a fiber will 'spin' down from a 'Taylor cone' (a stable fluid geometry reached at some critical potential) to be collected below (Fig. 4.2)[18-20].

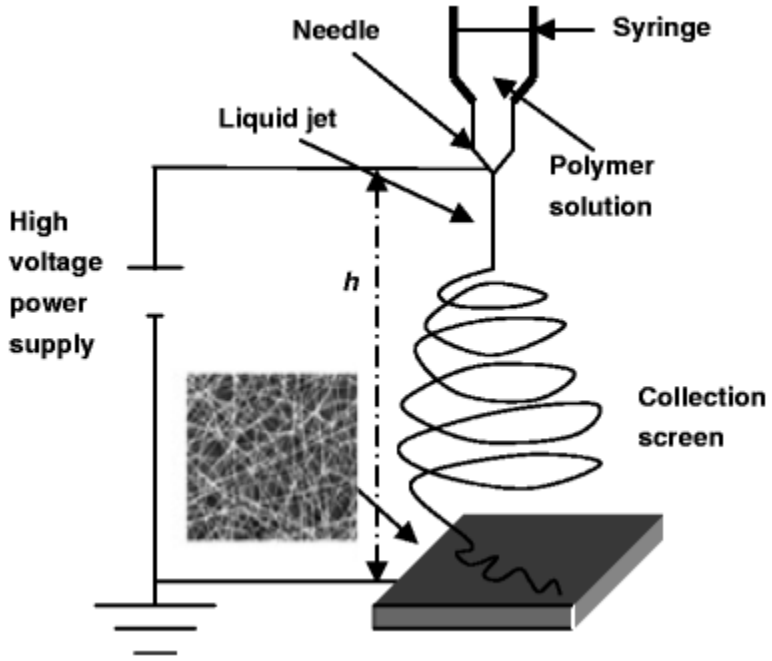

Figure 4.2: Schematic of electrohydrodynamic jetting (reprinted with permission by Kaul et al)[20].

Viscosity, surface tension, and solution conductivity are all important factors, along with velocity of the flow[21]. Bhaskar et al. jetted poly(lactide-*co*-glycolide) (PLGA) into fibers and particles[18], a biodegradable polymer often used in tissue engineering due to its biocompatibility and FDA approval. Key to this work is developing a technique for co-jetting two different variants of PLGA at the same time to create biphasic fibers; in this case unmodified PLGA is jetted alongside poly[lactide-*co*-(propargyl glycolide)] (i.e. acetylene-PLGA)[18]. This resulted in an anisotropic material that could be selectively altered depending on the material and functional properties of a particular phase. For example, one could modify the PLGA featuring acetylene via click chemistry (CuI-catalyzed Huisgen 1,3-dipolar cycloaddition), adding either cell resistant molecules like azido-PEG-amine or cell adhesive factors like the RGD or IKVAV peptide[18, 22]. Mandal et al. jetted acetylene-functionalized PLGA to create a fiber which promotes NIH3T3 fibroblast adhesion on one phase featuring IKVAV (derived from the extracellular matrix molecule laminin) clicked on beforehand[22].

Highly selective attachment resulted, with the majority of cells only attaching to the side containing the adhesive peptide[22].

Rationale, Project Goals, and Hypotheses

Bioactuators have been successfully created using cardiomyocytes, smooth muscle cells, or skeletal muscle cells[6, 14, 15]. However, many of these actuators can more accurately be described as cantilevers, where the actuator is fixed at one end to a solid support[14, 23-25]. While this makes sense in the context of overall device design (that is, building a cardiomyocyte cantilever as part of some larger design that is executed), these bioactuators have to be individually designed and fitted for each application and cannot be mass produced. Freely detached bioactuators on the other hand can almost be thought of better as 'biorobots' – while these could be inserted into larger devices as building blocks, so far most of them are large (on the order of millimeters) and thus unable to be used for microrobotic operations (whose main advantage is their ability to enter into small spaces) [9, 16, 17, 26]. One of the smallest free crawling devices was built by Xi et al., and even that was 138 μm[7]. We believe that smaller freely contracting bioactuators are possible.

We proposed creating a new bioactuator to address these issues and push the boundaries of this field towards more truly microbiorobots, taking advantage of EHD co-jetting to create anisotropic fibers. Previous work has already demonstrated that fibers can be aligned and cut at precise lengths to create microcylinders, using a microtome[27]. This allows for the mass production of tens of thousands of microcylinders – something that current methods for creating bioactuators and biorobots cannot achieve. Bhaskar et al. created several types of multiphasic microcylinders: with the right chemistry each phase in theory could be conjugated with a different functional group that can affect things like cell binding or behavior (Fig. 4.3)[27].

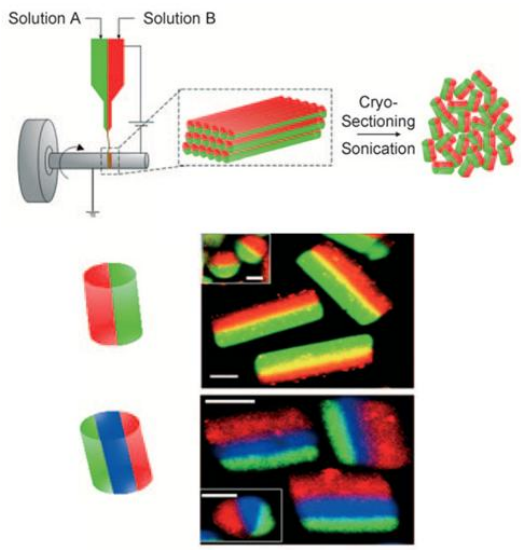

Figure 4.3: Microcylinders created from microtoming of EHD cojetted fibers. Bi and triphasic cylinders are possible (among other configurations) (reprinted and modified with permission from Bhaskar et al.)[27]

We took advantage of this platform to create a bioactuator. We jetted biphasic fibers (with one phase featuring either an acetylene or cyclooctyne functional group) constructed out of PLGA-PLGA/PLCL (e.g., one phase was PLGA-PLA, while the other phase was PLCL) and cut them into microcylinders. PLCL was used to provide increased flexability for bioactuation. With one side functionalized with PEG, we would prevent cells such as cardiomyocytes from binding to half of the cylinder – providing the critical anisotropy needed for uniaxial actuation. In order to promote cell adhesion to the other phase, the microcylinders were incubated with a solution of fibronectin. Fibronectin, a sticky and large protein, adsorbed to the phase not containing PEG. After we created our microactuators, we incubated them with rat neonatal cardiomyocytes until they began to contract, and then imaged and took videos via confocal microscopy. Fig. 4.4 shows step-by-step the process we used for creating our bioactuators.

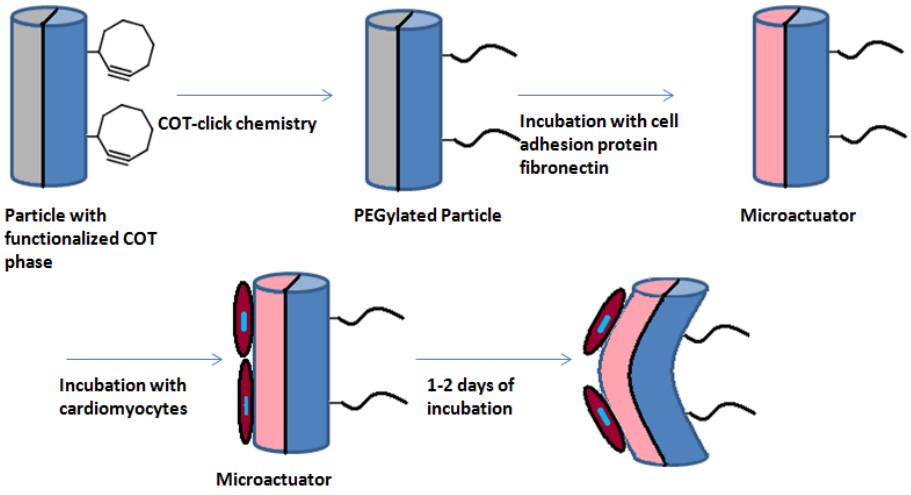

Figure 4.4: Microcylinder actuator schematic (based on a previous figure by Dr. Jaewon Yoon)[29]

In a survey of the literature, no one has yet constructed a free-floating bioactuator or biorobot with the dimensions reported here. The closest is a 20 μm diameter/40-45 μm long microcylinder propelled by attached bacteria via flagellar motion[28]. Significantly, this microcylinder also uses an anisotropic design strategy – by attaching Pluronic block copolymer F108 (a PEG triblock copolymer) to the sides of the cylinder (but not the back end), bacteria only attach to the end of the cylinder to propel it[28]. This does not really meet the definition of an actuator per se, as the bacteria are not deforming the material itself, but rather translating the entire device from one point to another[28].

In creating our microcylinder bioactuators, we came up with a series of experiments to characterize and demonstrate that they selectively adhere proteins and cells to one side due to their anisotropic properties. We first hypothesized that *EHD jetted biphasic fibers and microcylinders conjugated with PEG on one phase will only adsorb protein on the other phase.* We tested this hypothesis by incubating PEGylated fibers and cylinders (along with an unPEGylated control) with a fluorescently labeled protein, then observing where the protein binds. This hypothesis would be validated if the protein only attaches to the side without PEG. Next, we hypothesized that *cells will only attach to one side of the biphasic fibers*

and microcylinders if PEG is conjugated onto the other side and will attach to both phases indiscriminately if PEG is not present. We tested this hypothesis by incubating fibers and cylinders with NIH3T3 fibroblasts. This was done before using cardiomyocytes because we wanted to validate that cells would selectively bind the fibers and microcylinders before moving on to the far more sensitive and expensive cardiomyocytes. Finally, we hypothesized that *cardiomyocytes attached to biphasic microcylinders will only bind to the side not featuring PEG, will retain their ability to contract on microcylinders, and will be able to bend them inward as they contract*. We support this hypothesis by incubating the microcylinders with neonatal rat cardiomyocytes, then observing them in culture with a confocal microscope. The three hypotheses follow in logical order of complexity (from protein to simple fibroblasts to cardiomyocytes) and validate the most important aspect of our work: the anisotropy of our material and how this property translates to an anisotropic distribution of protein and cells.

Experimental Section

Parts of this experimental section were paraphrased from original text by collaborator Dr. Jaewon Yoon[29]

Fabrication of Bicompartmental Microfibers

Several different microcylinder polymer formulations were used throughout this work. For BSA incubation, 30% w/v PLGA and 30% w/v PLGA + 9% w/v COT-PLA with a blue dye (poly[(*m*-phenylenevinylene)-*alt*-(2,5-dihexyloxy-*p*-phenylenevinylene)]) were individually dissolved in a solvent mixture of chloroform and DMF (chloroform:DMF 95:5 (v/v)). For NIH3T3 cell incubation, 30% w/v PLGA + 0.9% w/v magnetite and 30% w/v PLGA + 9% w/v COT-PLA with a blue dye (poly[(*m*-phenylenevinylene)-*alt*-(2,5-dihexyloxy-*p*-phenylenevinylene)]) were individually dissolved in a solvent mixture of chloroform and DMF (chloroform:DMF 95:5 (v/v)). For cardiomyocytes bioactuators, a 25% w/v solution of PLCL with 7.5% w/v of iron oxide nanocrystals (3% by weight of PLGA) was dissolved in a solvent mixture of chloroform, cyclohexane and DMF (45:50:5, v/v/v), and a 30% w/v solution of PLGA and 9% w/v of COT-PLA was dissolved separately into a solvent of chloroform/DMF (95/5 v/v). A syringe pump (Fisher Scientific, Inc., USA), rotary collector, and powers supply (DC voltage, Gamma High Voltage Research, USA) comprised the electrohydrodynamic jetting station set-up. The polymers were put into vertically positioned syringes, and set to flow at a constant rate of 0.05 ml/hr through 26 G needles (Hamilton Company, USA). A Taylor cone was emitted from the liquid at the end of the needles after application of a 11-12 kV driving voltage, and collection occurred at a 7 cm distance.

Fabrication of Bicompartmental Microcylinders

Microfibers were sectioned using a cryostat microtome (Microm HM550, Thermo Fisher Scientific Inc., USA) after placement in a cryostat mold along with a freezing medium. After sectioning, the resulting microcylinders underwent washing with a solution of 0.01% v/v Tween in deionized (DI) water to remove the freezing medium.

Selective Surface Modification via Copper-Free Click Chemistry

Glass coverslips were PEGylated using atom transfer radical polymerization (ATRP) of oligo(ethyleneglycol) methacrylate (OEGMA) to form PEGMA in order to prevent unwanted cell and protein adhesion. After collection on these modified glass coverslips, microfibers functionalized with cyclooctyne (COT) were taped down and submerged in a 45 mg/ml deionized water solution of 8-armed PEG azide. The resulting click reaction took place at gentle agitation for 24 hours at room temperature, and leftover reactant was removed with a 0.01% v/v Tween20 solution in DI water. Microcylinders were PEGylated via a COT reaction in much the same fashion – ~50,000 microcylinders were placed in a 1.5 ml Eppendorf tube with a 45 mg/ml 8-armed PEG azide and 0.01% v/v Tween20 solution and rotated for 24 hours at room temperature.

Bovine Serum Albumin (BSA) Incubation

PEGylated microfibers on PEGMA-coated glass substrates were incubated with a solution of 100 μg/ml of bovine serum albumin (BSA) dissolved in phosphate buffer saline (PBS) at room temperature for 3 hours. These were washed with a 0.01% v/v Tween20 solution in PBS to remove unadsorbed BSA, and then imaged using a confocal microscope.

Incubation of NIH3T3 Fibroblasts on Microfibers

Microfibers were taped with double-sided tape to PEGMA-coated glass slides and incubated with a 50 μg/ml solution of fibronectin (FN) in PBS at room temperature for 1 hr under gentle orbital rotation. These were washed with PBS three times for 5 minutes each, then incubated with 1 ml of NIH3T3 cells (3.8×10^5 cells/ml at passage 1) for 6 hr in serum-free medium (DMEM). After incubation (6 hr), the cells were fixed with 4% paraformaldehyde in DPBS, stained with 1 μl/ml of cytocalasin D, and imaged using a confocal microscope.

NIH3T3 culture with cylinders

Cylinders were sterilized under a UV lamp overnight, and then incubated with 0.1 mg/ml of human fibronectin dissolved in H_2O at room temperature for one hour on a rotator. After washing the cylinders three times with DPBS at five minute increments, NIH3T3 cells (ATCC) at passages 3-5 (range over multiple trials; passages were not mixed for individual experiments) were thawed, centrifuged, and resuspended in DMEM (ATCC) + 10% calf bovine serum (ATCC). 3.8×10^5 cells/vial were incubated with the cylinders and rotated for 5 hr in a 5% CO_2 incubator at 37°C, after which they were transferred to a stationary PEG-coated glass surface on a 12 well plate and incubated in media under the same conditions as rotation. After 5 hr, the cells were fixed in 4% formaldehyde for 15 minutes at room temperature.

Rat Cardiomyocytes with Cylinders

Cylinders were sterilized under a UV lamp overnight, and then incubated with 0.1 mg/ml of human fibronectin dissolved in H_2O at room temperature for one hour on a rotator. After washing the cylinders three times with DPBS at five minute increments, neonatal rat cardiomyocytes (Lonza)

were thawed and carefully resuspended drop-by-drop (to avoid osmotic shock) in Rat Cardiac Myocyte Cell Medium (Lonza) supplemented with 5-bromo-2'deoxyuridine in order to prevent fibroblast proliferation. 80% of the media was replaced after 4 hr to remove dead cells, and thereafter if necessary 50% of the media was replaced every 72 hr. 8×10^5 cells/vial were incubated with the cylinders and rotated for various times in a 5% CO_2 incubator at 37°C, after which they were transferred to a 24-well plate for the remainder of the experiment. In some trials, 24 hours before imaging/filming via confocal microscope, 1 μmol/L of aldosterone dissolved in ethanol was added to the media in order to enhance cardiomyocyte beating. Some samples were stained with 15 μM of CellTracker Green CMFDA for 1 hr before imaging. Some samples were also fixed in 4% formaldehyde for 15 minutes at room temperature.

Results

Preliminary work was done with biphasic PLGA fibers, with one phase functionalized with acytalene for copper-catalyzed Huisgen's 1,3-dipolar cycloaddition (referred to as 'PLGA/PLGA-acetylene'). However, PLGA is too stiff of a material for cardiomyocytes to bend, as PLGA is a relatively inflexible material[30]. Previous work indicated that poly(L-lactide-co-caprolactone) (PLCA or PLCL) was far more flexible, and that blended with PLGA could result in materials less stiff than pure PLGA, but with better tensile strength than pure PLCL[31]. Pure PLCL microcylinders however were observed to deform during cell culture (performed at 37°C for multiple days). In addition, there was a desire to avoid using copper as a catalyst as copper is cytotoxic to cells[32]. Thus, the fiber composition was changed. While still biphasic, one phase is now a blend of PLGA and PLA (polylactic acid)-COT (cyclooctyne), while the other phase is pure poly(L-lactide-co-caprolactone) (PLCL). As discussed earlier, COT can undergo a strain-promoted azide-alkyne cycloaddition reaction similar to 1,3-dipolar cycloaddition, except a copper catalyst is not required[32]. Biphasic PLGA/PLCL fibers were measured to have far greater elasticity and lower Young's moduli than fibers composed of pure PLGA (data not shown)[29]. Microcylinders made from PLGA-PLA-COT/PLCL were subsequently picked as the ideal substrate for a cardiomyocyte bioactuator. These microcylinders maintained their shape after incubation at 37°C for several days, while microcylinders composed of pure PLCL slowly seemed to deform and melt (data not shown). For the initial experiments with bovine serum albumin and NIH3T3 fibroblast incubation, we use a slightly different formulation that does not include PLCL, as we do not need the added flexibility of this polymer for those projects. For the bovine serum albumin incubation experiments, we used microfibers and microcylinders composed of 30% w/v PLGA and 30% w/v PLGA + 9% w/v COT-PLA. For the NIH3T3 fibroblast incubation experiments, we used microcylinders composed

of 30% w/v PLGA + 0.9% w/v magnetite and 30% w/v PLGA + 9% w/v COT-PLA – the addition of magnetite was useful for both observing and isolating the microcylinders via a magnet.

To demonstrate that the PEGylated phase of the anisotropic fibers and cylinders effectively resisted protein adsorption, fibers were incubated with 200 μg/ml of Alexa Fluor 647-bovine serum albumin (647-BSA) for 3 hrs. Albumin is known for being a 'sticky' protein that binds to a large variety of other materials, so it is a good control for all protein binding [33]. Fibronectin has also been characterized as sticky [34]. A UV-fluorescent dye (poly[(*m*-phenylenevinylene)-*alt*-(2,5-dihexyloxy-*p*-phenylenevinylene)] - colored blue with the confocal microscope software) was included with the phase which was PEGylated to highlight the region which should be resistant to protein adsorption. 647-BSA bound to both sides of an unPEGylated fiber (Fig. 4.5-a), as expected. However, after PEG was "clicked" on using a copper-free cyclooctene (COT) reaction, 647-BSA only bound to the side which did not contain PEG (Fig. 4.5-b). This result was repeated with cylinders composed of the same polymers and also PEGylated on the blue-fluorescent side.

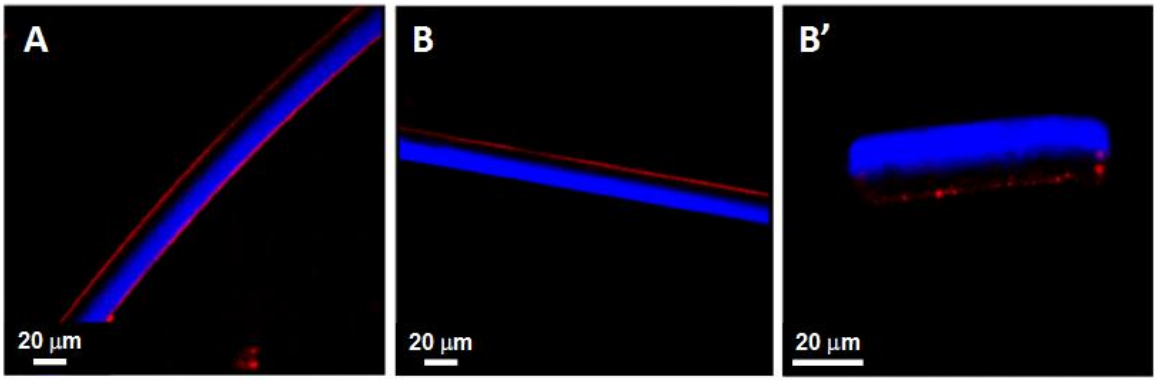

Figure 4.5: Confocal microscopy after 647-BSA incubation with (a) PLGA-PLA-COT/PLGA fiber without PEG (b) PLGA-PLA-COT/PLGA fiber with PEG (b') PLGA-PLA-COT/PLGA microcylinder with PEG (figure and experiment performed by Dr. Jaewon Yoon)[29]

This same experiment was earlier performed with PLGA/PLGA-acetylated fibers, with similar results (Fig. 4.6).

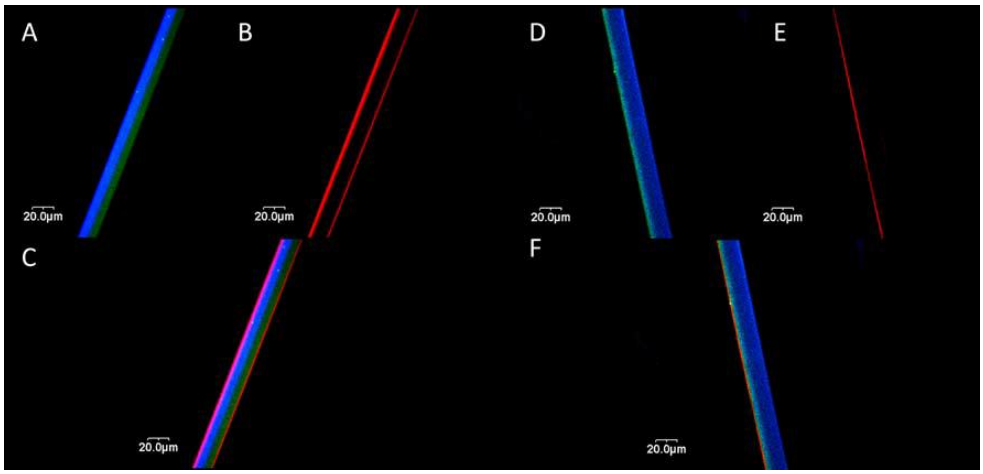

Figure 4.6: Confocal microscope demonstrating selectivity of PEG-modified PLGA fibers to protein adsorption. (a) PLGA/PLGA-acetylene fiber without PEG, (b) Alexa Fluor 647-BSA present on both sides, (c) compilation image, (d) PLGA/PLGA-acetylene fiber with clicked PEG on blue-stained side, (e) Alexa Fluor 647-BSA only attached to phase lacking PEG (stained green), (f) compilation image (experiment performed by Dr. Jaewon Yoon)

Before using cardiomyocytes (which cannot typically proliferate, making expansion in culture impossible and thus necessitating a newly purchased stock for each experiment), the fibers and microcylinders were tested for single-compartment cell selectivity using NIH3T3 fibroblasts. The NIH3T3 fibroblast line was derived from mouse embryonic tissue by Todaro and Green in an effort to establish new cell lines - they spontaneously became immortalized and are now a model fibroblast cell line [35]. They grow quickly, are hardy, and have simple media requirements (DMEM + 10% calf bovine serum). Cells were first cultured with fibers taped across PEGMA-coated glass slides (PEGMA prevents unwanted cell adhesion to the bottom of the well plate, which otherwise due to surface area would outcompete the fibers for cells). This was done to confirm the cell-selectivity of the jetted material, before moving on to the more complicated culture with microcylinders. When cultured with PLGA/PLGA-acetylene fibers clicked with PEG and subsequently incubated with fibronectin (100 μg/ml in H_2O for 1 hr at room temperature), they demonstrated some moderate

selectivity for the nonPEGylated side, though there were examples where cells were still found bound to the PEGylated side (Fig. 4.7).

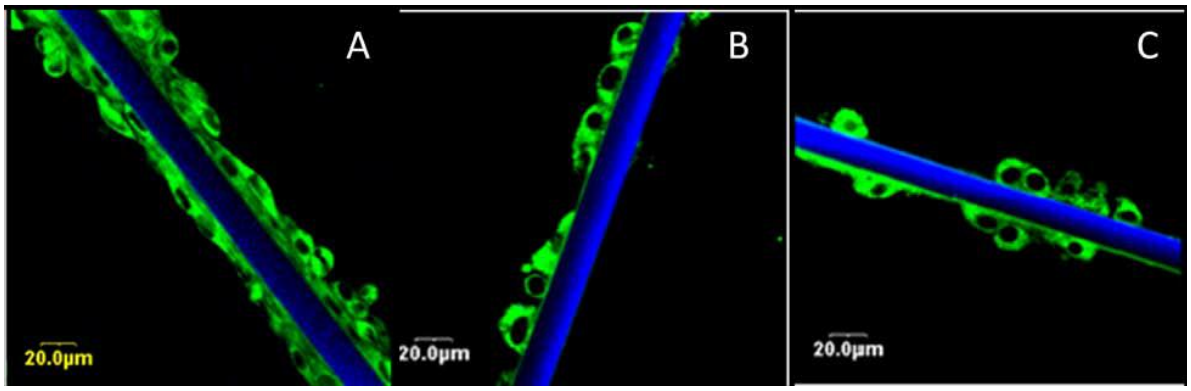

Figure 4.7: Confocal microscope demonstrating selectivity of PEG-modified PLGA fibers to cell adhesion (a) PLGA/PLGA-acetylene fiber without PEG incubated with NIH3T3 fibroblasts; note that cells readily attach to both sides (b) PLGA/PLGA-acetylene fiber with PEG; now cells are specific to one side (c) PLGA/PLGA-acetylene fiber with PEG and cells

However, NIH3T3 fibroblasts incubated with PLGA-PLA-COT/PLGA microcylinders were incredibly side-specific (Fig. 4.8). It was found that rotating the NIH3T3 cells first in an Eppendorf tube with the cylinders for five hours, followed by depositing them onto a static well plate with a PEGMA-coated glass substrate bottom covering (to prevent fibroblast adhesion to the well plate surface) lead to optimal cell attachment. Almost all the cells were found bound to the side PEGylated, with only a minimal number of contrarian counterexamples. Magnetite (a natural mineral composed mainly of iron oxides such as Fe_3O_4)[36] was added to the PLGA phase in order to provide further contrast for microscopy, and to create an easy method for isolating microcylinders when they were suspended in solution by simply pulling them to the wall of the Eppendorf tube with a powerful magnet (very useful when washing them after fibronectin incubation, or media changes). While not exploited further in this thesis, this incidentally leads to the creation of anisotropic magnetic cell transporters or building blocks, which in theory could be manipulated with

magnetic fields to move to a particular place and be isolated (perhaps for further experiments on individual cells), or to assemble a structure.

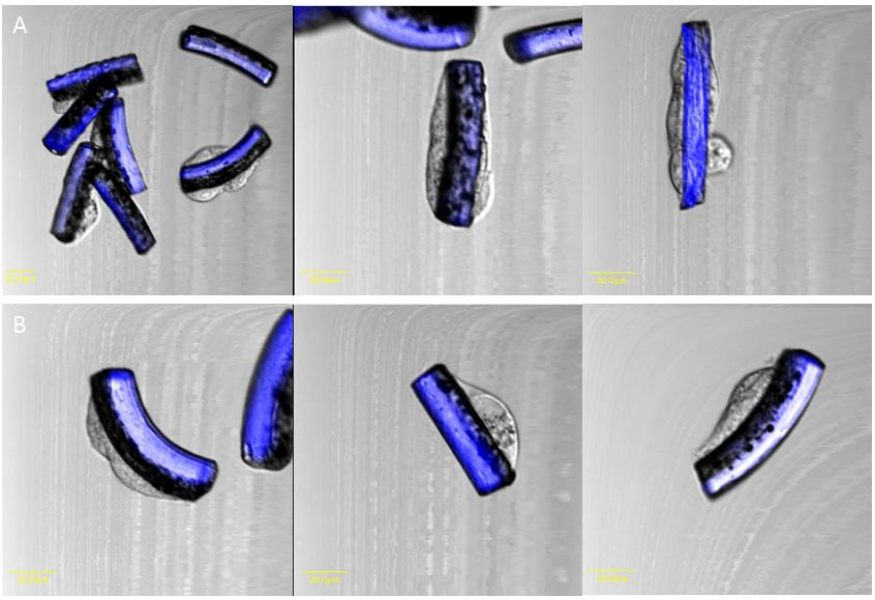

Figure 4.8: Confocal microscope demonstrating selectivity of PEG-modified PLGA-PLA-COT/PLGA microcylinders to cell adhesion (a) PLGA-PLA-COT/PLGA microcylinders without PEG incubated with NIH3T3 fibroblasts; cells readily attach to both sides (b) PLGA-PLA-COT/PLGA microcylinders with PEG; now cells are specific to one side

Upon successful selective attachment of NIH3T3 cells, PLGA-PLA-COT/PLCL microcylinders were incubated with neonatal rat cardiomyocytes (purchased from Lonza). Cardiomyocytes cannot normally divide in culture (though there exist the immortalized line HL-1 which can divide and continues to spontaneously contract, these are difficult to obtain), so these experiments were performed with a fresh vial of cardiomyocytes each time[37]. We continued to incubate our microcylinders in fibronectin in order to attach cardiomyocytes, though laminin has also been used[14].

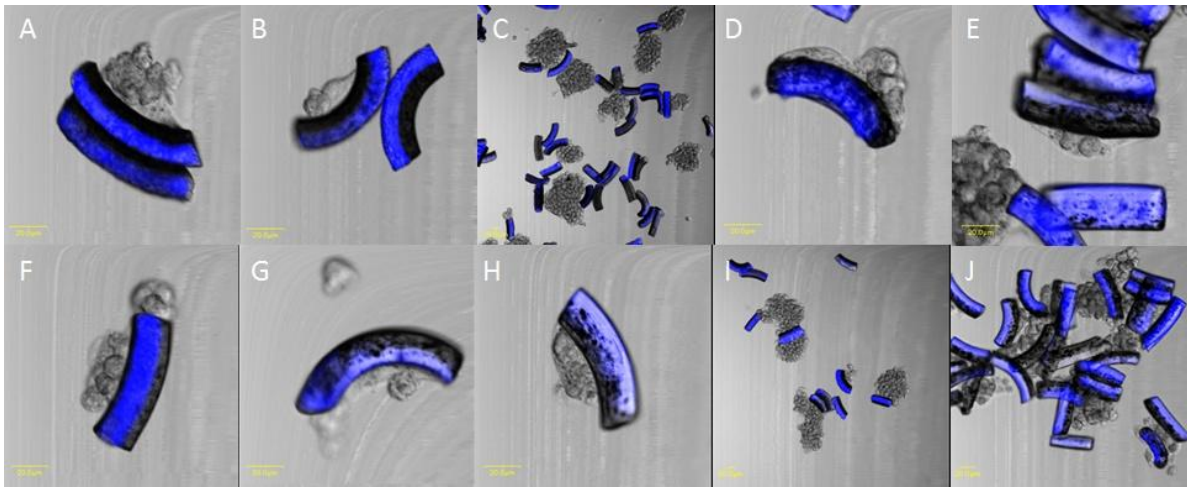

Figure 4.9: Microcylinders cultured with cardiomyocytes. PEG (when present) is on the blue side. Cells primarily attach to the non-PEGylated side on PEGylated cylinders (a-e), while on non-PEGylated micocylinders (f-j) cells can be observed attaching to either side more often.

Cardiomyocytes were first allowed to rotate with the cylinders for 8 hours, and then were deposited onto well plates with PEGMA substrates (to prevent unwanted attachment) for 16 hours before imaging. As shown in Fig. 4.9, cardiomyocytes prefer to attach to the non-PEGylated side on PEGylated cylinders (Fig. 4.9, a-e), while on non-PEGylated cylinders cardiomyocytes may be observed binding to either side (Fig. 4.9, f-j, especially Fig 4.9-g). Of course, there were counterexamples present as well (see Fig. 4.9, c), but overall this pattern held for the majority of cylinders observed. Generally, there were fewer cells on the blue-stained side even when not PEGylated, in comparison to the NIH3T3 experiments. As expected, the cardiomyocytes would spontaneously contract on the microcylinders.

It became apparent that the amount of time we allowed cells to incubate on the rotator versus on a static well plate needed to be optimized. We cultured cardiomyocytes with PEGylated PLGA-PLA-COT/PLCL cylinders and rotated them for 24, 48, and 72 hr. The 24 hr sample was then incubated in a well plate for 48 hr, the 48 hr sample in a well plate for 24 hr, and the 72 hr sample was not

incubated at all in a well plate. In this experiment, cardiomyocytes were stained with 15 μM of CellTracker Green CMFDA for 1 hr before imaging, in order to better differentiate them from the other components present in the media.

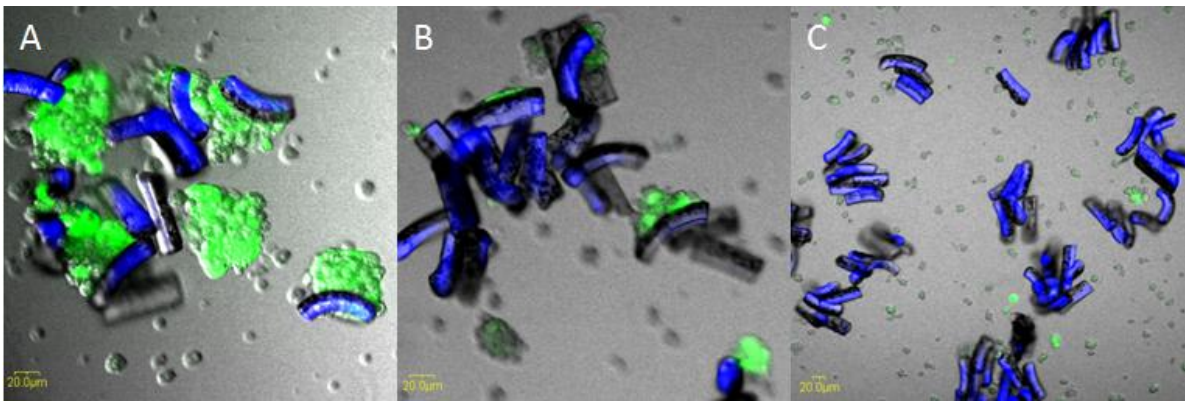

Figure 4.10: Cardiomyocytes (a) rotated for 24 hr and incubated in a well plate for 48 hr, (b) rotated for 48 hr and incubated in a well plate for 24 hr, and (c) rotated for 72 hr with no subsequent well plate incubation

Cardiomyocytes rotated for 24 hr and incubated on well plates for 48 hr (Fig. 4.10-a) showed the highest amount of cell attachment, with cardiomyocytes often forming large aggregates of cells on the microcylinders. These aggregates were commonly observed through all experiments, and would often beat. Cardiomyocytes rotated for 48 hr and incubated on well plates for only 24 hr still showed cell adhesion to the microcylinders, but it was overall lower than that for the 24 hr rotated/48 hr well plate samples with far fewer aggregates. Cardiomyocytes rotated for 72 hr with no subsequent well plate incubation were mostly found still suspended in the media and completely unattached to the microcylinders, with a few exceptions. Thus, it seems that by varying the time spent rotating versus the time spent in an incubator, we can control and optimize the amount of cell adhesion and aggregation on our microcylinders.

Beating frequency and contractile force was found to be further optimized by the addition of 1 μmol/L aldosterone 24 hours before inspection – aldosterone has been previously demonstrated to

raise neonatal rat cardiomyocyte's beating frequency[38]. Cardiomyocytes were rotated for 8 hr, then transferred to a well plate and allowed to incubate for roughly 72 hours before imaging. We took many movies via confocal microscopy to observe the cardiomyocytes beating, in an attempt to capture one bending a microcylinder and thus functioning as a bioactuator. After finding one, we analyzed it using software to determine the extent of bending (Fig. 4.11).

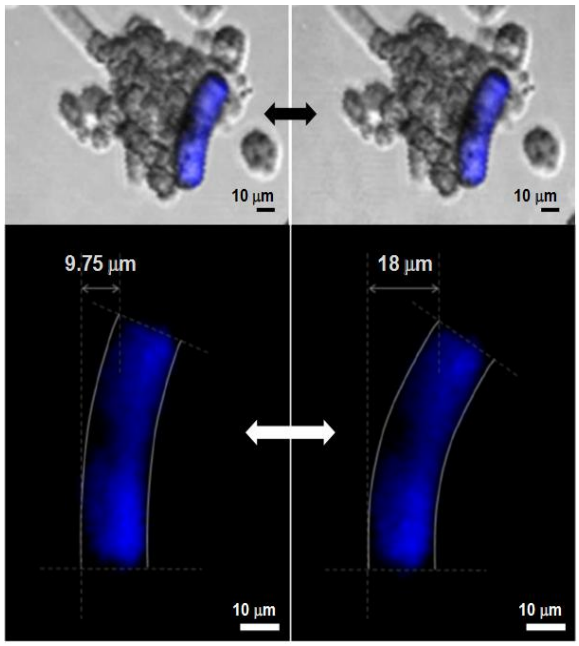

Figure 4.11: Cardiomyocytes after rotation and well plate incubation bending a microcylinder (figure by Dr. Jaewon Yoon, modified)[29]

By fixing the bottom left corner of the cylinder and looking at the movie frame-by-frame, we could measure the extent of displacement performed by the cardiomyocytes. The cylinder's upper displacement was nearly double that of its initial starting point. With fixing the bottom to estimate the amount of displacement by the top, the stress can be modeled like that for a micropillar, which has been worked out by Tan et al. (Fig. 4.12)[39]. This equation assumes that the cells bending the microcylinder are concentrating their force on the top, which is not entirely true – nevertheless, it is

a reasonable first approximation, and the force needed to bend it from the sides would be even higher according to Tanaka et al. [23].

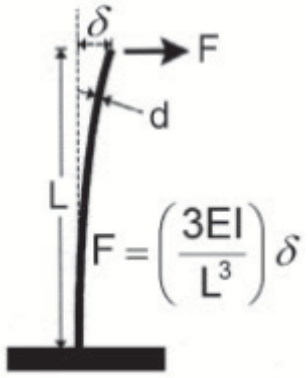

Figure 4.12: Model for calculating the amount of force needed to bend a micropillar (reprinted with permission from Tan et al.)[39]

Here, L is the length of the microcylinder, I is the geometric moment of inertia (here $\pi d^4/64$ for a bending bar, where d is the diameter of the microcylinder,)[24], δ is the cylinder's upper displacement, and E is the Young's modulus of the microcylinder[39]. We measured E to be 476 ± 31 MPa, L is 78.5 μm, d is 20 μm, I is 7.854 x 10^{-21} m^4, and δ is 8.25 μm. The following equation is then used to calculate the force of displacement[39]:

$$F = \left(\frac{3EI}{L^3}\right)\delta$$

From this, we get a total force of 191 ±12 μN. This is very large in comparison to those measured for other bioactuators, but not surprising given that our biomicroactuators have a far greater number of cardiomyocytes tethered in comparison. For example, Akiyama's dorsal vessel tissue robot exerted a force of 4.7 μN for bending of their microcylinders (though they were calculating the contracting force at the center of the pillar rather than the top)[24]. Tanaka's peg micropillars were bent with a force of 3.8 μN, which is unsurprising given that they only have one or a few cardiomyocytes attached [23]. Nishimura et al. averaged the amount of force generated by a single

adult rat cardiomyocyte (with a population of 18 measured) with isometric conditions as 5.720 ±0.41 μN [40]. Visual inspection of the cylinder reveals there are ~ 26 cardiomyocytes attached (this is a rough figure), giving them an average individual force of ~7.3 μN. This is not too far from the forces measured by Nishimura et al. for a single cardiomyocyte. Unfortunately, the number of experiments undertaken with the aldosterone added was limited, and we could only isolate this single cylinder in film for analysis. Clearly, more experiments are necessary for further analysis and measurement of more bending forces.

Conclusions and Future Work

Bioactuators are a novel idea for confronting some of the issues that face traditional bioactuators. As shown by several previous groups, material anisotropy can be very important for creating a functional bioactuator. We have successfully used EHD-cojetting to create a biphasic fiber to which cells are selective for only one side. While Mandel et al. have accomplished this as well, we took it a step further by also developing key protocols for attaching our cells to microcylinders created via microtoming and rotation culture[22]. In essence we created a sort of magnetized cell carrier, which in itself is an accomplishment. Finally, we cultured these microcylinders with neonatal rat cardiomyocytes, and while we need to further optimize our protocols for creating successful microcylinder-cardiomyocyte hybrids that bend, we were able to isolate and take video of one actuating. This is one of the smallest free floating bioactuators that has been developed by any group. The force generated by our bioactuator was measured to be much higher than that of those previously reported in the literature, chiefly due to the far larger number of cardiomyocytes present in comparison. All three hypotheses posited have been supported by the experiments performed herein.

For future work, as previously pointed out further experiments are needed to optimize and continue to observe other cardiomyocytes bending our cylinders. Furthermore, it would be a good idea to try other compounds to further stimulate beating force and frequency – while aldosterone worked well, compounds such as epinephrine could also be used (Baar et al. measured that application of epinephrine to a culture of cardiomyocytes increased force production by 253 ± 58%)[41]. It is true that not every PEGylated fiber and microcylinder was cell selective, but after optimization the majorities observed were. It would be beneficial to optimize this further. Finally, other contracting cell types previously mentioned such as C2C12 could be used in addition to cardiomyocytes –

skeletal muscle may be preferable as it does not spontaneously contract and is thus easier to control with an outside electrical stimulus.

References

1. Bell, D.J., Lu, T.J., Fleck, N.A. & Spearing, S.M. MEMS actuators and sensors: observations on their performance and selection for purpose. *J Micromech Microeng* **15**, S153-S164 (2005).
2. Ricotti, L. & Menciassi, A. Bio-hybrid muscle cell-based actuators. *Biomedical microdevices* **14**, 987-998 (2012).
3. Anquetil, P.A., Rinderknecht, D., Vandesteeg, N.A., Madden, J.D. & Hunter, I.W. Large strain actuation in polypyrrole actuators. *P Soc Photo-Opt Ins* **5385**, 380-387 (2004).
4. Spinks, G.M., Liu, L., Wallace, G.G. & Zhou, D.Z. Strain response from polypyrrole actuators under load. *Advanced functional materials* **12**, 437-440 (2002).
5. Kuttel, C., Stemmer, A. & Wei, X. Strain response of polypyrrole actuators induced by redox agents in solution. *Sensor Actuat B-Chem* **141**, 478-484 (2009).
6. Feinberg, A.W. et al. Muscular thin films for building actuators and powering devices. *Science* **317**, 1366-1370 (2007).
7. Xi, J., Schmidt, J.J. & Montemagno, C.D. Self-assembled microdevices driven by muscle. *Nature materials* **4**, 180-184 (2005).
8. Woledge, R.C., Curtin, N.A. & Homsher, E. Energetic aspects of muscle contraction. (Academic Press, London ; Orlando; 1985).
9. Herr, H. & Dennis, R.G. A swimming robot actuated by living muscle tissue. *Journal of neuroengineering and rehabilitation* **1**, 6 (2004).
10. Shimizu, K. et al. Multi-scale Reconstruction and Performance of Insect Muscle Powered Bioactuator from Tissue to Cell Sheet. *2010 3rd Ieee Ras and Embs International Conference on Biomedical Robotics and Biomechatronics*, 425-430 (2010).
11. Johnson, J.A. & Mochly-Rosen, D. Inhibition of the spontaneous rate of contraction of neonatal cardiac myocytes by protein kinase C isozymes. A putative role for the epsilon isozyme. *Circulation research* **76**, 654-663 (1995).
12. Mitcheson, J.S., Hancox, J.C. & Levi, A.J. Cultured adult cardiac myocytes: Future applications, culture methods, morphological and electrophysiological properties. *Cardiovascular research* **39**, 280-300 (1998).
13. Agarwal, A., Goss, J.A., Cho, A., McCain, M.L. & Parker, K.K. Microfluidic heart on a chip for higher throughput pharmacological studies. *Lab on a chip* (2013).
14. Tanaka, Y. et al. Demonstration of a bio-microactuator powered by vascular smooth muscle cells coupled to polymer micropillars. *Lab on a chip* **8**, 58-61 (2008).
15. Sun, Y., Duffy, R., Lee, A. & Feinberg, A.W. Optimizing the structure and contractility of engineered skeletal muscle thin films. *Acta biomaterialia* **9**, 7885-7894 (2013).
16. Nawroth, J.C. et al. A tissue-engineered jellyfish with biomimetic propulsion. *Nature biotechnology* **30**, 792-797 (2012).
17. Hoshino, T., Imagawa, K., Akiyama, Y. & Morishima, K. Cardiomyocyte-driven gel network for bio mechano-informatic wet robotics. *Biomedical microdevices* **14**, 969-977 (2012).
18. Bhaskar, S., Roh, K.H., Jiang, X.W., Baker, G.L. & Lahann, J. Spatioselective Modification of Bicompartmental Polymer Particles and Fibers via Huisgen 1, 3-Dipolar Cycloaddition (vol 29, pg 1655, 2008). *Macromolecular rapid communications* **29**, 1973-1973 (2008).
19. Yarin, A.L., Koombhongse, S. & Reneker, D.H. Taylor cone and jetting from liquid droplets in electrospinning of nanofibers. *J Appl Phys* **90**, 4836-4846 (2001).

20. Kaul, P.B., Singh, U. & Prakash, V. In situ Characterization of Nanomechanical Behavior of Free-standing Nanostructures. *Exp Mech* **49**, 191-205 (2009).
21. Andrady, A.L. & Wiley online library. Science and technology of polymer nanofibers. (Wiley, Hoboken, N.J.; 2008).
22. Mandal, S., Bhaskar, S. & Lahann, J. Micropatterned Fiber Scaffolds for Spatially Controlled Cell Adhesion. *Macromolecular rapid communications* **30**, 1638-1644 (2009).
23. Tanaka, Y. et al. Demonstration of a PDMS-based bio-microactuator using cultured cardiomyocytes to drive polymer micropillars. *Lab on a chip* **6**, 230-235 (2006).
24. Akiyama, Y., Iwabuchi, K., Furukawa, Y. & Morishima, K. Long-term and room temperature operable bioactuator powered by insect dorsal vessel tissue. *Lab on a chip* **9**, 140-144 (2009).
25. Morishima, K. et al. Demonstration of a bio-microactuator powered by cultured cardiomyocytes coupled to hydrogel micropillars. *Sensor Actuat B-Chem* **119**, 345-350 (2006).
26. Akiyama, Y., Hoshino, T., Iwabuchi, K. & Morishima, K. Room Temperature Operable Autonomously Moving Bio-Microrobot Powered by Insect Dorsal Vessel Tissue. *PloS one* **7** (2012).
27. Bhaskar, S., Hitt, J., Chang, S.W.L. & Lahann, J. Multicompartmental Microcylinders. *Angew Chem Int Edit* **48**, 4589-4593 (2009).
28. Behkam, B. & Sitti, M. Bacterial Propulsion of Chemically Patterned Micro-Cylinders. *P Ieee Ras-Embs Int*, 841-845 (2008).
29. Yoon, J. 2013).
30. Tran, R.T. et al. Synthesis and characterization of a biodegradable elastomer featuring a dual crosslinking mechanism. *Soft Matter* **6**, 2449-2461 (2010).
31. Wang, L.S., Zhang, Z.P., Chen, H.C., Zhang, S.L. & Xiong, C.D. Preparation and characterization of biodegradable thermoplastic Elastomers (PLCA/PLGA blends). *J Polym Res* **17**, 77-82 (2010).
32. Agard, N.J., Prescher, J.A. & Bertozzi, C.R. A strain-promoted [3+2] azide-alkyne cycloaddition for covalent modification of blomolecules in living systems. *Journal of the American Chemical Society* **126**, 15046-15047 (2004).
33. Dixon, R. & Brunskill, N.J. Albumin stimulates p44/p42 extracellular-signal-regulated mitogen-activated protein kinase in opossum kidney proximal tubular cells. *Clin Sci (Lond)* **98**, 295-301 (2000).
34. Wu, C.S. & Chen, G.C. Adsorption of proteins onto glass surfaces and its effect on the intensity of circular dichroism spectra. *Analytical biochemistry* **177**, 178-182 (1989).
35. Todaro, G.J. & Green, H. Quantitative studies of the growth of mouse embryo cells in culture and their development into established lines. *The Journal of cell biology* **17**, 299-313 (1963).
36. Harrison, R.J., Dunin-Borkowski, R.E. & Putnis, A. Direct imaging of nanoscale magnetic interactions in minerals. *Proceedings of the National Academy of Sciences of the United States of America* **99**, 16556-16561 (2002).
37. Claycomb, W.C. et al. HL-1 cells: A cardiac muscle cell line that contracts and retains phenotypic characteristics of the adult cardiomyocyte. *Proceedings of the National Academy of Sciences of the United States of America* **95**, 2979-2984 (1998).
38. Lalevee, N. et al. Aldosterone increases T-type calcium channel expression and in vitro beating frequency in neonatal rat cardiomyocytes. *Cardiovascular research* **67**, 216-224 (2005).
39. Tan, J.L. et al. Cells lying on a bed of microneedles: an approach to isolate mechanical force. *Proceedings of the National Academy of Sciences of the United States of America* **100**, 1484-1489 (2003).

40. Nishimura, S. et al. Single cell mechanics of rat cardiomyocytes under isometric, unloaded, and physiologically loaded conditions. *American journal of physiology. Heart and circulatory physiology* **287**, H196-202 (2004).
41. Baar, K. et al. Self-organization of rat cardiac cells into contractile 3-D cardiac tissue. *Faseb Journal* **18**, 275-+ (2004).

CHAPTER 5

Cell Sheet Engineering with PLGA Grid Scaffolding Generated via EHD Co-jetting

Overview

We use three-dimensional PLGA grid scaffolds to induce the formation of cell sheets. These scaffolds are constructed using electrohydrodynamic co-jetting and a programmable x-y collection stage. In the **Introduction and Background**, we examine how others generate cell sheets and their relative importance to the field of tissue engineering. The cell sheets currently created lack mechanical robustness, making it difficult to shape them into higher ordered structures (other than simply stacking them atop one another). We propose generating cell sheets that contain a PLGA grid, making them less flimsy and easier to manipulate by comparison to other cell sheets. We demonstrate this technology with a series of cell lines, beginning with fibroblasts and concluding with mesenchymal stem cells and keratinocytes. We examine such things as extracellular matrix protein deposition, dynamic gross cell morphology and organization as they form the sheets, and use co-culture techniques to create a keratinocyte sheet that otherwise would not form easily.

Introduction and Background – Tissue Engineering

As the name suggests, tissue engineering proposes the creation of designed functional tissue *de novo* and *ex vivo* for use in a clinical setting (potentially for repairing injured or diseased tissue, or even completely replacing a dysfunctional organ), or for better *in vitro* assays than 2D culture[1]. Given that allogenic sources for organs can be on short supply, the ability to recapitulate these tissues for patients would be a very powerful tool for medicine[2]. Native tissue is composed of a variety of cells,

structural proteins/proteoglycans/glycosaminoglycans/connective proteins/etc. that make up the extracellular matrix, and a vast number of proteins and small molecules that regulate the cells within [3]. The ECM is particularly important as it gives tissue its mechanical properties and serves as a scaffold onto which cells can attach while also playing an active role in regulating them through mechanotransduction and serving as a reservoir for growth factors [2-4]. The current paradigm for tissue engineering is then creating microenvironments which are composed of cells, a scaffold of some sort, and growth factors (Fig. 5.1); furthermore, how cells interact with each other, their scaffold, and the growth factors present greatly dictates the viability and behavior of the overall tissue construct [5].

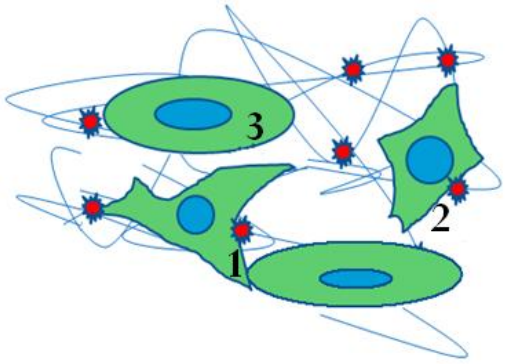

Figure 5.1: A conceptual framework for tissue engineering. Interactions between cells themselves (1), growth factors present (2), and their matrix (3) dictate outcome behavior

There are several important parameters when it comes to creating scaffolding for tissue engineering, and each must be optimized depending on the type of tissue being engineered. These include biocompatibility, geometry (i.e. the design of the structure needs some porosity for nutrient transport), and material properties such as stiffness/mechanical strength/flexibility/etc.[6]. It is also often desired for scaffolds to eventually degrade as the implanted engineered tissue creates its own matrix after surgery and becomes incorporated into the native tissue surrounding it[7]. The ability to promote cell adhesion and surface area can also be important parameters as well[7]. Collagen is often

used for creating scaffolding for tissue engineering, thanks to its biocompatibility and porosity[8]. The carbohydrate chitosan has also been used for creating scaffolds used to generate cartilage *in vitro* – like other materials, it was selected partly due to its biocompatibility and ease in processing[9]. There are advantages in creating scaffolds from a predetermined design –one can specify exactly the desired mechanical properties/architecture/etc. using a large array of available natural and synthetic materials (primarily biocompatible and biodegradable polymers such as PLGA) [6, 7]. Artificial materials have the advantage of being more customizable than natural structural proteins like collagen to the particular mechanical and microstructural needs of the engineered tissue, given that they are completely chemically defined and can be fine-tuned via functionalization or surface modification to alter how cells behave when attached to them[6]. PLGA is a common synthetic polymer which degrades into harmless lactic and glycolic acid – it is popular partly because of its approval by the FDA for implantation in people[7, 10]. PLGA also has other properties that make it appealing – it is a stiff material that is still easy to shape, and can be made very porous through several techniques (such as room-temperature compression molding/particulate leaching)[10]. Furthermore, its mechanical properties and rate of degradability can be tuned by adjusting the ratio of lactic to glycolic acid groups in the polymer (for example, increasing the amount of glycolic acid groups in PLGA will increase the degradation rate)[10]. Huang et al. used PLGA to create a scaffold embedded with poly(β-hydroxybutyrate-co-β-hydroxyvalerate) (PHBV), which was then seeded with hMSCs[11]. Cartilage-like engineered tissue has also been created using a PLGA-collagen hybrid scaffold seeded with hMSCs which were subsequently incubated in chodrogenic differentiation media[12]. These and many other examples demonstrate that PLGA is a widely used biomaterial for scaffolding able to host a large variety of cells. Other artificial materials used for tissue engineering include ceramics, other polymers such as poly(ε-caprolactone), and even metals[13-15].

Electrospinning has been heavily exploited for constructing scaffolds, given its ability to form meshes that have similar features to extracellular matrices[16, 17]. Many electrospun scaffolds are a matting of randomly oriented fibers, which cells are then seeded[18]. Yoshimoto et al. jets a randomly distributed PCL scaffold onto which they culture hMSCs that they go on to differentiate into osteocytes, while Shalumon et al. electrospins a blended scaffold of carboxymethyl chitin/poly(vinyl alcohol) (CMC/PVA) also for hMSC seeding [18, 19]. The random orientation of the fibers can be seen in Fig. 5.2. This can be an advantage, as it allows for the creation of a highly porous material that has a thickness on the order of hundreds of nanomaters and a high surface area[18-20].

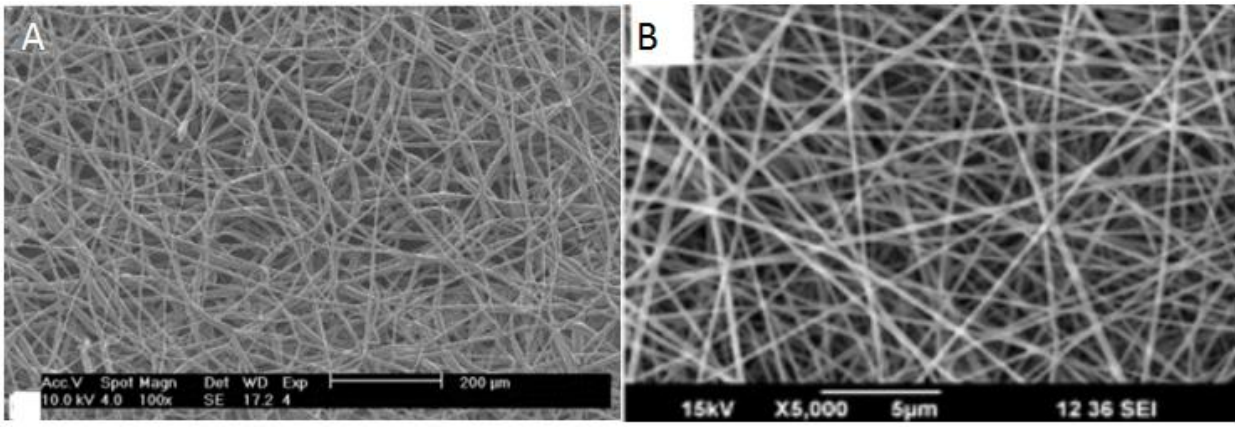

Figure 5.2: (a) PCL scaffold jetted by Yoshimoto et al, and (b) CMC/PVA scaffold jetted by Shalumon et al (figures used with permission by Yoshimoto et al. and Shalumon et al.)[18,19]

Melt electrospinning has also been used to create scaffolds for tissue engineering[21, 22]. Brown et al. was able to create patterned grid scaffolds from stacks of poly-(ε-caprolactone) (PCL) using melt electrospinning and a movable x-y stage – the resulting scaffolds could be composed of stacked fibers or a weave [21]. Tubular PCL scaffolds for bone tissue engineering were also generated using a similar technique (except with a rotating collector) – Brown et al. then cultured osteblasts on these scaffolds and demonstrated their ability to support the proliferation of cells [22]. While melt electrospinning does not require (potentially toxic) solvents, it has several disadvantages in comparison to electrohydrodynamic jetting – it normally requires high temperatures (which can

degrade the polymer or any drugs loaded into it for later release), and has only been performed with a limited number of polymers (listed by Hutmacher et al.) [23, 24].

Furthermore, scaffolds created via EHD-cojetting can be made multicompartmental and functionalized for further modification with proteins or peptides or other biomolecules (as discussed earlier) – as of the writing of this thesis, the author could find no examples of multicompartmental fibers generated by melt electrospinning in the literature[25]. Recently a collaborator set out to develop a similar technique for creating geometrically defined scaffolds *à la* Brown et al. (i.e. through the use of a movable x-y stage), except using EHD jetting instead of melt electrospinning. As before, instead of a rotating drum that simply collects the fibers, a stage moves at precise intervals (programmed via MATLAB) while the jet is descending from its Taylor cone. Thus, the jet deposits on the surface of the stage in a pattern. Furthermore, that pattern could be repeated, resulting in a stacked three dimensional structure (Fig. 5.3, b-d). A ring electrode was necessary in order to stabilize the jet. We used this apparatus to create PLGA stacks, in which the fibers were laid on top of one another in a continuous pattern (Fig. 5.3, b-d). While nearly any stacked geometric shape can be created with the right MATLAB program, the first was a simple square grid pattern, with each square having a side length of 750 μm. PLGA was chosen because of its mechanical strength and biocompatibility, along with a lack of brittleness (a PLGA scaffold created with this method can be easily manipulated with forceps, and rolled up into a tube or any other shape without breaking the fibers). This scaffold was created in order to produce intact sheets of cells that can be mechanically manipulated after formation.

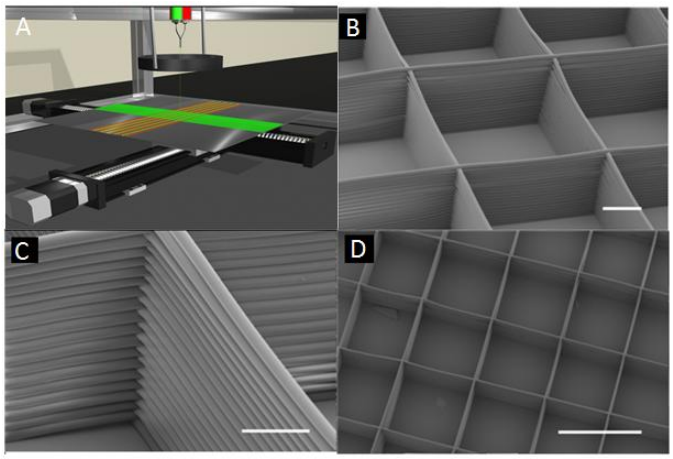

Figure 5.3: (a) Movable stage and ring electrode apparatus for controlled electrohydrodynamic jetting. (b-d) Various SEM images of stacked PLGA grid scaffolds (scale bars are 100 μm for b and c, 1 mm for d) (cartoon in (a) by Jacob Jordahl)

Cell Sheet Engineering

Tissue architecture can be conceptualized as a hierarchy in complexity, as Atala et al. propose[26]. The bottom of this hierarchy is the flat cell sheet, followed by rolling this structure into a tube shape for the simple transport of fluids such as blood (which feature two layers of cells with one acting as a barrier and the other acting as supportive tissue), then the formation of hollow shapes (like spheres or cylinders such as the stomach), and finally solid tissues and organs like the brain[26]. Thus, there has been a recent focus on engineering cell sheets for clinical applications, as they form a basic unit of tissue architecture and could be used like building blocks to create more complicated tissue shapes.

One method of creating cell sheets was developed by Teruo Okano at the Tokyo Women's Medical University. His group developed a method for isolating sheets of cells from 2D culture intact, along with their extracellular matrix without using any sort of proteolysis (e.g., trypsin)[27]. Furthermore, it requires no scaffold to support the sheet, as Okano et al. worried about the chances of it causing infection[28]. Instead, they grew the cells on a poly(N-isopropylacrylamide) surface (PIPAAm), which

has a tunable wettability depending on the temperature[29]. At temperatures below 32°C it shows a low contact angle (and is thus very hydrophilic), but above this temperature the surface rapidly becomes hydrophobic (this has to do with changes in the chain conformation which directly controls the level of hydration)[29]. When the surface is placed in a cooler temperature and becomes hydrophilic, the cells growing on top of it will detach as complete sheets along with their extracellular matrix (Fig. 5.4)[27, 30]. These cell sheets can be used as is, or layered on top of each other to create thicker tissues – more complicated tissues can be generated by layering different cell lines on top of one another as well[27]. Okano et al. have successfully generated sheets composed of many types of cells, ranging from cardiomyocytes to bone, all without requiring any sort of premade scaffold [28, 31-36]. Multilayered sheets of corneal epithelial cells generated with this method were transplanted into a ocular-injury rabbit model (via keratectomy), and successfully regenerated the cornea[28]. In order to mechanically lift and transport the relatively flimsy cell sheets, a PVDF donut-shaped membrane was applied to the cell sheets before they were harvested, which allowed the sheets to be easily moved via forceps[28].

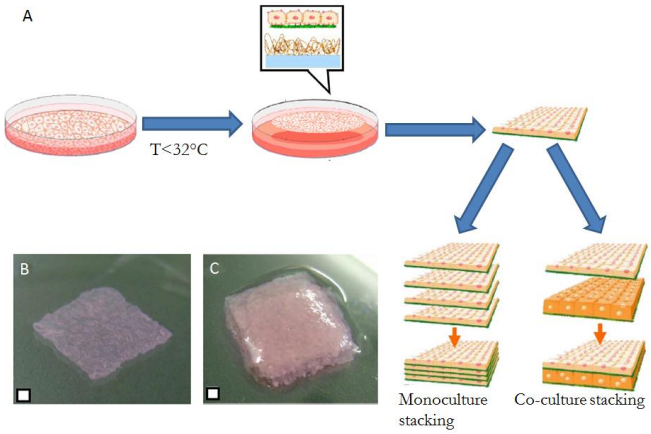

Figure 5.4: (a) General process used by Okano et al. to detach cell sheets from PIPAAm in order to harvest cell sheets, which can then be layered on top of one another (either in mono or co-culture). (b) A single sheet of smooth muscle cells created by this method; (c) five sheets of smooth muscle cells stacked on top of each other (figure modified with permission from Yang et al.)[30]

Other co-culture sheets created include stacking sheets of myoblasts onto a culture of endothelial cells using a complicated system whereby the myoblast sheet is released from a surface via PIPAAm and cold temperature, then harvested with a gelatin stamp, which is then placed on top of a layer of pre-grown HUVECs (the gelatin is subsequently removed, leaving behind only a top layer of myoblasts) – these are then allowed to incubate together[34]. They observed that the HUVECs migrated through the myoblast sheets and formed various shapes and networks depending on the myoblast sheet thickness – demonstrating how cell sheets can be used to look at fundamental cell biology and interactions between two distinct populations[34]. The gelatin stamp was likely used because handling the cell sheets otherwise appears to be difficult, as they are very thin. A similar gelatin stamp manipulator was used to stack endothelial cell sheets on top of hepatocytes in co-culture[31].

There are alternative methods for reliably creating a multi-cell stack. Ito et al. tethered magnetic particles to heptaocytes and feeder NIH3T3 cells with a cationic liposome containing magnetite[37]. They could then be cultured on a low-cell adhesion surface via an underlying magnet which would provide the necessary force the cells need to attach and spread - the cells could then easily be detached by removal of the magnet after they form confluent sheets[37].

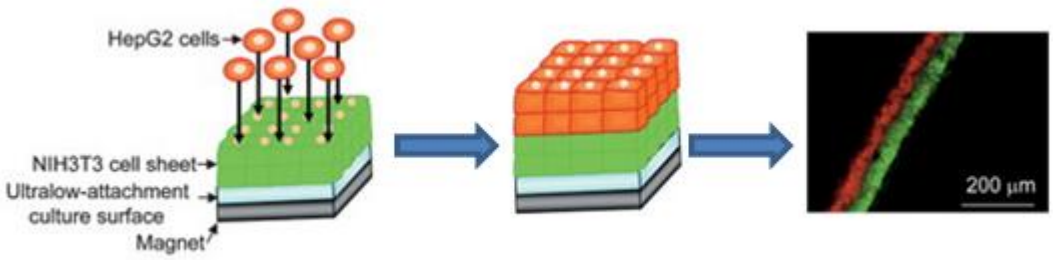

Figure 5.5: NIH3T3 and hepatocytes tagged with magnetic particles sequentially layered onto a magnetic surface, creating an ordered stack of cells that can clearly be observed via confocal microscopy (modified and reprinted with permission by Ito et al.)[37]

Ito et al. were able to generate well defined layers of hepatocytes and feeder NIH3T3 cells (Fig. 5.5)

with this method, and showed that hepatocytes would secrete more albumin when co-cultured with the fibroblasts[37]. This represents another scaffold-less technique for creating cell sheets – but yet again the sheets themselves are thin (and can even be seen to crumple in their figures after being manipulated with forceps). Matsusaki et al. created 3D co-cultures of cell sheets in a microwell plate via inkjet printing, printing each cell one at a time[38]. This 'bottom-up' approach is commonly advocated for by other biomedical scientists, and allows for precise construction of all sorts of complicated cell arrangements in a layer-by-layer fashion – all with no pre-constructed scaffold required[39]. Matsusaki et al. would first print a bottom layer of cells, then a layer of fibronectin and gelatin, then another layer of cells – slowly building up a *de novo* tissue for use in assays that require more physiologically relevant models than 2D cell culture[38]. Using this technique, Matsusaki et al. generated multiple layers of C2C12 cells, and hepatocytes layered with HUVECs[38].

Cell sheets have also been generated with scaffolds before, particularly in the work of Jennifer Lewis at Harvard University. Lewis et al. created a grid-like silk fibroin scaffold by 3D direct ink writing [40]. Through extrusion (rather than electrospinning), the scaffolds were generated layer-by-layer through a programmable movable nozzle, and then cultured with hMSCs that were differentiated into chondrocyte-like cells (Fig. 5.6) [40]. These cells seem to form sheets (Fig. 5.6-C) that span across the grid, though they are relatively small squares (~100 μm sides). This suggests that similar sheets of cells could be formed using the scaffolds generated by Jordahl et al.

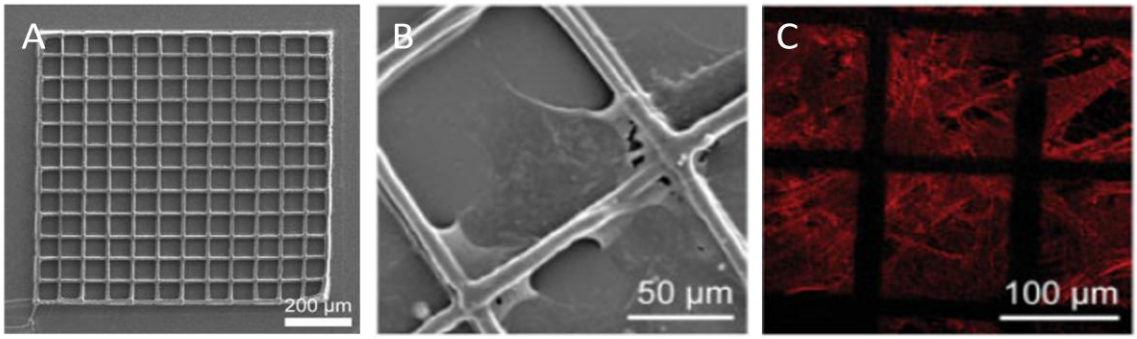

Figure 5.6: (a) SEM of extruded silk fibroin scaffold; (b) close up of the scaffold with differentiating hMSCs, and (c) actin immunofluorescence of differentiating hMSCs, showcasing the formed cell sheets (modified with permission by Ghosh et al.)[51]

Sun et al. later used the same technique to generate silk/hydroxyapatite grid scaffolds – as hydroxyapatite is the mineral found in bone, it was felt that these could potentially be ideal for osteogenic tissue engineering[41]. Shepherd et al. created poly(2-hydroxyethyl methacrylate) hydrogel grid scaffolds through a direct-writing method to grow networks of hippocampal neurons[42]. In all three examples, cells grew on grid scaffolds and could span across the squares, though only Sun et al. generate large (~750 µm sides) grid sizes[41].

Rationale, Project Goals, and Hypotheses

The work of Okano, Matsusaki, and Lewis has all advanced the field of cell sheet engineering significantly. However, each has disadvantages which need to be addressed. The sheets created by Okano have little to support them beyond the extracellular matrix created by the sheets themselves, likely making them difficult to handle with a pair of forceps – gelatin stamps, PVDF donut membranes, and complex cell cartridges with polycarbonate membranes appear to be how they solved this problem, but all are somewhat complicated to use (for example, the gelatin stamps are custom built)[28, 31]. Also, it would be difficult to shape the sheets Okano develops into higher architectures (such as tubes or spheres) – the most complicated structures generated are co-cultures of different cell sheets stacked onto one another[31]. Unlike Okano, Matsusaki can precisely place individual cells into any sort of pattern desired, even cells of a different lineage[38]. However, his methodology is not designed for easily removing the sheets after their generation (they are pulled off mechanically) – given that his goal is to create more physiologically relevant *in vitro* assays (rather than engineered tissues for clinical use), this is not surprising[38]. Finally, while Lewis et al. have created grid scaffolds that cell sheets have been grown on, their use of silk fibroin limits their ability to be functionalized[40]. Her scaffolds are created through simple extrusion[40], and thus could not be made multicompartmental like those scaffolds that can be generated via EHD co-jetting.

As discussed above, Jordahl recently developed a method for EHD co-jetting that uses a programmable x-y stage to create scaffolds from multiple layers of stacked or weaved PLGA in precise patterns. A ring electrode added to stabilize the jet was a breakthrough essential for getting the fibers to stack on each other; the viscosity and solvent choice were also critical. Unlike any other grids previously made, the fibers could be multicompartmental, allowing potentially for cell-selectivity or enhancement of differentiation by the attachment of growth factors (Fig. 5.7). The

scaffolds themselves are strong, yet flexible and easy to manipulate into multiple shapes (Fig 5.7-c), and can be made on the order of centimeters. They provide a 3D culture environment for the cells to grow on (as opposed to the 2D platforms used by Okano). Furthermore, unlike the work of Brown et al.[21], these were made with EHD co-jetting rather than melt electrospinning, thus avoiding the disadvantages associated with that technique (such as the required high temperatures). PLGA is a biocompadable and degradable material, and ideal for tissue engineering[10]. Cell sheets generated through rotary culture on these scaffolds could be used to create complex 3D cultures *in vitro* for assay development a la Matsusaki, or potentially even used in for clinical applications.

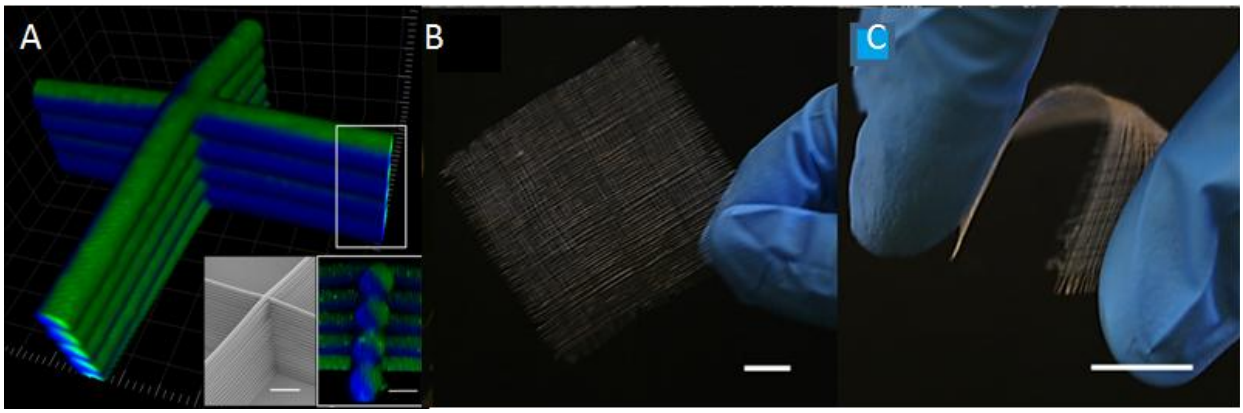

Figure 5.7: (a) Confocal and SEM of biphasic PLGA grid deposited using an x-y movable platform and EHD co-jetting (confocal scale bar: 20 μm, SEM scale bar: 50 μm; figure by Jacob Jordahl). (b) Macroscopic photo of a grid scaffold, and (c) demonstration of their flexibility (scale bar – 1 cm)

We proposed using these scaffolds to create cell sheets. Unlike the sheets created by Okano (which purposefully avoid the use of scaffolding), we believe that cells grown on these scaffolds could be subsequently bent and shaped into a complicated 3D conformation, then potentially placed in a gel of collagen or Matrigel to form a complex 3D cell culture. Furthermore, like Okano's sheets, the cell sheets generated with these scaffolds can also be stacked, but unlike Okano et al. do not require a complicated gelatin stamping mechanism. We also have the added benefit of making our scaffolds multicompartmental, though for this initial study we do not take advantage of this feature as we first

would like to characterize and optimize the production of cell sheets on unmodified single-phase PLGA. Nevertheless, it is a built in advantage that other methods lack.

The general protocol for generating sheets was largely adapted from the bioactuator project discussed in Chapter 4 (Fig. 5.8). We adsorbed fibronectin onto the scaffolds in order to enhance cell attachment (necessary for cell sheet formation), then incubated the scaffolds with a variety of cell lines on a rotator. The time of incubation, cell concentration, and grid spacing were optimized for NIH3T3 fibroblasts, which were used as a model cell line for cell sheet formation given their robustness and fibroblastic morphology. We used confocal and scanning electron microscopy to look at both cell/sheet morphology and the expression of various extracellular matrix proteins, as we believed these were important for the formation of stable and confluent cell sheets given their role as supportive scaffolding for other cell sheets (such as those created by Okano). We hypothesized the following: *fibroblasts grown on scaffolds will form denser sheets at longer incubation times, and the deposition of fibronectin can be correlated to sheet formation*. We tested this hypothesis by culturing NIH3T3 fibroblasts with the scaffolds, then fixing them at various time points and staining for fibronectin via immunofluorescence.

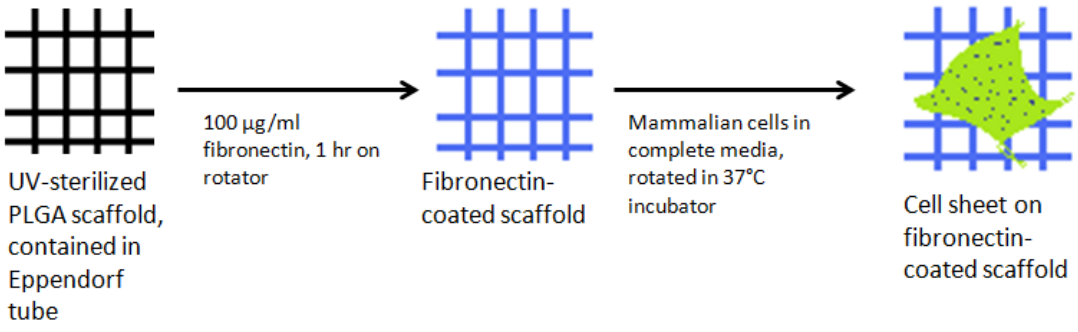

Figure 5.8: General protocol for create cell sheets with stacked grid PLGA scaffolds

Next, we hypothesized that *there is an optimal grid size, and grid sizes which are too large will fail to generate cell sheets*. Scaffolds of different grid spacing were created to test this hypothesis. We also hypothesized that *keratinocyte epithelial cells will have a difficult time forming sheets in comparison to fibroblasts due to their morphology. However, they will form sheets on top of a pre-formed sheet of fibroblasts grown on the scaffold.* We tested this by growing NIH3T3 cells first on a scaffold, then we incubated the resulting sheet with keratinocytes and characterized the resulting sheet after various incubation times. Throughout this project, we demonstrate that we can reliably and continuously create sheets of cells that span across our scaffold, paving the way for a multitude of projects ranging from the creation of bone-like scaffolds after differentiation of hMSC sheets to other complex co-cultures such as hepatocytes and endothelial cells.

Experimental Section

Parts of this experimental section were paraphrased from original unpublished text by collaborator Jacob Jordahl.

Electrohydrodynamic Co-Jetting

A jetting solution composed of 30 w/v% PLGA dissolved in 93:7 v/v% chloroform:N,N-dimethylformamide and a polymeric fluorescent probe at a concentration of <0.01 w/v% was loaded into two side-by-side syringes. Next, the solution was pumped through two side-by-side 26 gauge needles via a syringe pump (Fischer Scientific Model 78-0100I). An electrostatic lens composed of a copper cylindrical ring (5 cm in diameter and 2.5 cm tall) stabilized the jet and allowed it to be stacked. A positive potential was applied using a DC power supply (Gamma High-Voltage Research ES30P-10W), while a nominal potential of16 kV and 9kV was applied to the needle and the band respectively (with a needle to ground electrode distance of 5 cm). The resulting fibers were collected on a grounded stainless steel plate attached to an x-y moving axis (Velmex Inc.). The motion of the x-y axis was controlled via a proprietary programming language. After collection, the structures were put in a vacuum for solvent removal, and then subsequently cut via razor blade.

NIH3T3 Fibroblast and hMSC Culture on Scaffolds

The scaffolds were sterilized overnight using UV irradiation. After this process, the scaffolds contained in 1.5 ml Eppendorf tubes were incubated in 100 μg/ml human fibronectin (Sigma Aldrich) for 1 hr at room temperature on a rotator. These were then washed three times at five minute intervals with DPBS (Life Technologies, Inc). NIH3T3 fibroblasts (ATCC) were thawed from liquid nitrogen and diluted to a concentration of 6 x 10^5 cells/ml in DMEM (ATCC) + 10% calf bovine serum (ATCC) at passage 6. hMSCs (a kind gift from Dr. Paul Krebsbach) were also

thawed from liquid nitrogen and diluted to a concentration of 3 x 10^5 cells/ml. Cells were then seeded onto the scaffolds (1 ml/scaffold) and rotated in the incubator at 37°C and 5% CO_2. These were fed at 24 hr, and then every 48 hr thereafter if needed. The scaffolds were fixed at various time points in 2.5% gluteraldehyde for 20 minutes, then immunostained for fibronectin with a primary antibody (monoclonal anti-fibronectin antibody produced in mouse, Sigma Aldrich) diluted 1:400 and secondary antibody (Alexa Fluor® 488 Goat Anti-Mouse IgG (H+L) Antibody, Life Technologies) diluted to 1:400. Collagen I was also sometimes stained for, with a primary antibody (Anti-collagen I antibody, rabbit polyclonal, Abcam) diluted 1:100 and secondary antibody (Marina Blue® Goat Anti-Rabbit IgG (H+L) Antibody, Life Technologies) diluted to 1:100. Phalloidin 555 (Life Technologies) was also added at a concentration of 40 μl/ml to stain actin, and TO-PRO®-3 Iodide (642/661) at a dilution of 1:400 for nuclear staining. Scaffolds were then imaged using a confocal microscope – some were then further prepped for scanning electron microscopy (SEM). Scaffolds were submerged in 10%, 30%, 50%, and 70% solutions of ethanol/water for 7 minutes each sequentially. Then they were submerged in a 90% solution of ethanol/water for two 7 minute incubations, then 100% ethanol for another two 7 minute incubations. Finally, the scaffolds were incubated three times at 7 minute increments with pure hexamethyldisilazane (HMDS) and allowed to dry overnight. The scaffolds were then mounted on an SEM stand, sputtered, and then imaged using an AMRAY 1910 Field Emission Scanning Electron Microscope (FEG-SEM).

Co-Culture of NIH3T3/GFP Fibroblasts and Keratinocytes

The scaffolds were sterilized overnight using UV irradiation. After this process, the scaffolds contained in 1.5 ml Eppendorf tubes were incubated in 100 μg/ml human fibronectin (Sigma Aldrich) for 1 hr at room temperature on a rotator. These were then washed three times for five minute intervals with DPBS (Life Technologies, Inc). NIH3T3 fibroblasts stably transfected with

green fluorescent protein (GFP) (Cell Biolabs, Inc) were thawed from liquid nitrogen and diluted to a concentration of 6 x 10^5 cells/ml in DMEM + 10% fetal bovine serum (FBS) + 1% L-Glutamine (L-Glut) + 1% Non-essential amino acids (NEAA) + 1% penicillin/streptomycin (P/S) (media and all from supplements Life Technologies, Inc) at passage 2. 1 ml of the cell-media mixture was incubated with each scaffold, and the scaffolds were placed on a rotator in an incubator at 37 °C and 5% CO_2. The media was replaced at 24 hr. After 72 hr, normal human epithelial keratinocytes (NHEKs) (Lonza) were thawed from liquid nitrogen and diluted to a concentration of 3 x 10^5 cells/ml in KGM-Gold complete media (Lonza) + 10% FBS + 1% NEAA + 1% L-Glut (Life Technologies, Inc.). The cell-media mixture then replaced the media with the scaffolds, and media was replaced after 24 hr and then after every 48 hr. As a control, NHEKs were also incubated with freshly prepared scaffolds (UV-irradiated and coated in fibronectin by methods described earlier) that were not previously incubated with NIH3T3/GFP cells. At various time points, the scaffold-cell constructs were fixed with 2.5% gluteraldehyde (Sigma Aldrich), then stained via immunofluorescence with a pan-keratin antibody (Pan-Keratin (C11) mouse mAb #4545) at a concentration of 1:400 in a 1% BSA/Triton-X 100 solution.

Results

Characterization of the scaffolds by SEM and fluorescence microscopy was first performed in order to demonstrate the high fidelity stacked PLGA grids generated via EHD jetting (data not shown). Biphasic grids were generated with co-jetting, adding a functional alkyne group to one side. Furthermore, other patterns were generated via changes in the MATLAB code which controls the movable platform. However, for the cell experiments the grid pattern was almost exclusively used, and the fibers were not biphasic.

We initially worked with fibroblasts to create cell sheets as they were easy to grow, robust, and relatively inexpensive. A fibroblastic morphology and behavior also seemed desirable with regards to generating sheets, as fibroblasts tend to show a great deal of motility in culture and spread out on most amenable surfaces (as opposed to epithelial cells, which mostly display a 'cobble stone' morphology with less motility). This cell motility was felt to be important for generating cell sheets. The scaffolds were first cultured with NIH3T3 fibroblasts for 18 hr, then stained with Cell Tracker (Life Technologies Inc) and Hoescht probe (Fig. 5.9). As can be seen from microscopy, sheets formed over the majority of the scaffold, though there are gaps in coverage. Scaffolds not incubated beforehand in fibronectin did not form sheets and had few fibroblasts attached to them (data not shown). From the walls, via SEM we could observe the fibroblasts actively beginning to form a cell sheet (Fig. 5.9-c).

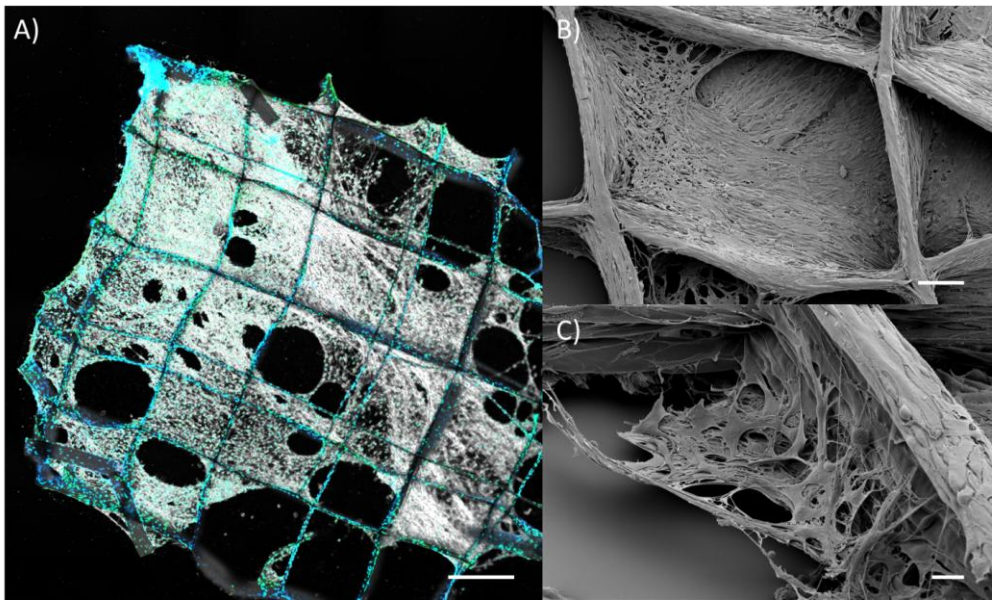

Figure 5.9: (a) Fluorescent CLSM image overlaid with a differential interference contrast image showing NIH3T3 cells forming sheets on a PLGA scaffold (scale bar: 500 μm) (b) SEM of cell sheet (same conditions as a, scale bar: 100 μm) (c) Early formation of a cell sheet (scale bar: 10 μm) (figure by Jacob Jordahl)

In Fig. 5.9-c, we see fibroblasts attached to both the wall of the scaffold and while also reaching out towards the space between the grids. Further out, cells which are not directly attached to the scaffold are attached to cells which are, suggesting several possible mechanisms by which the sheets are generated. First, it is possible that cells initially attached to the scaffolds will begin to protrude across the void, then while undergoing cell division will generate attached cells which jut out farther. It is also possible that cells which jut out serve as initial platforms for other cells on the scaffold to move across, adding another cell 'further' out (like a self-building bridge) until they eventually reach the other side. 'Bridges' of cells can be seen in other images, adding weight to this hypothesis (Fig. 5.10). Cells were ubiquitous on the walls of the scaffolding themselves (Fig. 5.10-b). It has been hypothesized that while incubating the scaffolds with fibronectin, a small sheet of it formed in between the grids as well as adsorbing onto them, providing some initial base to which the fibroblasts could reach out to and form the sheets. However, no evidence of this sheet has ever

been observed in either confocal microscopy or the SEM, even when staining for fibronectin via immunofluoresence.

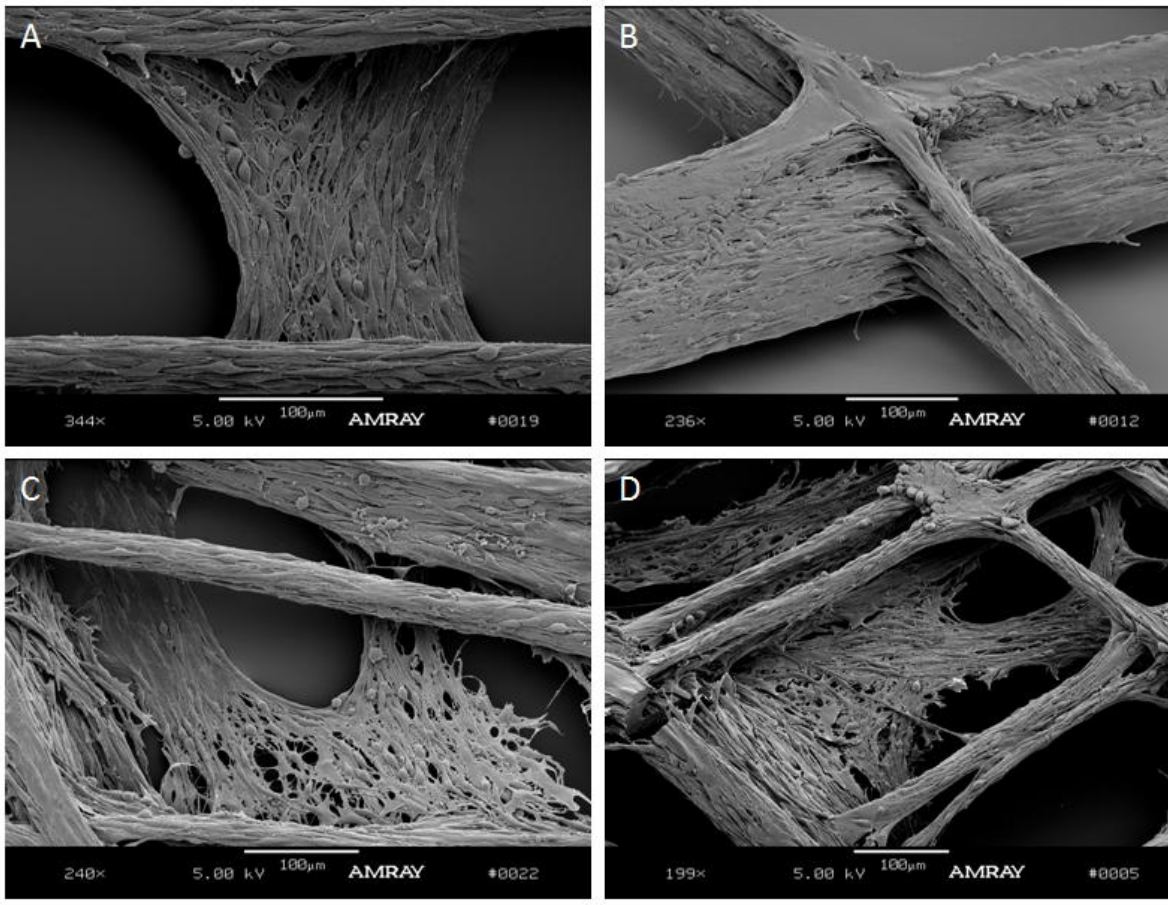

Figure 5.10: (a) Fibroblast 'bridge' that spans across the gridding of a scaffold (b) Even when not forming sheets, fibroblasts will cover the scaffold completely (c and d) Cell sheets at various stages of completion

In order to delve further into this hypothesis, we next cultured NIH3T3 fibroblasts with the scaffolds at three different time points: 6 hr, 18 hr, and 72 hr. Cells were stained with TO-PRO (a far-red stain for nuclei false colored blue in Fig. 5.11, found to work much better for z-stacks than DAPI or Hoescth probe, which tended to 'smear' in the image) and phalloidin (red). ECM proteins likely play a major role in giving the cells needed support while they make sheets, so we also stained

via immunofluorescence for fibronectin (green). After fluorescence imaging, we also imaged the same scaffolds via SEM.

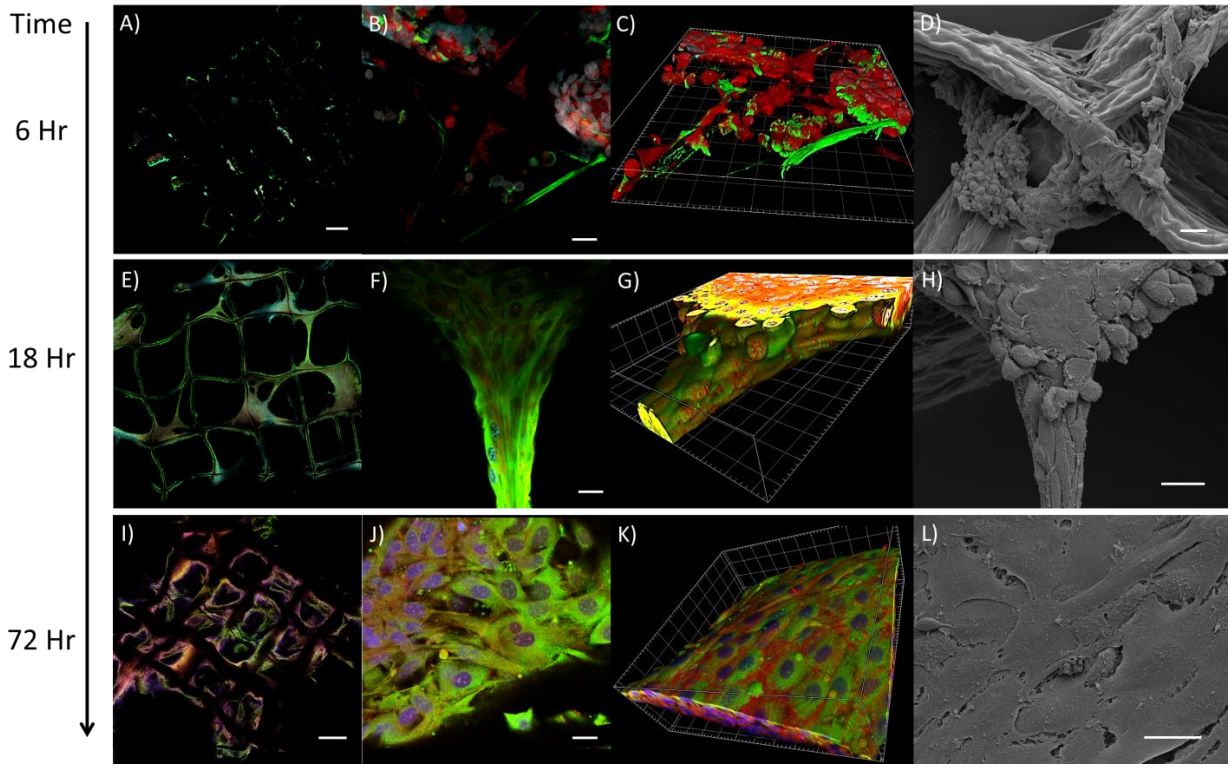

Figure 5.11: (a) Confocal micrograph of a scaffold seeded with NIH3T3 and incubated for 6 hours, then immuostained for fibronectin (green) along with phalloidin (red) and TO-PRO (blue) ; (b) Confocal of zoomed in area from (a); (c) z-stack of (b); and (d) SEM of region from (b) and (c). (e) Confocal micrograph of a scaffold seeded with NIH3T3 and incubated for 18 hours; (f) Confocal of zoomed in area from (e); (g) z-stack of (f); and (h) SEM of region from (f) and (g). (i) Confocal micrograph of a scaffold seeded with NIH3T3 and incubated for 72 hours (j) Confocal of zoomed in area from (i); (k) z-stack of an area from (i); and (h) SEM of region from (j). (figure by Jake Jordahl)

After six hours of incubation, the fibroblasts do not form any sheets, and are relatively small and not spread out. In both the confocal (Fig. 5.11-c) and SEM (Fig. 5.11-d) images, clumps of the fibroblasts can be seen sticking to each other and the scaffold, forming grape-like clusters which are ubiquitous. The fibronectin is patchy (Fig. 5.11-c) and only present on some cells, which implies that the extracellular matrix is still under development at this time point. There does seem to be a leading edge of fibronectin on the surfaces of some fibroblasts, which can be seen via confocal z-

stack (Fig. 5.12). We can however observe a few cells beginning to branch out towards the space between the grids, hinting at an eventual cell sheet.

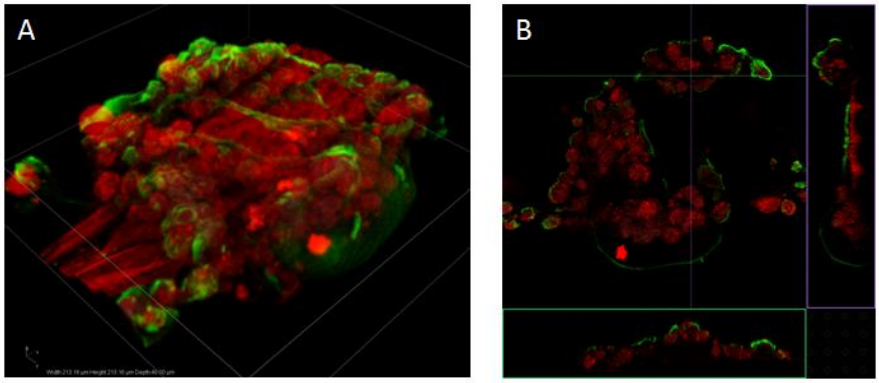

Figure 5.12: z-stack analysis of the fibroblasts on the scaffold after 6 hours of incubation

At 18 hours, the fibroblasts are now beginning to form sheets. In some areas the sheets cover nearly half of the grid space, while in other areas we only see rope-like 'bridges' of cells spanning from one end of the grid to the other. We took a z-stack of one of these cell bridges, and discovered that the fibronectin essentially wrapped around the bridge like an encasing sheath (Fig. 5.11-f and Fig 5.13).

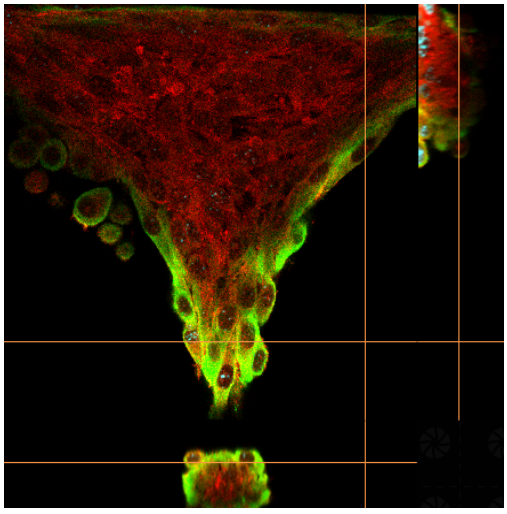

Figure 5.13: z-stack analysis of the fibroblast bridge after an 18 hour incubation

As Fig. 5.13 shows, the fibronectin (green) almost circles around the cells in the middle as they bridge out (red). A z-stack (Fig. 5.11-f) shows that the top of the cell bridge is completely covered

in fibronectin. This is strong evidence that the fibronectin (and by extension the extracellular matrix) plays an early key role in supporting the cells as they form nascent sheets. This is different from what Hitani et al. observed when they created cell sheets of corneal epithelial cells – after immunostaining they saw that fibronectin was weakly present on the surface of the sheet, but strongly present in between cells [43]. However, their sheets were cultured for a week on a flat surface before being removed – perhaps fibronectin is stronger on the surfaces of the forming cell sheet at earlier times. As shown in the SEM and confocal images (Fig. 5.11-h), fibroblast morphology at 18 hours is not as rounded like those at 6 hours, but more flattened out.

Finally, after 72 hours of incubation the fibroblasts formed thick sheets across the entire scaffold, with almost no gaps in coverage present. The cell bridges observed at 18 hr are mostly gone, replaced by the sheets which are now nearly ubiquitous. The sheets are roughly 2-3 cells thick, and the fibronectin is now found coating one side as a sort of support (Fig. 5.14). Fibronectin was also present somewhat in the intercellular region, but was not strong as observed by Hitani et al [43]. However, we do observe that the fibronectin (and by extension the ECM) tends to form mainly on one side (it is difficult to delineate one side as 'apical' or the other 'basolateral' as they did not form on a solid structure) – this can be seen especially well with z-stack confocal microscopy (Fig 5.14-c). In the SEM, the cell morphology was observed to be extremely flat and spread out (Fig 5.11-l). Thus, it seems that 72 hr is an ideal time point for generating a confluent cell sheet layer with fibroblasts. Given the results obtained from all three time points, we can correlate sheet formation with fibronectin deposition. Initially, cells attach in clumps and only just begin to spread out after 6 hours of incubation. No sheets are present as we believe there is no underlying extracellular matrix yet. The ECM is still being constructed, as evidenced by the 'patchiness' of the fibronectin. At 18 hr, we begin to see sheets at various stages of development. The fullest sheets take up the entire grid, but we also find plenty of examples of half sheets and earlier cell bridges, where a fiber of cells

(just a few cells thick at the center) spans across the grid to attach one side to the other. How these bridges form remains an open question, but one must keep in mind that theses scaffolds are kept rotating at all times. It is possible that cells remaining in suspension continue to hit and attach to cells that are slowly probing out towards the grid space, slowly building the bridge piece by piece. However, we rarely find these bridges at a 'half-way' point (it's possible that the ones we do see are a result of breakage during handling for microscopy) – they always are found already spanning the grid, suggesting that this action occurs quickly and likely involves cells from both sides of the spanned area.

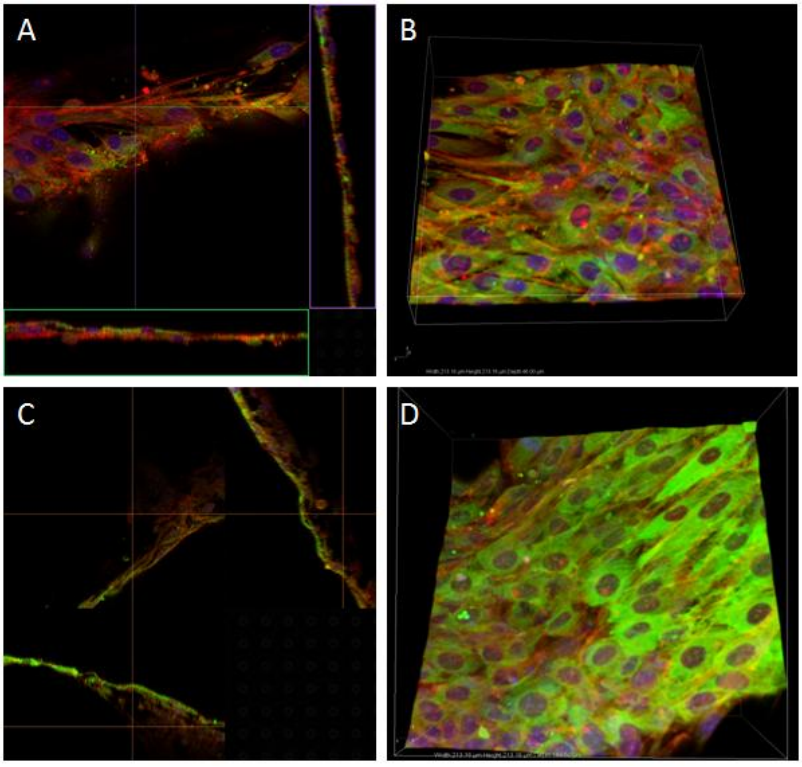

Figure 5.14: NIH3T3 fibroblast sheets immunostained for fibronectin (green) after 72 hr of growth (a). Side-slice of the confocal image in (b); (c) side slice of the confocal image in (d)

At 18 hr, the fibronectin covers the entire thickness of the cell bridges as they thrust across the grid, providing essential support for the cells as they span with no solid substrate underneath. We hypothesize that the half sheets and full sheets are likely then generated by cell proliferation; this

could be confirmed with live-cell confocal microscopy and NIH3T3/GFP cells, though the scaffolds would need to be removed from rotation after a set period of time so for the remainder they could be dynamically observed. It is clear that cell proliferation plays a role given the extent of cell sheet coverage present at 72 hr – the media is changed at 24 hr, so any non-anchored cells from the initial seeding would be removed by then. Thus, the other cells most likely come from cell division. Finally, at 72 hr the fibronectin appears to primarily coat one side of the cell sheet, though it is present intercellularly and on the other side too. This polarity is only evident with fully-formed sheets. Now fully formed, the fibroblasts seem to show the usual polarity cells display when arranged as sheets. The ECM serves as a base to support the sheets as they continue to proliferate. We can see that the sheets are as two or even three cells thick in some areas (Fig. 5.14), though other areas of the sheet are only one cell thick. Thus, as the fibronectin changes where it is deposited over time, the cells go from clumps adhered to a scaffold, to small bridges which span across a grid, to full sheets that are confluent across the entire scaffold. Furthermore, we measured the number of fibroblasts after 72 hr of confluent growth to be 7.4×10^4 cells/scaffold (with the dimensions of the scaffolds as 3 mm x 3 mm).

We also incubated fibroblasts with the scaffolds for 15 days as a long-term culture, in order to see if the cells would survive and continue to thrive as sheets. We wanted to know if the cell sheets would become any thicker than those observed after 72 hr of culture. We used an NIH3T3 line that was stably transfected with green fluorescent protein (GFP) (Cell Biolabs, Inc) which will be titled NIH3T3/GFP for the rest of this thesis. Cells were incubated with the scaffolds for a full fifteen days, with the media first changed post 24 hr after seeding, and then regular media changes every 48 hr. The cells formed confluent sheets that were not any thicker than those observed with 72 hr of

culture (Fig. 5.15). The scaffolds also remained very intact with only minor warping, showing the robustness of their construction despite over two weeks of submersion in media at 37°C.

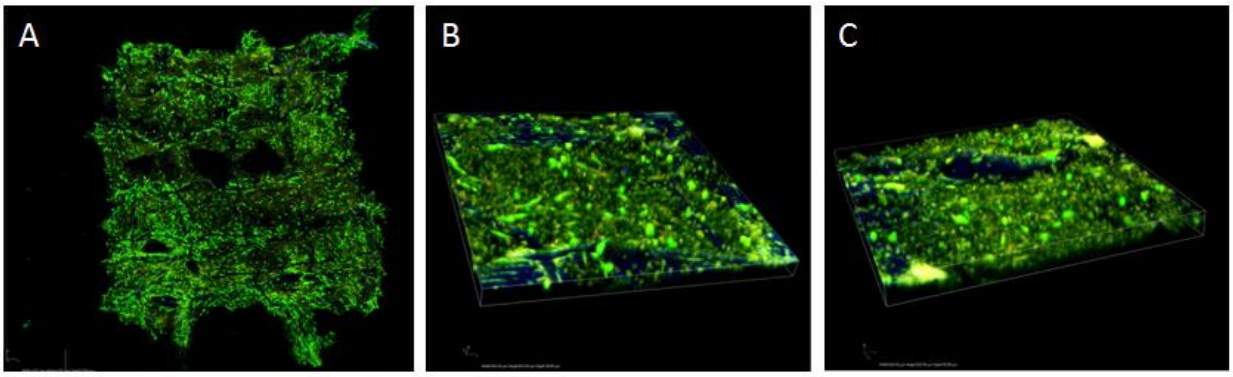

Figure 5.15: NIH3T3/GFP fibroblast sheets on a scaffold after 15 days of continuous rotation culture. (a) Full scaffold, and (b,c) z-stacks of sheets spanning between grids

The role of the scaffold size in cell sheet formation was also tested. In addition to the 750 μm grid sized scaffolds previously used to generate NIH3T3 sheets, we also tested scaffolds with a 500 μm and 1500 μm sized grid. Based on previous work, we looked at scaffold development at both 18 hr and 72 hr. The 500 μm sized grid scaffolds had multiple sheets in formation at 18 hr just like the 750 μm grids, and were completely confluent by 72 hr (Fig. 5.16). In contrast, at 18 hr the 1500 μm sized grid scaffolds showed no cell sheet formation at all. By 72 hr, they had sufficiently warped enough in culture to allow some sheets to form – nevertheless they were nowhere near confluent like those seen on the 750 μm and 500 μm scaffolds. Thus, it seems that the geometry of the scaffolds plays an important role in cell sheet establishment. Also, the larger 1500 μm grid sized scaffolds tended to more easily deform in culture than the 750 μm. Deformation to some extent occurs with all scaffolds due to continual shearing by the media under rotation and the forces the cell sheets exert as they grow. However, the 1500 μm scaffolds were observed to undergo far worse deformation than the other sizes, showing the importance of mechanical rigidity in design.

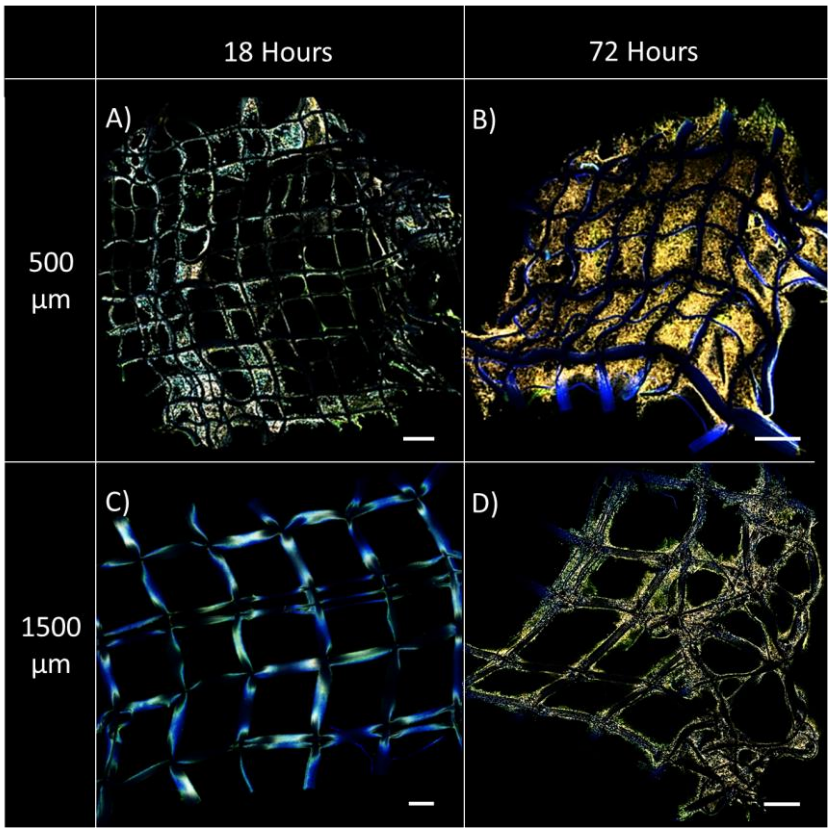

Figure 5.16: NIH3T3 fibroblast sheets on a 500 µm grid-sized scaffolds for (a) 18 hr and (b) 72 hr. 1500 µm grid-sized scaffolds were also tested at (c) 18 hr and (d) 72 hr (figure by Jacob Jordahl)

Given the success of generating fibroblast cell sheets, we decided to branch out to other cell types that are more physiologically interesting than NIH3T3. We first cultured hMSCs on the scaffolds for 72 hr to generate fully confluent sheets. As the importance of fibronectin became apparent, we also examined collagen I expression via immunofluorescence. Collagen provides tensile strength to extracellular matrices (while fibronectin provides a cell attachment anchor), so we thought it would be interesting to see if we could view its formation on hMSC sheets.

After 72 hr, the hMSCs form confluent sheets of across the scaffold. A confocal z-stack shows that while the cells are very flat one side of the sheet, the other side shows an almost chaotic frenzy of

hMSCs reaching into the space above them as if to branch out further. This was not observed with the fibroblasts.

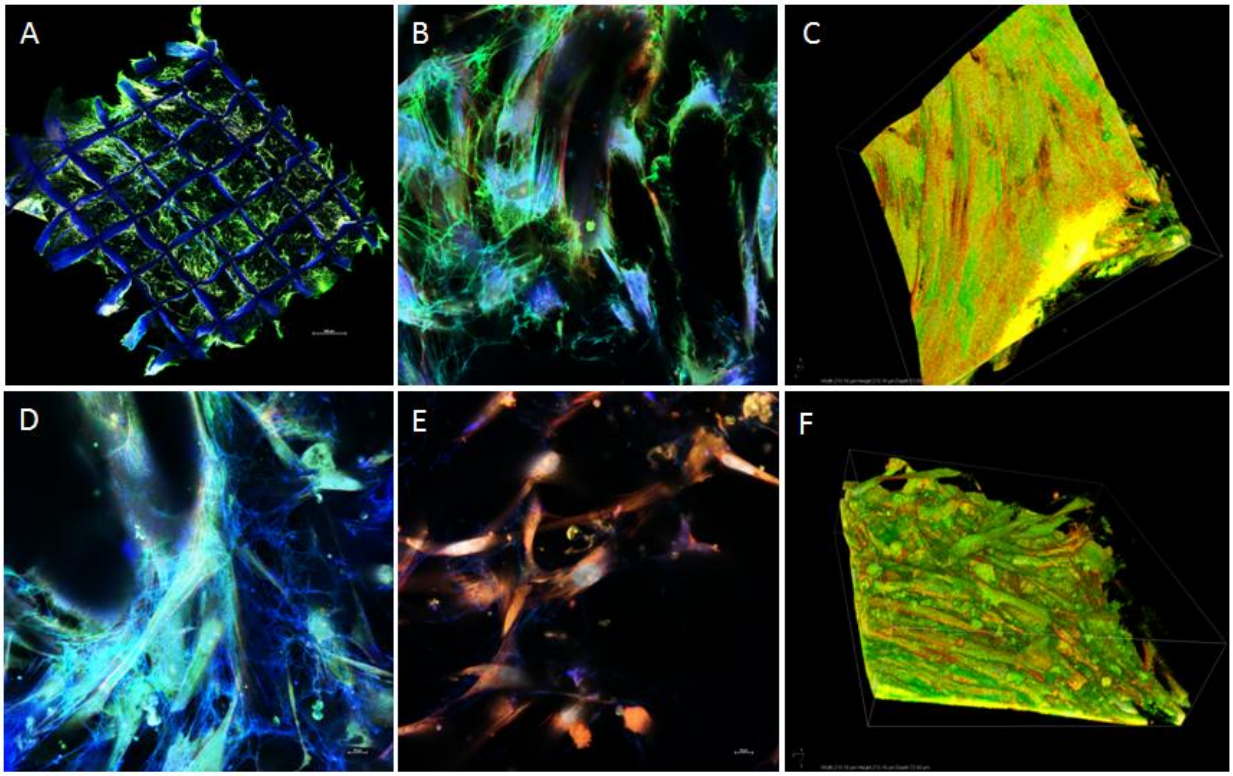

Figure 5.17: (a) hMSCs grown on a scaffold into a confluent sheet after a 72 hr incubation (b, d, e) Immunofluoresence of collagen (dark blue) and fibronectin (green), (c, f) z-stacks of two sides of the same hMSC sheet

The collagen is easy to distinguish as long fibers that appear almost cagelike around the cells (dark blue, Fig. 5.17-b, d, e). This is precisely what we hypothesized collagen would look like on cell sheets. The fibronectin can also be seen as almost fiberlike (especially in Fig. 5.17-b) on the hMSCs. The relative ease with which hMSCs form sheets on scaffolds was not particularly surprising, given their fibroblastic morphology and the success we had with NIH3T3 cells earlier. Nevertheless, it is an important first step in potentially creating scaffolds of bone-like or cartilage-like cells.

We next attempted to create sheets of keratinocytes, as skin tissue engineering is a major area of biotechnology[44]. Products such as Apligraf and Permaderm are already on the market for use in

chronic skin wounds and burns, respectively [44]. As our scaffolds are sheetlike (like skin), we thought it was a natural area to explore. We first attempted to grow NHEKSs (normal human epithelial keratinocytes, a primary cell line) by themselves on scaffolds for 72 hr, as that time point had previously given us confluent sheets of fibroblasts. Like the fibroblasts, we immunostained the NHEK cells for fibronectin, and counter stained with phalloidin and TO-PRO.

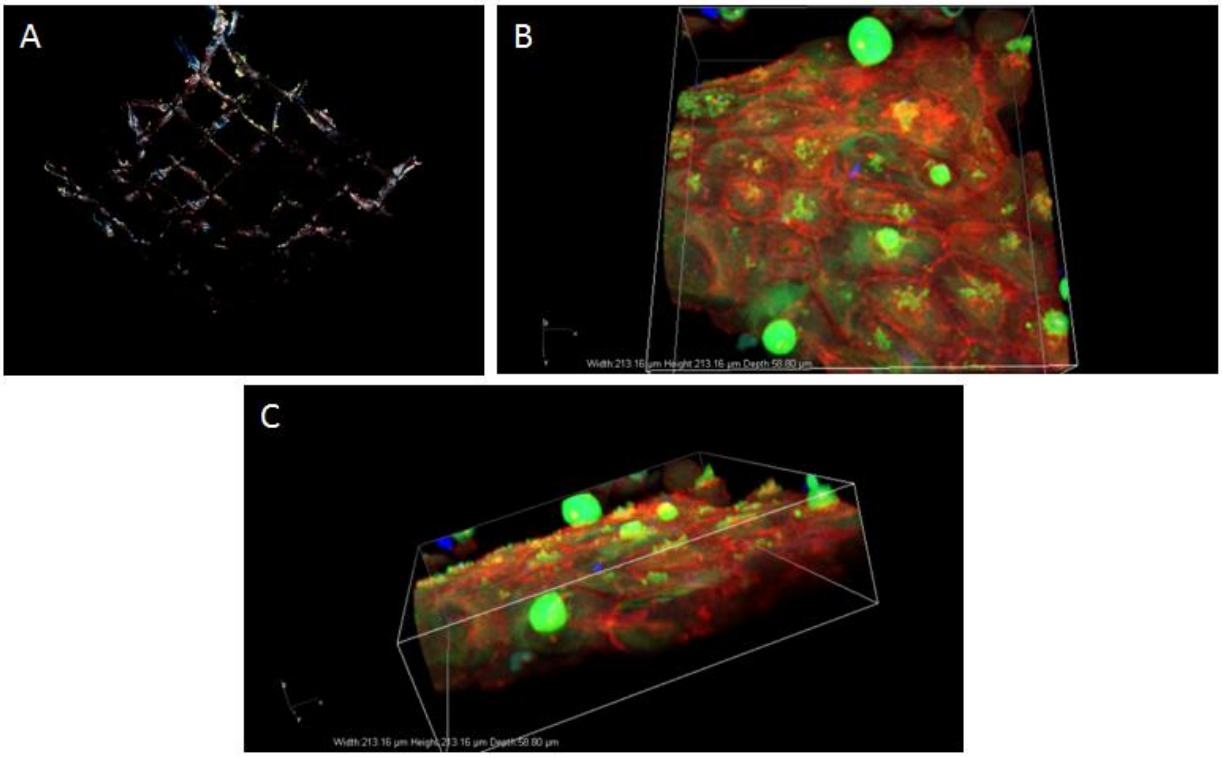

Figure 5.18: (a) Scaffold incubated with NHEKs for 72 hr (b) z-stack showing the top and (c) side of NHEK sheet

Unfortunately, the NHEKs did not form anything like a confluent sheet, and most of the spaces between the grids were devoid of cells, though the keratinocytes readily attached to the scaffolding itself (Fig. 5.18-a). However, there were a few isolated areas where sheets were present, and with z-stacking we saw that the keratinocytes retained their epithelial morphology ('cobblestone') (Fig. 5.18-b). The sheets formed were no thicker than those formed by fibroblasts, and the fibronectin appeared to be on the surfaces of the cells as seen earlier (Fig. 5.18-b). Encouraged, we next tried a

different strategy. Previous work suggested that NHEKs co-cultured with fibroblasts could be beneficial[45, 46]. Rheinwald et al. documented one of the first instances of keratinocyte/fibroblast co-culture in 1975, by mixing irradiated NIH3T3 cells (the irradiation prevents further proliferation of the fibroblasts while allowing them to maintain their supportive role) with keratinocytes from foreskin[47]. They were subsequently able to culture human keratinocytes, a feat previously found to be extremely challenging[47]. Wang et al. found that keratinocytes co-cultured with fibroblasts would proliferate quicker than those without fibroblasts[45]. In fact, feeder layers of fibroblasts for clinical keratinocyte expansion remain part of the standard protocol for rapid proliferation (though the NHEKs grown for the experiments in this thesis did not require them)[46]. As fibroblasts form excellent sheets on scaffolds and have been shown in previous literature to support keratinocyte culture, we hypothesized that a co-culture of NHEKs on a pre-formed fibroblast sheet would lead to keratinocyte sheets[47]. Another strategy could be to grow hMSCs into sheets as we have already demonstrated, then differentiate them into keratinocyte-like cells – previous studies have been able to differentiate hMSCs towards an epidermal-like cell line[48, 49]. In order to distinguish between fibroblasts and NHEKs, we used NIH3T3 cells that have been stably transfected with green fluorescent protein. Keratinocytes were identified by immunostaining for keratin with an anti-pan-keratin antibody (a marker for epithelial cells), followed by a red fluorescent secondary antibody[48]. Thus, the fibroblasts would fluoresce with a green light, and the keratinocytes with a red light. Fibroblasts were cultured first for 72 hr to form sheets – then keratinocytes were co-cultured for 3 days, 5 days, and 7 days in an optimized co-culture media (described in the Experimental Section). We then imaged them using confocal microscopy and took z-stacks to observe how the two cell populations sorted themselves in space relative to each other.

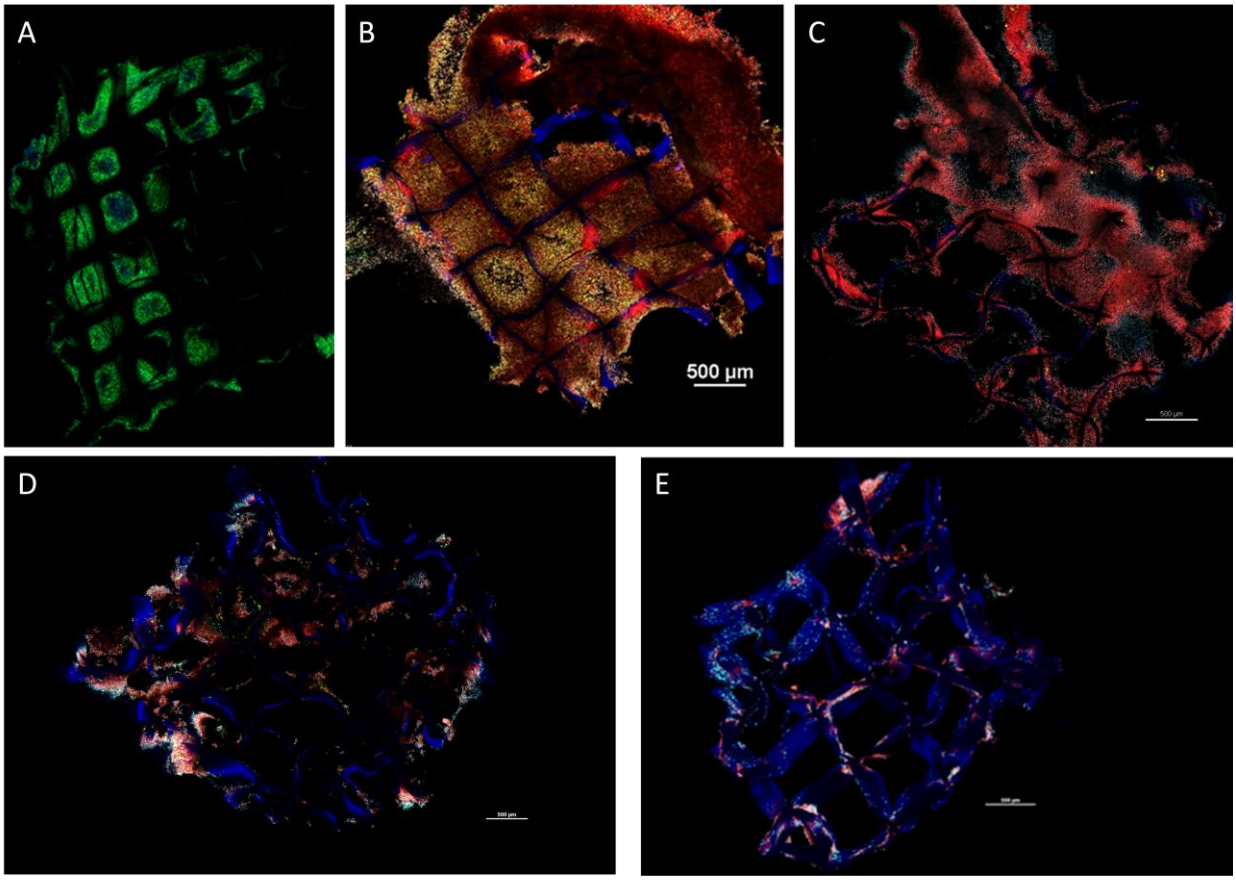

Figure 5.19: (a) NIH3T3/GFP cells cultured for 72 hr prior to keratinocyte seeding. Keratinocytes were then seeded with NIH3T3/GFP-confluent sheets on scaffolds for (b) three, (c) five, and (d) seven days. (e) NHEK cells cultured on scaffolds for 7 days without fibroblasts

NIH3T3/GFP fibroblasts formed fully confluent sheets by 72 hr post-seeding as expected (Fig. 5.19-a). After 3 days of co-culture, sheets of keratinocytes co-existed with that of fibroblasts (Fig. 5.19-b); however, they did not two distinct layers. z-stacks indicate that they actually became mixed together in the same plane, with some areas having a heavy number of fibroblasts and some areas only the keratinocytes (Fig. 5.20-b). After 5 days of co-culture however, the fibroblasts are almost completely gone and replaced by a confluent NHEK sheet (Fig. 5.19-c). Only a few fibroblasts could be spotted on top of the sheet that now existed. This largely held true for 7 days of co-culture as well, although there were now more fibroblasts (Fig. 5.19-d). They seemed to have been relegated to a sort of supportive role, with one or two fibroblasts clinging to a dense sheet of NHEK cells

(Fig. 5.20-c,d). Nevertheless, our hypothesis of NHEK sheet formation via fibroblast co-culture was supported by the formation of the keratinocyte sheets. Even after 7 days of culture, NHEKs seeded onto scaffolds with no prior fibroblasts failed to form any sheets of significant size (Fig. 5.19-e).

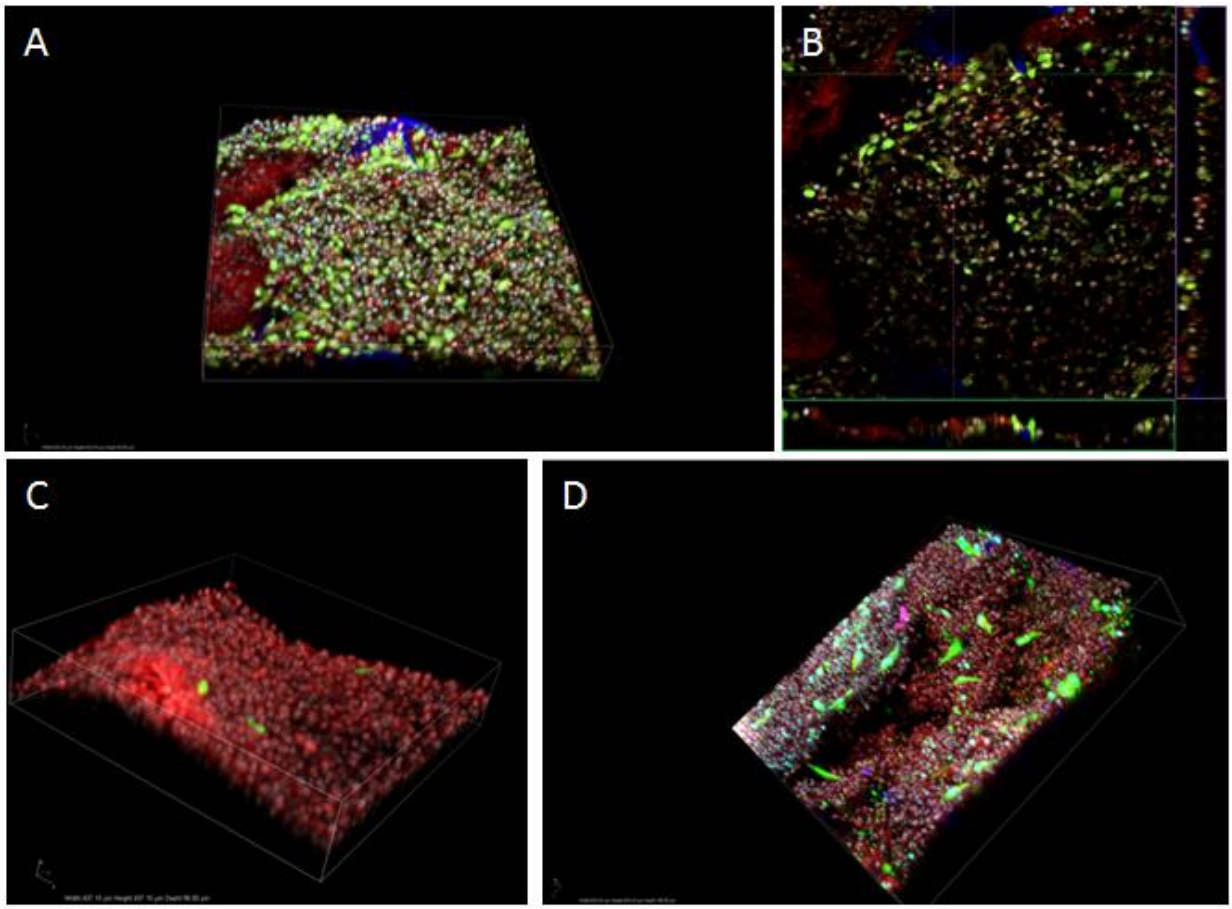

Figure 5.20: (a) z-stack of NHEK-NIH3T3/GFP co-culture incubated for 3 days (b) cross-sectional images of z-stack shown in (a); z-stack of NHEK-NIH3T3/GFP co-culture incubated for (c) 5 days and (d) 7 days

What leads to this massive loss of fibroblasts between 3 and 5 days is not clear. Irradiated fibroblasts (which cannot proliferate) used in co-culture eventually detach and die after extended culture with keratinocytes[46]. Using non-irradiated human fibroblasts, Jubin et al. observed that in a 6:1 ratio of keratinocytes to fibroblasts the resulting co-culture was composed of over 90%

keratinocytes after 15 days, while lower ratios of keratinocytes to fibroblasts led to fibroblast dominance instead[46]. Given that there are approximately 60,000-80,000 fibroblasts per scaffold at the end of 72 hr, maybe subsequently seeding over 300,000 keratinocytes onto them (a ratio of approximately 4-5:1, not too far from what Jubin et al. used) allows the keratinocytes to overwhelm the fibroblasts by sheer numbers and subsequent proliferation rates[46]. Of course Jubin et al. did their culture on flat 2D substrates while we did ours on 3D scaffolds, and we know that not all 300,000 keratinocytes attach to the scaffold. Still, there are a lot more keratinocytes present in the culture than fibroblasts initially. One way of testing this hypothesis would be to try seeding different concentrations of NHEKs with the scaffolds after generated confluent fibroblast layers. To test if it is the co-culture medium (which is not used until the NHEKs are seeded), we could simply continue to grow the NIH3T3/GFP cells in it without NHEKs to see if it is toxic.

We also noticed that the keratinocytes after co-culture looked different from those that were cultured without fibroblasts. While the keratinocytes grown by themselves had the classic cobblestone morphology as observed by confocal microscopy (Fig. 5.18), keratinocytes grown in co-culture appeared more fibroblastic and spindle-shaped, almost even balled up (Fig. 5.20-c). In order to investigate this further, we performed SEM with keratinocytes grown without fibroblasts (which will form a few small sheets one can examine), and keratinocytes that had been co-cultured with fibroblasts. Both were cultured for 5 days before fixation and SEM.

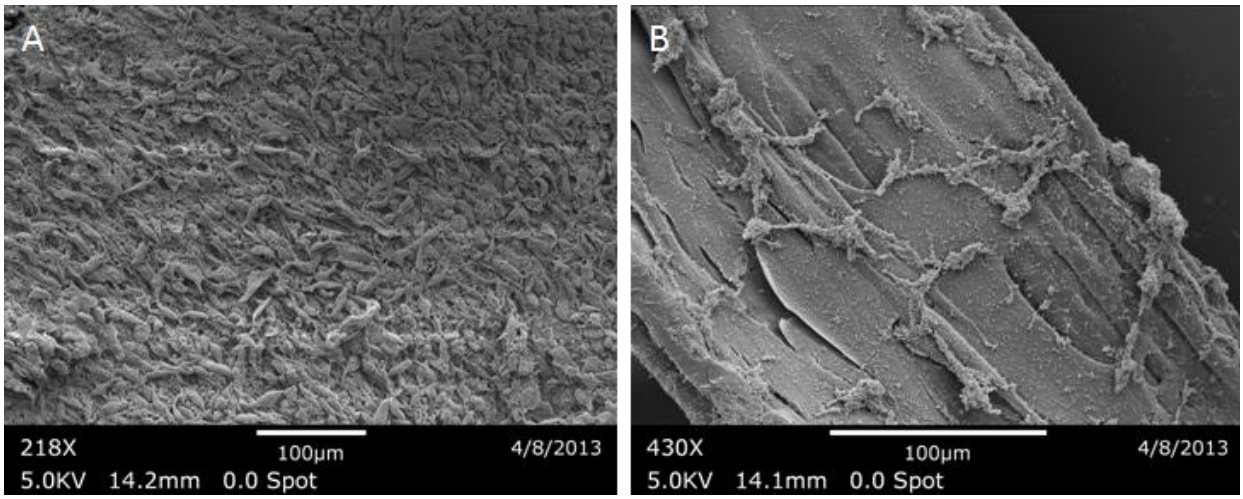

Figure 5.21: (a) SEM of NHEK cells grown in co-culture for 5 days in co-culture with NIH3T3/GFP cells (b) SEM of NHEK cells grown without NIH3T3/GFP cells

While we do see a marked difference in morphology, we believe that this is just a confinement effect. Thus, we are unconcerned about this difference, though it is striking (Fig. 5.21). These cultures were grown in a hypoxic environment – hypoxia induces the downregulation of e-cadherins in keratinocytes [50]. Perhaps we are observing the effects of this downregulation, as the keratinocytes dethatch from one another.

Conclusions and Future Work

By using a ring electrode to stabilize our jetted polymer and a controllable collecting stage, we are able to generate high fidelity scaffolds with precise geometric spacing. While many different types of scaffolds were created, we initially focused on using a simple square grid pattern for generating our cell sheets. We characterized the deposition of fibrocetin by NIH3T3 fibroblasts over time, and correlated its appearance and distribution to the formation of cell sheets. SEM also further elucidated how cells beginning to form sheets do so by anchoring part of their cell body to the scaffold wall while another part reaches out into the space between the grid walls, allowing for other cells to attach at these ends and further 'bridge' out until they form a span across. Multiple cell sheets have been formed with our scaffolds, including mesenchymal stem cells and keratinocytes with a co-culture of fibroblasts.

Many tissues can be thought of as being organized into sheets, and future work will involve growing more cell types to create sheets, including hepatocytes, endothelial cells, and eventually neurons. As of the writing of this thesis however, we are actively working on differentiating our sheets of mesenchymal stem cells towards osteogenic fates. While one obvious application would be to use the scaffolds and cell sheets as a platform for creating bone-like sheets that could be used in a clinical setting, another use would be as a model *in vitro* osteogenic platform for studying the interactions of tumor cells with bone. The scaffolds are flexible, yet provide a strong platform for generating sheets that does not tear or break easily. Thus, we plan to expand our co-culture strategy towards growing two or more types of cells on individual scaffolds (such as osteogenic cells and chrondrogeneic cells, or liver cells and endothelial cells) and then stacking the individual scaffolds on top of one another. As tissues are composed of multiple cell types and our scaffolds are flexible enough to be contorted into various possible shapes (including three- dimensional ones such as tubes or spheres), we potentially have a technology platform that allows us to recapitulate very

complicated tissue architectures *in vitro*. This is an advantage over other cell sheet methods reviewed. For example, we could grow a sheet of hepatocytes and a sheet of endothelial cells on separate scaffolds, then fold the endothelial cell sheet into a tube, and then wrap that tube with the hepatocyte sheet. We also plan to exploit the fact that these scaffolds can be jetted to contain multiple phases featuring reactive functional groups. We could jet a PLGA scaffold containing a cyclooctyne (much like what was done for Chapter 4), click on an ATRP bromo-initiator, then create zwitterionic polymer brushes of PMEDSAH. This would potentially then allow us to grow hESCs or iPSCs onto our scaffolds, which can then be exploited to differentiate into a wide array of cell lines. We could even create multimodal fibers with one or more biomolecules immobilized via bio-orthogonal chemistries to illicit synergistic effects on the cells we culture, or to influence differentiation of stem cells down a certain path. For example, we could tether an azido-TGF-β to our scaffolds to induce hMSC sheets to differentiate down an chondrogenic pathway – McCall et al. did precisely this and demonstrated that immobilized TGF-β induced encapsulated hMSCs to differentiate into chondrocyte-like cells[51]. EGF on the other hand has been shown to stimulate hMSCs into differentiating down an osteogenic pathway[52]. If one could selectively tether TGF-β to one side of a scaffold while tethering EGF to the other side, it is possible that one could make alternating grids of osteocytes and chondrocytes. This could then be a useful *in vitro* model for studying multi-tissue interfaces.

References

1. Berthiaume, F., Maguire, T.J. & Yarmush, M.L. Tissue engineering and regenerative medicine: history, progress, and challenges. *Annual review of chemical and biomolecular engineering* **2**, 403-430 (2011).
2. Bhatia, S.K. & SpringerLink (Online service) (Springer Science+Business Media, LLC, New York, NY; 2012).
3. Badylak, S.E. The extracellular matrix as a scaffold for tissue reconstruction. *Semin Cell Dev Biol* **13**, 377-383 (2002).
4. Kanematsu, A. et al. Type I collagen can function as a reservoir of basic fibroblast growth factor. *Journal of Controlled Release* **99**, 281-292 (2004).
5. Ikada, Y. Challenges in tissue engineering. *Journal of The Royal Society Interface* **3**, 589-601 (2006).
6. Chan, B.P. & Leong, K.W. Scaffolding in tissue engineering: general approaches and tissue-specific considerations. *European spine journal : official publication of the European Spine Society, the European Spinal Deformity Society, and the European Section of the Cervical Spine Research Society* **17 Suppl 4**, 467-479 (2008).
7. Peppas, N.A. & Langer, R.S. Biopolymers II. (Springer, New York; 1995).
8. Glowacki, J. & Mizuno, S. Collagen scaffolds for tissue engineering. *Biopolymers* **89**, 338-344 (2008).
9. Nettles, D.L., Elder, S.H. & Gilbert, J.A. Potential use of chitosan as a cell scaffold material for cartilage tissue engineering. *Tissue engineering* **8**, 1009-1016 (2002).
10. Pan, Z. & Ding, J. Poly(lactide-co-glycolide) porous scaffolds for tissue engineering and regenerative medicine. *Interface Focus* **2**, 366-377 (2012).
11. Huang, W., Shi, X., Ren, L., Du, C. & Wang, Y. PHBV microspheres – PLGA matrix composite scaffold for bone tissue engineering. *Biomaterials* **31**, 4278-4285 (2010).
12. Kawazoe, N., Inoue, C., Tateishi, T. & Chen, G. A cell leakproof PLGA-collagen hybrid scaffold for cartilage tissue engineering. *Biotechnology Progress* **26**, 819-826 (2010).
13. Seitz, H., Rieder, W., Irsen, S., Leukers, B. & Tille, C. Three-dimensional printing of porous ceramic scaffolds for bone tissue engineering. *Journal of Biomedical Materials Research Part B: Applied Biomaterials* **74B**, 782-788 (2005).
14. Elomaa, L. et al. Preparation of poly(ε-caprolactone)-based tissue engineering scaffolds by stereolithography. *Acta biomaterialia* **7**, 3850-3856 (2011).
15. Alavi, S.H. & Kheradvar, A. Metal mesh scaffold for tissue engineering of membranes. *Tissue engineering. Part C, Methods* **18**, 293-301 (2012).
16. Pham, Q.P., Sharma, U. & Mikos, A.G. Electrospinning of polymeric nanofibers for tissue engineering applications: A review. *Tissue engineering* **12**, 1197-1211 (2006).
17. Di Martino, A. et al. Electrospun scaffolds for bone tissue engineering. *Musculoskeletal surgery* **95**, 69-80 (2011).
18. Yoshimoto, H., Shin, Y.M., Terai, H. & Vacanti, J.P. A biodegradable nanofiber scaffold by electrospinning and its potential for bone tissue engineering. *Biomaterials* **24**, 2077-2082 (2003).
19. Shalumon, K.T. et al. Electrospinning of carboxymethyl chitin/poly(vinyl alcohol) nanofibrous scaffolds for tissue engineering applications. *Carbohydrate Polymers* **77**, 863-869 (2009).

20. Meng, Z.X. et al. Electrospinning of PLGA/gelatin randomly-oriented and aligned nanofibers as potential scaffold in tissue engineering. *Mat Sci Eng C-Mater* **30**, 1204-1210 (2010).
21. Brown, T.D., Dalton, P.D. & Hutmacher, D.W. Direct Writing By Way of Melt Electrospinning. *Advanced Materials* **23**, 5651-+ (2011).
22. Brown, T.D. et al. Design and Fabrication of Tubular Scaffolds via Direct Writing in a Melt Electrospinning Mode. *Biointerphases* **7** (2012).
23. Hutmacher, D.W. & Dalton, P.D. Melt Electrospinning. *Chem-Asian J* **6**, 44-56 (2011).
24. Andrady, A.L. & Wiley online library. Science and technology of polymer nanofibers. (Wiley, Hoboken, N.J.; 2008).
25. Mandal, S., Bhaskar, S. & Lahann, J. Micropatterned Fiber Scaffolds for Spatially Controlled Cell Adhesion. *Macromolecular rapid communications* **30**, 1638-1644 (2009).
26. Atala, A., Kasper, F.K. & Mikos, A.G. Engineering complex tissues. *Science translational medicine* **4**, 160rv112 (2012).
27. Yang, J. et al. Cell delivery in regenerative medicine: The cell sheet engineering approach. *Journal of Controlled Release* **116**, 193-203 (2006).
28. Nishida, K. et al. Functional bioengineered corneal epithelial sheet grafts from corneal stem cells expanded ex vivo on a temperature-responsive cell culture surface. *Transplantation* **77**, 379-385 (2004).
29. Yamada, N. et al. Thermo-responsive polymeric surfaces; control of attachment and detachment of cultured cells. *Die Makromolekulare Chemie, Rapid Communications* **11**, 571-576 (1990).
30. Yang, J. et al. Cell sheet engineering: Recreating tissues without biodegradable scaffolds. *Biomaterials* **26**, 6415-6422 (2005).
31. Kim, K., Ohashi, K., Utoh, R., Kano, K. & Okano, T. Preserved liver-specific functions of hepatocytes in 3D co-culture with endothelial cell sheets. *Biomaterials* **33**, 1406-1413 (2012).
32. Matsuura, K., Haraguchi, Y., Shimizu, T. & Okano, T. Cell sheet transplantation for heart tissue repair. *Journal of controlled release : official journal of the Controlled Release Society* **169**, 336-340 (2013).
33. Nakajima, R. et al. Fabrication of transplantable corneal epithelial and oral mucosal epithelial cell sheets using a novel temperature-responsive closed culture device. *J Tissue Eng Regen Med* (2013).
34. Ngo, T.X. et al. Endothelial cell behavior inside myoblast sheets with different thickness. *Biotechnology letters* **35**, 1001-1008 (2013).
35. Pirraco, R.P. et al. Development of osteogenic cell sheets for bone tissue engineering applications. *Tissue engineering. Part A* **17**, 1507-1515 (2011).
36. Takagi, R. et al. Cell sheet technology for regeneration of esophageal mucosa. *World journal of gastroenterology : WJG* **18**, 5145-5150 (2012).
37. Ito, A., Jitsunobu, H., Kawabe, Y. & Kamihira, M. Construction of heterotypic cell sheets by magnetic force-based 3-D coculture of HepG2 and NIH3T3 cells. *Journal of bioscience and bioengineering* **104**, 371-378 (2007).
38. Matsusaki, M., Sakaue, K., Kadowaki, K. & Akashi, M. Three-dimensional human tissue chips fabricated by rapid and automatic inkjet cell printing. *Advanced healthcare materials* **2**, 534-539 (2013).
39. Huebsch, N. & Mooney, D.J. Inspiration and application in the evolution of biomaterials. *Nature* **462**, 426-432 (2009).

40. Ghosh, S., Parker, S.T., Wang, X.Y., Kaplan, D.L. & Lewis, J.A. Direct-write assembly of microperiodic silk fibroin scaffolds for tissue engineering applications. *Advanced functional materials* **18**, 1883-1889 (2008).
41. Sun, L. et al. Direct-write assembly of 3D silk/hydroxyapatite scaffolds for bone co-cultures. *Advanced healthcare materials* **1**, 729-735 (2012).
42. Hanson Shepherd, J.N. et al. 3D Microperiodic Hydrogel Scaffolds for Robust Neuronal Cultures. *Advanced functional materials* **21**, 47-54 (2011).
43. Hitani, K. et al. Transplantation of a sheet of human corneal endothelial cell in a rabbit model. *Molecular vision* **14**, 1-9 (2008).
44. MacNeil, S. Progress and opportunities for tissue-engineered skin. *Nature* **445**, 874-880 (2007).
45. Wang, Z., Wang, Y., Farhangfar, F., Zimmer, M. & Zhang, Y. Enhanced keratinocyte proliferation and migration in co-culture with fibroblasts. *PloS one* **7**, e40951 (2012).
46. Jubin, K., Martin, Y., Lawrence-Watt, D.J. & Sharpe, J.R. A fully autologous co-culture system utilising non-irradiated autologous fibroblasts to support the expansion of human keratinocytes for clinical use. *Cytotechnology* **63**, 655-662 (2011).
47. Rheinwald, J.G. & Green, H. Serial cultivation of strains of human epidermal keratinocytes: the formation of keratinizing colonies from single cells. *Cell* **6**, 331-343 (1975).
48. Ma, K., Laco, F., Ramakrishna, S., Liao, S. & Chan, C.K. Differentiation of bone marrow-derived mesenchymal stem cells into multi-layered epidermis-like cells in 3D organotypic coculture. *Biomaterials* **30**, 3251-3258 (2009).
49. Han, C.M., Wang, S.Y., Lai, P.P. & Cen, H.H. Human bone marrow-derived mesenchymal stem cells differentiate into epidermal-like cells in vitro. *Differentiation* **75**, 292-298 (2007).
50. Straseski, J.A., Gibson, A.L., Thomas-Virnig, C.L. & Allen-Hoffmann, B.L. Oxygen deprivation inhibits basal keratinocyte proliferation in a model of human skin and induces regio-specific changes in the distribution of epidermal adherens junction proteins, aquaporin-3, and glycogen. *Wound repair and regeneration : official publication of the Wound Healing Society [and] the European Tissue Repair Society* **17**, 606-616 (2009).
51. McCall, J.D., Luoma, J.E. & Anseth, K.S. Covalently tethered transforming growth factor beta in PEG hydrogels promotes chondrogenic differentiation of encapsulated human mesenchymal stem cells. *Drug delivery and translational research* **2**, 305-312 (2012).
52. Kratchmarova, I., Blagoev, B., Haack-Sorensen, M., Kassem, M. & Mann, M. Mechanism of divergent growth factor effects in mesenchymal stem cell differentiation. *Science* **308**, 1472-1477 (2005).

CHAPTER 6

Conclusions and Future Work

General Conclusions

In this work, we have characterized the behaviors of mammalian cells after they are cultured with a variety of microenvironments, ranging from two-dimensional surfaces tethered with multiple biomolecules, to three-dimensional scaffolds that could host entire sheets of cells. In Chapter 2, we successfully demonstrated that we could modify a substrate by immobilizing two biomolecules independently (or 'orthogonally') of each other. We then showed that these biomolecules could still interact as expected with the model cell lines HUVEC and A431. Chapter 3 dealt with the development of a microenvironment for feeder-free culture of hESCs, and characterizing how hMSCs behaved on it. By designing an anisotropic microenvironment featuring spatially distributed areas of cell-selective and cell-resistant domains, we successfully built and characterized a bioactuator powered by rat neonatal cardiomyocytes in Chapter 4. Finally, in Chapter 5 we used a novel grid PLGA scaffold generated from EHD-cojetting and a movable/programmable x-y stage to create sheets of various cell lines (including hMSCs and keratinocytes).

The advances generated by this work add to the overall body of scientific knowledge and 'toolboxes' available to biomedical engineers. The ability to create microenvironments is a powerful tool because these niches do so much *in vivo* to guide and support cells in performing their physiological roles, especially stem cells[1]. They can also play a pathological role, as it is well known that the microenvironment of cancer cells is critical to their development [2]. By developing methods for

bioorthogonal surface reactions, we have pushed the field forward towards better techniques for the precise immobilization of biomolecules. We also now have a much clearer idea of how hMSCs behave on PMEDSAH, and how the method of coating PMEDSAH can play a major role in their proliferation. Stem cells will continue to play an increasingly important role in medicine and in studies of fundamental cell physiology, so coatings like PMEDSAH that result in feeder-free conditions will be more and more prevalent – being able to differentiate hESCs into hMSCs and continue to culture them on the same substrate will represent another step towards a 'universal' substrate that can be used for all the steps of stem cell culture, from growth to maintenance to differentiation. Even though hMSCs can be grown and maintained on TCPS, other groups have moved towards developing xeno-free conditions for their expansion, including a using surface with an immobilized peptide (PQVTRGDVFTMP) – their growth rate on these modified substrates was significantly higher in comparison to TCPS [3]. Thus, it is important that we continue to characterize hMSC proliferation on substrates intended for xeno-free culture, and that's precisely what Chapter 3 explored.

In the burgeoning field of bioactuators, we created free-floating actuators which are much smaller than many others that have been developed, and found that they are able to host a large number of cardiomyocytes which together exert a calculated force nearly an order of magnitude larger than many of those previously created (detailed in Chapter 2). We also advanced the field of cell microcarriers by developing a spatially selective magnetic microcylinder that could host both fibroblasts and cardiomyocytes. Finally, the field of cell sheet engineering now has a new method for creating cell sheets that addresses several of the shortcomings currently present with other techniques.

In Chapter 1, we discuss the historical context and modern scientific relevance of biomaterials to medicine and engineering, and emphasize that the field of biomaterials is rapidly moving from simple and basic materials like metals and unmodified polymers to complex substrates that in many cases directly incorporate biomolecules such as proteins or nucleic acids in order to better integrate with a patient after transplantation, or to influence the behavior of cells in some way. Even the topology of the surfaces can play a role in dictating cell behavior (e.g., rough vs. smooth surfaces, or stiff vs. flexible substrates) and can be modified to induce some specific biological outcome, as reviewed by Ross et al[4]. Biomaterials should be thought of as creating microenvironments just as we currently think of niches in the body where cells reside as microenvironments. In this dissertation, we leverage this paradigm to characterize the biological outcomes of a variety of biomaterials, and we continue to build on our knowledge of this fascinating field.

Future Work

As discussed earlier, our successful dual immobilization strategy for biomolecules should be exploited to attempt more intriguing biological phenomenon. For example, by microcontact printing different growth factors or small molecules to our surface sequentially, we could create patterns of factors that would differentiate mesenchymal stem cells towards different lineages. Other groups have demonstrated the feasibility of this approach[5]. Other possible ways forward include attempting to create gradients of biomolecules on our surface, rather than just a homogeneous density[6]. This would allow us to induce behaviors such as neural guidance[7]. This could also potentially allow us to create surfaces or substrates that can induce morphogenesis with cell lines, along the French Flag model espoused by Wolpert [8]. With opposing gradients of our co-polymer, we could even create a system where one population of cells undergoes morphogenesis in one direction, while another does so in the opposite. Gradients of biomolecules can be created in

CVD by coating a gradient of the co-polymer (this is done by not rotating the sample stage), creating a thin polymer film with a spatially increasing amount of reactive functional groups (and thus after immobilization a gradient of tethered molecules such as proteins)[6]. Opposing co-culture gradients can be generated with two-source CVD. One of the chief difficulties with this way forward is non-specific adsorption of the proteins (negating the advantages of the polymer gradient).

There is still much work to be done with the hMSCs grown on PMEDSAH. It is not clear whether the differences in the number of hMCSs after 1 week of culture on UV-grafted and ATRP PMEDSAH are solely due to proliferation, or if initial attachment rates also play a role. Several experiments designed to measure initial cell attachment were not successful – however, we believe these technical issues can be overcome. We also must continue to investigate why hMSCs show such a radical difference when cultured on UV-grafted PMEDSAH over ATRP PMEDSAH. We also still need to confirm that hMSCs grown on PMEDSAH still differentiate down their key lineages. We plan to exploit the EDTA effect we observed during this work to generate patterned PMEDSAH surfaces that can resist cell adhesion.

We hope to continue our work with the bioactuators and the culture of cardiomyocytes on substrates for tissue engineering (particularly our scaffolds discussed in Chapter 5). We would like to further optimize our protocols in order to get only a few cardiomyocytes on our cylinders (and avoid the giant balls of cells that currently accumulate on them) – in order for these to then bend we likely will need to make our cylinders even less stiff than they currently are (perhaps by making them smaller in diameter). We also would like to explore the possibility of using our cylinders as spatially selective cell microcarriers. Their magnetic properties could potentially allow for self-assembly, or for them to act as 'cell trains' that carry cells from location to location based on magnetic fields.

Finally, we are very excited about the results we have obtained from our PLGA grid scaffolds. We are currently working on differentiating hMSCs down an osteogenic lineage on our scaffolds, and hope to place them in an *in vivo* model such as a mouse both to demonstrate their safety and potential for use in tissue engineering. We have plans to create sheets of cells from a wide variety of sources, including the liver, endothelial cells, cardiomyocytes, and gastric cells. We would like to move beyond simple sheets and attempt to create more complicated structures by post-incubation manipulation. The scaffolds will hopefully provided the necessary structural support needed to do this, without breaking the cell sheets. These can then be arranged by stacks or overlaying structures of various gross geometric conformation (such as tubes) to create complicated 3D cell co-cultures. Furthermore, we can take advantage of our library of functionalized PLGAs and our ability to jet multicompartmental fibers to create scaffolds which can be enhanced with tethered biomolecules and other functional groups – these could be picked to enhance proliferation, or induce differentiation, or even to resist cell adhesion.

References

1. Ghafar-Zadeh, E., Waldeisen, J.R. & Lee, L.P. Engineered approaches to the stem cell microenvironment for cardiac tissue regeneration. *Lab on a chip* **11**, 3031-3048 (2011).
2. Friedl, P. & Alexander, S. Cancer invasion and the microenvironment: plasticity and reciprocity. *Cell* **147**, 992-1009 (2011).
3. Dolley-Sonneville, P.J., Romeo, L.E. & Melkoumian, Z.K. Synthetic surface for expansion of human mesenchymal stem cells in xeno-free, chemically defined culture conditions. *PloS one* **8**, e70263 (2013).
4. Ross, A.M., Jiang, Z.X., Bastmeyer, M. & Lahann, J. Physical Aspects of Cell Culture Substrates: Topography, Roughness, and Elasticity. *Small* **8**, 336-355 (2012).
5. Ker, E.D. et al. Engineering spatial control of multiple differentiation fates within a stem cell population. *Biomaterials* **32**, 3413-3422 (2011).
6. Elkasabi, Y. & Lahann, J. Vapor-based polymer gradients. *Macromolecular rapid communications* **30**, 57-63 (2009).
7. Cao, X. & Shoichet, M.S. Defining the concentration gradient of nerve growth factor for guided neurite outgrowth. *Neuroscience* **103**, 831-840 (2001).
8. Wolpert, L. Positional information and the spatial pattern of cellular differentiation. *Journal of theoretical biology* **25**, 1-47 (1969).